International Erasmus Mundus Master in
QUATERNARY AND PREHISTORY

Comparative Analysis of Two Microscopy Techniques for Use Wear Research on Stone Tools: laser scanning confocal microscopy (Olympus LEXT OLS5100) and microdisplay scanning confocal microscopy (Sensofar S neox)

BITCHASHVILI Tamar

Supervisor

Antony Borel
Andreu Ollé Cañellas

Academic year 2022/2023

Acknowledgments

Expressing my profound gratitude for the transformative two years I have experienced presents a daunting challenge, as finding adequate words seems a formidable task. These years have ushered me into a wondrous world, teeming with knowledge, fresh perspectives, and boundless innovation.

First and foremost, I extend my heartfelt appreciation to my esteemed supervisors, Dr. Antony Borel and Dr. Andreu Ollé Cañellas. Their profound expertise, unwavering dedication, and consistent guidance have been pivotal in shaping my academic journey and navigating the complexities of my chosen field. I am genuinely indebted to their wisdom, patience, and willingness to impart knowledge.

The European Union Commission's Erasmus Mundus program holds a special place in my heart for enabling me to pursue my master's degree abroad. My participation in the Quaternary and Prehistory International Master (IMQP) opened up an array of remarkable opportunities at prestigious institutions such as the Muséum National d'Histoire Naturelle de Paris in France and the esteemed Universitat Rovira i Virgili in Tarragona, Spain. Additionally, I had the privilege to be part of this program with esteemed institutions like Università degli Studi di Ferrara in Italy and Instituto Politécnico de Tomar in Portugal.

I must also express my heartfelt thanks to the Institute of Archaeological Sciences of the University Eötvös Loránd (ELTE) in Budapest, Hungary, and Institut Català de Paleoecologia Humana i Evolució Social (IPHES) in Tarragona, Spain. Their invaluable assistance in orchestrating this program and providing crucial resources, particularly the microscopes in the laboratories, played a pivotal role in my academic journey (The laser scanning confocal microscope (LSCM) was funded by the grant no. K 132857 of the National Research, Development and Innovation Office (NRDI fund) of Hungary“).

I must acknowledge and convey my sincere gratitude to Dr. Ketevan Esakia, a Senior Researcher at the Georgian National Museum O. Lordkipanidze Archaeological Research Center, for her unwavering support and constant presence by my side throughout this incredible journey.

A special debt of gratitude is owed to my family, colleagues, and friends, whose unwavering support and encouragement have kept me motivated and focused on this rewarding path.

I extend a heartfelt thank you to all the individuals involved in creating and organizing this extraordinary program—from the organizers to the lecturers and support staff. Your efforts are instrumental in providing individuals like me with the opportunity to embark on a transformative learning journey, granting us a new chance to succeed at a crucial stage in our careers.

In conclusion, my gratitude knows no bounds, and I remain forever appreciative to all who have played a part in shaping this memorable chapter of my life.

Thank you; Merci; Gracias; Grazie; Obrigado; დიდი მადლობა;

"Stone tools are an appropriate choice,
as they reflect the fossilized acts and goals
of the hominins that created them"
Foulds, F.W.F.

Abstract

This study presents the outcomes of experimental and laboratory research, representing the first investigation within this specific discipline. The primary objective of the research focuses on the comparative assessment of microscopic techniques to ascertain their congruence when analyzing stone tool surfaces.

With a focus on advancing scientific understanding and resolving existing inquiries, advanced microscopy techniques are employed, including laser scanning confocal microscopy (Olympus LEXT OLS5100) and microdisplay scanning confocal microscopy (Sensofar S neox).

The study unfolds in two integral components: Part I encompasses experimental work, while Part II involves rigorous laboratory appraisal. The study aims to compare data measured with both confocal microscopes, from the surfaces of the experimental stone tools, used by different contact materials.

The pivotal findings of this research unequivocally establish the comparability of data acquired from both microscopy techniques. However, our study illustrates that the implementation of a series of surface roughness analyses, such as tailored workflows and precise measurement filters, effectively mitigates these inter-microscope differences. This revelation holds profound significance, underscoring the reliability of these instruments for use-wear analysis, as they consistently yield congruent results.

.....

Keywords:

Use-wear analysis, Lithic tools, Microscopy, Laser scanning confocal microscopy, LED confocal microscopy, Comparative analysis, Experimentation

Abbreviations List:

- DMTA - dental microwear texture analysis
- ELTE - Eötvös Loránd University
- HPA - high power approach
- IPHES - Institut Català de Paleoecologia Humana i Evolució Social
- LED - light emitting diode
- LPA - low power approach
- LSCM - laser scanning confocal microscopy
- MWA - microscopic use-wear analysis
- OLM - optical light microscopy
- SEM - scanning electron microscopy
- SSFA - Scale-sensitive fractal analysis
- TEM - transmission electron microscopy
- QAMA - Quantitative artifact microwear analysis

Table of Contents

Chapter I. Introduction, Framework, and Objectives

1.1. Beyond the Surface: Importance of Use Wear Analysis and Experimental Work in Archaeology

The use-wear analysis is a crucial archaeological method to gain insights into the past by examining the wear patterns found on Prehistoric tools and artifacts (Odell 2004). These patterns provide valuable information about the ways in which these tools were used, the activities they were involved in, and the materials they interacted with (Tafelmaier *et al.* 2022). It goes beyond merely looking at the artifact's features appearance, and delves into the functional aspects, helping archaeologists reconstruct past human societies' daily lives and behaviors.

A wide range of wear patterns, emanating from use, could be observed on lithic tools. These include micro-scarring, striation, edge rounding, smoothing, beveling and micro polish (Borel *et al.* 2014; Ibáñez *et al.* 2014; Ibáñez & Mazzucco 2021), for example, some tools were designed for specific tasks, and use-wear analysis can reveal these specialized functions. For instance, a tool designed for woodworking might exhibit unique wear patterns different from a tool intended for hide processing (Álvarez-Fernández *et al.* 2020; Liu *et al.*).

Since the middle of the 20th century, use-wear analysis was as one of a potent method for studying archaeological materials (Dumont 1982; Keeley 1982; Gijn 1990; Kimball *et al.* 1995). Among these materials, lithic artifacts have been of particular interest, and the advent of use-wear analysis has significantly enriched our understanding of the functions of lithic tools beyond the traditional approach based on morphology and typology (Andrefsky 1998). Early research into use-wear analysis on lithic artifacts have provided compelling evidence that the physical characteristics of stone tools do not always align with the functions attributed to them (Andrefsky 1998; Stemp 2014) . This revelation has opened up new avenues for interpreting the multifaceted roles that these ancient tools played in prehistoric societies. This goes to show the role use-wear analysis played in refuting some of the deeply entrenched beliefs regarding prehistoric objects and providing reinforcement to interpretations (Nunziante Cesaro & Lemorini 2012; Ibáñez & Mazzucco 2021).

Throughout the past five decades, the incorporation of numerous tools and methodologies in this research domain has sparked a significant surge in interest regarding

use-wear analysis through microscopic research of the traces found on stone tools (Stemp *et al.* 2015; Borel *et al.* 2021).

Presently, observation also involves conducting experiments focused on the observation, the possibility of repetition, and the quantification of surface alterations. These experiments employ diverse methodologies, with a especially emphasis on using confocal and other high-resolution microscopes (Arman *et al.* 2016; Pedergnana *et al.* 2020b; Borel *et al.* 2021b). The primary objective is to gain a comprehensive understanding of the factors influencing the formation of distinct traces observed on archaeological materials during the use-wear analysis process.

In the past couple of decades, the incorporation of numerous tools and methodologies in this research domain has sparked a significant surge in interest regarding use-wear analysis through microscopic observation of the traces found on stone tools (Borel *et al.* 2014; Stemp 2014; Ibáñez & Mazzucco 2021).

Conducting experiments plays a pivotal role, as it is through this process that we glean the most crucial information (Keeley 1982; Ibáñez *et al.* 2019; Marreiros *et al.* 2020). Experiments stand as a cornerstone in use-wear analysis and prehistoric stone tools research, serving as a rigorous scientific approach to explore ancient tool use and gain insights into prehistoric societies (Stemp & Stemp 2003; Ollé & Vergès 2014; Ibáñez *et al.* 2019; Waber 2020). This comprehensive discussion highlights the pivotal role of experiments, encompassing the creation of reference collections, empirical validation, insights into past technologies and behaviors, and the establishment of methodological rigor (Ollé & Vergès 2014; Stemp 2014: 1; Borel *et al.* 2021a; Ibáñez & Mazzucco 2021).

Experiments in use-wear analysis involve subjecting meticulously crafted replicas of prehistoric stone tools to controlled use activities representative of past human behaviors. These activities encompass cutting, scraping, drilling, grinding, and more (Stemp *et al.* 2013; Marreiros *et al.* 2020). By intentionally inducing wear on these replicas under controlled conditions, researchers create a comprehensive reference collection that documents distinct wear patterns corresponding to specific tool-use actions (Ibáñez & Mazzucco 2021). This reference collection forms the foundation for comparative analysis, allowing scholars to identify and interpret wear patterns on archaeological artifacts with greater accuracy and confidence (Marreiros *et al.* 2020).

Through the systematic execution of experiments, use-wear analysts can empirically validate their interpretations of wear patterns on ancient stone tools. By comparing the wear patterns observed on replicas to those found on actual artifacts, researchers can confirm the

accuracy of their analytical methods and interpretations. This empirical validation enhances the reliability of use-wear analysis, reducing potential subjectivity and fortifying the credibility of research findings (Ollé & Vergès 2014).

Experiments offer a unique window into past technologies and the behaviors of ancient societies. By replicating prehistoric stone tools and employing them in controlled scenarios, researchers can gain invaluable insights into the functional capabilities and limitations of these tools (Rots & Taipale 2023). Such experimentation allows for a deeper understanding of tool performance, the selection of raw materials, and the tasks for which these tools were optimized. Consequently, use-wear analysis supplemented by experimental data provides a more holistic view of prehistoric societies, shedding light on their subsistence strategies, craftsmanship, and cultural practices (Vergès & Ollé 2011; Bencomo *et al.* 2023).

The controlled environment provided by experiments ensures methodological rigor and standardization in use-wear analysis. By systematically manipulating variables and carefully documenting experimental procedures, researchers can establish reliable protocols for use-wear studies (Borel *et al.* 2021b; Stemp 2023). This rigorous approach minimizes potential biases and errors, allowing for more consistent and objective interpretations of wear patterns across different researchers and archaeological sites (Ollé & Vergès 2014).

In conclusion, experiments hold immense importance in the realm of use-wear analysis and prehistoric stone tools research. They contribute significantly to the construction of reference collections, empirical validation of interpretations, insights into past technologies and behaviors, and the establishment of methodological rigor. The use-wear analysis complements traditional typologies by providing functional information about artifacts, through the fusion of experimental data and archaeological evidence, researchers gain a more profound appreciation for the intricacies of prehistoric tool use, enabling them to reconstruct and comprehend the lives of ancient human societies with greater accuracy and depth (Stevens *et al.* 2010; Marreiros *et al.* 2020; Pal *et al.* 2020).

Undoubtedly, mastering specific aptitudes and methodologies is crucial for proficiently identifying and interpreting surface modifications resulting from use. By employing materials and techniques relevant to use-wear analysis in prehistoric archaeology, these experiments serve as valuable methodological tools to enhance the practitioner's familiarity and expertise with essential skills.

Looking ahead, continued exploration of experiments in use-wear analysis may uncover new insights and innovative approaches, further advancing our understanding of prehistoric tool use and the lives of ancient human societies.

1.2 Research Objectives:

The main objective of this master's thesis is to conduct a comparative analysis of two microscopy techniques, namely laser scanning confocal microscopy (Olympus LEXT OLS5100) and microarray scanning confocal microscopy (Sensofar S neox), for their application in use-wear research on stone tools. The study aims to investigate the suitability of both microscopy techniques by exploring their principles, working mechanisms, spatial resolution, scanning speed, optical setups, surface adaptability, depth measurement ranges, and additional features. We also aim to test if both microscopes provide similar results when they are used for the discrimination of different contact materials.

The research seeks to thoroughly examine and evaluate each microscopy technique's capabilities, limitations, and potential applications within the context of use-wear analysis. The experiment is divided into two parts: The first involves conducting an experimental study where flint flakes are used on different contact materials, employing distinct movements and divergent numbers of strokes. Subsequently, the second part of the research was laboratory work carried out using the two microscopes with different magnifications. After this, the MountainsMap®9 system was employed on which different filters and workflows are applied. The results obtained from the laboratory work are then used for statistical analysis.

The achievement of these objectives is expected to have a notable contribution regarding the questions related to microscopic techniques in use-wear analysis, providing valuable insights into the study of stone tool use in archaeological contexts. By comparing and assessing the effectiveness of laser scanning confocal microscopy and Microdisplay scanning confocal microscopy for use-wear research, this study aims to enhance the understanding of stone tool use patterns, shedding light on past human activities and their historical significance.

1.3 Research Questions:

-What are the key features and technical specifications of laser scanning confocal microscopy (Olympus LEXT OLS5100) and Microdisplay scanning confocal microscopy (Sensofar S neox) relevant to use wear research on stone tools?

-How do laser scanning and Microdisplay scanning confocal microscopy differ in resolution, imaging capabilities, and sample preparation requirements for use-wear analysis?

-What are the strengths and weaknesses of each microscopy technique in identifying and characterizing use-wear traces on stone tools?

-How do laser scanning confocal microscopy and Microdisplay scanning confocal microscopy perform in the analysis of different types of use wear (e.g., cutting, scraping, grinding) on stone tools?

-How do the cost, accessibility, and ease of use of these microscopy techniques impact their applicability in use wear research for academic and practical archaeological settings?

-What are the challenges and potential sources of error associated with the use of laser scanning confocal microscopy and Microdisplay scanning confocal microscopy in use-wear analysis, and how can these be mitigated?

-To what extent can the findings from this comparative analysis inform best practices and recommendations for future researchers employing microscopy techniques in use wear studies on stone tools?

-How can the data obtained from laser scanning confocal microscopy and Microdisplay scanning confocal microscopy be integrated and complemented to enhance the overall understanding of stone tool use and technology in past human societies?

By addressing these research questions, this thesis aims to establish a comprehensive and critical assessment of the capabilities of laser scanning confocal microscopy and Microdisplay scanning confocal microscopy in studying use-wear on stone tools. The results of this study are expected to contribute significantly to the field of use-wear analysis and provide valuable guidance for researchers in selecting appropriate microscopy techniques for their studies.

Chapter II. State of the art

2.1 Use-Wear Analysis in Prehistoric Archaeology and Evolution of the Methods

The fundamental objective of archaeological research revolves around the piecing together of subsistence patterns that were characteristic of human populations in the prehistoric period. This goal requires a collaborative and multidisciplinary approach, with analysis of a diverse array of archaeological materials undertaken by specialists from various fields (White & Folkens 2005).

Prehistoric archaeology stands as a gateway to understanding the origins of human civilizations, revealing the remarkable journey of our ancestors through the artifacts they left behind. Among these artifacts, stones hold particular importance due to their abundance, durability, and versatility in various prehistory societies. The study of stones tools and their use-wear has emerged as a critical tool for prehistoric archaeologists, enabling them to study and shed light on the evolution of human culture, technology, and social dynamics. Use-wear analysis provides the key to decipher the functional and technological aspects associated with prehistoric tools.

Use-wear refers to the alterations on the edges and surfaces of an implement that is linked with its utilization (Keeley 1982; Odell 2004). The ultimate goal of use-wear analysis is to identify the forms of use of archaeological materials as well as the wider implication of this for understanding the subsistence economies based on the functional analysis of the materials (Keeley 1974; Grace 1989; Ollé & Vergès 2008). That is exceptionally important for modern archaeological studies because this kind of research allows us to examine the wide range of substance activities inferred from the study of wear patterns observed on prehistoric tools (Fuentes *et al.* 2019; Borel *et al.* 2021).

The use-wear analysis (Traceology) is a term that may refer to the study of any traces, whether residues or surface alterations, usually in the context of tool use (Odell 2004). Potentially applicable to all material classes, artifacts made of wood, bone, stone, shell, and metal, specific methods and interpretive rules have been developed for particular tool materials (Fullagar & Matheson 2014; Stemp *et al.* 2015; Stemp 2023).

The Use of wear analysis and experimental work in archaeology gained significant attention and refinement in the latter half of the 20th century, but the history can be traced back to the early 20th century, and possible that it began laying the groundwork even before that. The evolution of its development can be categorized into specific periods: The period

from the mid-19th to the early 20th centuries, followed by the early 20th to mid-20th century, then the 1970s to 1980s, further advancing into the 1990s, and finally, spanning from 2000 to the present (Stemp *et al.* 2015).

One of the earliest researcher period the mid-19th to the early 20th centuries who made significant contributions to the study of stone tools and prehistoric artifacts is John Evans, an early British archaeologist. In his work "The Ancient Stone Implements, Weapons and Ornaments of Great Britain" (Evans 1897). Evans developed a classification system for stone tools based on their functional purposes. This marked an important shift in archaeological thinking, as previous approaches often focused solely on typological classifications based on morphological similarities. Following Evans' lead, subsequent archaeologists and lithic analysts recognized the importance of considering the functional aspects of stone tools in addition to their typological characteristics. Function refers to the purpose and use of a tool in the past, while typology involves grouping artifacts based on shared morphological features. Technology, on the other hand, relates to the methods and techniques used by prehistoric societies to produce tools.

For most of the researchers, the history of use-wear studies is tied to developments since the mid-20th century. Research works from this period onwards had a significant impact in bringing use-wear analysis to the forefront. Because of this, currently, two main schools of use-wear analysis are commonly recognized. The first was formed the Eastern scholars, which is also known as the St. Petersburg school, and the second Western European research.

During this period, one of the notable figures was Sergei Alexandrovich Semenov, whose research formed the foundation for a significant impact on the researche of use-wear analysis (Semenov 1957). He is particularly renowned for developing systematic approaches to the study of use-wear traces on stone tools. Semenov's first major publication in the field of archaeology is widely considered to be "Prehistoric Technology: An Experimental Study of the Oldest Tools and Artifacts from Traces of Manufacture and Wear" which was published in 1957 (Semenov 1957). The translation and publication of Semenov’s early results in 1964 laid the basis for subsequent studies. His corpus of work from this period involved the study of wear traces such as striations on metal, lithic, and bones observed using different used both low-power stereoscopic microscopes and significantly more potent metallographic variants, but employ the primary reliance was placed on the former (Stemp *et al.* 2015). Furthermore, his works had drawn upon ethnographic analogies, an approach that largely dictated research methodologies during this period (Semenov 1964; Semenov & Shchelinsky 1971).

Following Semenov's contributions, the period spanning from the 1970s to the 1980s stands out as a period of significant transformation in the realm of functional, use-wear analyses. During this timeframe, a considerable portion of the efforts were directed toward refining the experimental methodologies and adapting the microscope methodology initially introduced by Semenov and Eastern scholars (Keeley 1982; Stemp *et al.* 2015). Consequently, researchers in archaeology placed a pronounced emphasis on rigorous experimentation, task replication, and the application of various microscopic techniques to unravel the diverse functions of tools (Keeley 1980; Odell 1981). However, during this period, there was notable progress in the evolution of microwear analysis techniques. One of the first scholars who demonstrated early interest in this particular approach included Ruth Tringham (Tringham *et al.* 1974), and her doctoral student George Odell, (Odell 1977, 1981) and Lawrence Keeley (Keeley 1974, 1980). After identifying specific limitations in the application of Semenov's method by Western researchers (Keeley 1974; Keeley & Newcomer 1977), Ruth Tringham and her colleagues took on the challenge of developing a novel technique during their research studies at Oxford University (Keeley 1974; Stemp *et al.* 2015; Tumung 2019) .

In the 1970s, notable efforts to analyze residues on stone tools emerged which is focuses on identifying microscopic traces of organic materials, such as plant remains, animal tissues, blood, and other substances, left behind on artifacts (Kealhofer *et al.* 1999; Fullagar 2004; Wadley *et al.* 2004). In particular, researchers utilized a low-power microscope to examine tools and made attempts to detect predominantly plant-based remnants through the use of chemical reagents (Briuer 1976). They explored the concept of systematically measuring observed variations in wear formation during their investigation into wear patterns that result from contact with different materials (Keeley 1980; Lerner *et al.* 2007). There have been studies on a range of residues, encompassing phytoliths, plant fibers, and starch grains (Fullagar & Matheson 2014). In this regard, notable works were carried out on the identification of the traces resulting from these remains on stone tools. During this period, alongside the study of obsidian, flint, quartzite and other kind of stone tools, there was also a focus on the analysis and experimental examination of bone and antler tools (Tringham *et al.* 1974; Chomko 1975; Odell & Odell-Vereecken 1980; Levi Sala 1986), as well as organic materials. Prehistoric cultures utilized bone and antlers to craft a diverse range of implements, including awls, needles, and harpoons. Additionally, shell tools were potentially employed for creating ornaments, cutting tools, and containers in various cultures (Banning 2020).

Use-wear analysis has undergone remarkable developments from 1990 to the present day. During this period, a substantial body of research was dedicated to the domain of microwear analysis, employing conventional microscopic techniques (Grace 1990; Anderson *et al.* 1998). The focal point of investigation revolved around scrutinizing wear patterns manifested on stone tools fashioned from diverse raw materials, encompassing flint, chert, obsidian, quartz, and limestone, (Stemp & Chung 2011; Pedergnana & Ollé 2017; Pedergnana *et al.* 2020b; Halbrucker *et al.* 2021; Paixão *et al.* 2021). An augmented interest emerged in probing contact materials hitherto underexplored, such as horn, root, tuber, and pottery. Within this period, certain researchers advocated for the utilization of singular microwear techniques, while others embraced a complementary approach, amalgamating disparate techniques to harness their distinct analytical merits. Researchers use high, and lower-power microscopy and micro-wear analysis techniques, enabling more accurate identification of tool use and function. Experiments during this period were pivotal in replicating wear patterns found on artifacts. Researchers conducted controlled experiments with stone tools, shedding light on how distinct materials and activities generate unique use-wear traces.

Empirical outcomes have demonstrated the critical significance of minutiae in advancing this discipline and elucidating outcomes. From the 2000s onwards, researchers focused more on developing methodological standardization for the analysis of use-wear on tools. Analysts often adopt methods of their predecessors, leading to methodological diversity. This era saw significant efforts directed towards establishing systematic approaches to interpret wear patterns present on archaeological artifacts (Macdonald 2014b; Gibaja & Gassin 2015). These endeavors aimed to enhance the objectivity and accuracy of wear identification and functional interpretation.

The realm of use-wear analysis revolves around intricate specifics, wherein even the tiniest nuances have the capacity to yield noteworthy disparities. As has been vividly demonstrated in the early work of Eliot Cecil Curwen who investigated to discern the origins of polished surfaces found on the edges of certain ancient serrated blades of Neolithic origin, spanning Europe, the Near East, and North Africa (Curwen 1930; Evans & Donahue 2005). Considering the prevailing hypothesis attributing these tools to grain cutting, Curwen conducted experiments using flint implements resembling sickle blades. Upon examination, he noted a pronounced extent of surface polishing along the edge of the experimental sickle blades, surpassing that observed on archaeological blades from the British region. Consequently, Curwen inferred that these serrated blades were possibly intended for woodworking rather than grain harvesting. However, this interpretation was subsequently

deemed inaccurate. It is plausible that a meticulous cleansing of Curwen's experimental specimens would have revealed a comparable degree of surface polishing on the experimental blades as observed on the archaeological counterparts (Evans & Donahue 2005; Macdonald 2014a).

In the last two decades, technological innovations have played a pivotal role in the evolution of use-wear analysis. Interdisciplinary collaborations between archaeologists, material scientists, and engineers have significantly enriched use-wear analysis . There has been a noticeable trend toward the integration of diverse methodologies within the realm of microwear analysis. This integration encompasses a spectrum of techniques, ranging from low- to high-power microscopy, as well as the amalgamation of traditional microscopic methods with cutting-edge approaches such as scanning electron microscopy (SEM). Furthermore, a pronounced emphasis has been directed towards the quantification of surface wear, facilitated by the application of assorted image analysis methodologies. Parallel to these developments, there has been a discernible augmentation in investments directed toward engineering technologies and computational applications. This augmentation is particularly pronounced in domains like metrology and tribology, which bear significance in the context of microwear analysis (Stemp *et al.* 2015; Borel *et al.* 2018).

The introduction of a multitude of tools and methods in this type of research over the past decades had led to a marked increase in research interest in the qualitative and quantitative analysis, by microscopy, of the traces on the stone tools (Evans & Donahue 2008a; Macdonald 2014b). The qualitative commences with a macroscopic visual assessment, constituting the initial phase, wherein the primary objective pertains to distinguishing use-wear traces on the surface distribution that correlates with the technical and functional attributes inherent in the implementation (Calandra *et al.* 2019; Borel *et al.* 2021a). Within this preliminary scrutiny lies the identification of wear patterns ascribed to both the manufacturing process and those indicative of patterns arising from usage.

The first attempts at applying quantitative methods for wear identification date back to the 1970s, with the seminal work of Semenov who measured the intensity of polishes and compared microreliefs between used and unused surfaces (Borel *et al.* 2021b). Subsequent to this, the quantitative analysis adopts a meticulously structured methodology, meticulously measuring and quantifying specific attributes residing on the surface of the tool that holds indications of its historical use (Stemp *et al.* 2013; Borel *et al.* 2021a; Ibáñez & Mazzucco 2021). Advanced imaging techniques, coupled with precision measurement methods, underpin these stages, yielding data of exactitude and standardization. This collective

endeavor serves to enrich the comprehension of wear patterns through a more stringent and objective lens.

However, while wear analysis and the study of surface alterations are powerful tools in archaeological interpretation, they inherently involve challenges related to subjectivity and uncertainty. Because of this, an interdisciplinary approach, combining multiple lines of evidence, using advanced analytical techniques, and incorporating experimental archaeology, helps to mitigate these challenges and build more reliable interpretations of prehistoric artifact use (Borel *et al.* 2021b).

It is important that the research on prehistoric tools should be aided by rigorous experiments, which make the research process more reliable. The comparison of the results that can be obtained with different types of microscopies, acquisition, and the 3D surface traces of use at nanometric scales allow for detecting and characterizing the traces of use. The analysis of these traces is done by the calculation of various metrological parameters processed.

2.2 Microscopy Techniques, Surface Metrology and Approaches in Use-Wear Research

Accurate execution of use-wear analyses is contingent upon possessing the appropriate equipment. The techniques necessary for conducting use-wear analysis underscore the methodical essence of archaeological research (Evans & Donahue, 2008a). A comprehensive toolkit, encompassing microscopes, cameras, lighting, reference collections, replication tools, software, and measurement instruments, is essential for delving into the histories of tools and their users. Progress in the field has been propelled by advancements in equipment, accompanied by a series of experimental endeavors. In the 1950s, the application of microscopy in archaeology began to gain momentum (Keeley, 1974; Evans & Donahue, 2008a). Microscopes became a pivotal tool for scrutinizing the microscopic wear traces on stone tools, allowing deductions about their functions and patterns of use.

The contributions of microscopes to unraveling technological, and functional aspects of prehistoric tool use are priceless (Ollé & Vergès 2008; Borel *et al.* 2014; Ibáñez *et al.* 2019). Microscopy techniques have emerged as an indispensable tool for this discipline, allowing researchers to investigate microscopic traces on lithic artifacts, revealing details of

tool function, use context, and socio-economic activities (Álvarez-Fernández *et al.* 2020; Rodriguez *et al.* 2021; Ibáñez & Mazzucco 2021).

Historically, the examination of wear traces on stone tools has primarily involved the utilization of a stereomicroscope and reflected-light microscopy. The stereomicroscope, operating at low power, was designed to present samples in a three-dimensional view. Reflected-light microscopy, on the other hand, entails illuminating a sample from above and recording the light reflected off its surface. This approach enables the meticulous observation and documentation of diverse surface attributes. However, up until now, numerous experiments have been conducted involving various types of microscopes. The selection of a particular microscope hinges upon the nature of the investigative focus and the desired level of resolution. Consequently, the choice between differing microscopes is predicated upon the nuanced intricacies of the analytical objectives at hand.

Microscope as SEM provides high-resolution images of wear patterns at the microscale, revealing intricate details of tool-edge modifications and wear debris. The capability to observe micro-fractures, striations, and residues contributes to deciphering tool use and raw material sourcing This technique unveils ultrafine details of micro-wear, facilitating the study of cutting edges, abrasives, and contact interactions. Other advantage of SEM is that it does not lose depth with increasing magnifications, and point are always focused (Ollé & Vergès 2008, 2014; Frahm 2014).

Optical Light Microscopy (OLM) involves examining tool surfaces under visible light, enabling the identification of macroscopic wear features such as polish, striations, and rounding. This technique aids in distinguishing tool functions, wear types, and the materials worked upon (Borel *et al.* 2014).

Nowadays, aided by technological advancements, various experimental tools, and methods are employed in surface analysis. Especially, surface metrology has been increasingly employed by archaeologists and anthropologists in their research endeavors aimed at comprehending tool use and gaining enhanced insights into the processes of use-wear, particularly on stone. The application of a confocal microscope has consistently yielded promising results in surface metrology.

The possibility of controlling numerous functions on mechanical components and manufactured objects is facilitated by surface metrology. This entails the measurement and characterization of surface features at the micro or nanoscale level. Specifically, confocal microscopy serves as a non-destructive imaging technique wherein a focused laser is employed to capture intricate three-dimensional images of a sample's surface (Stemp *et al.*

2015; Borel *et al.* 2018). Through this technique, highly detailed data about the topography and wear features of stone tools can be acquired. Today, with technological advancements, several experimental tools and methods are employed in surface analysis. LSCM, in particular, has gained traction for its ability to assess subsurface cracks and provide comprehensive insights into wear mechanisms. The best results in surface metrology studies are being achieved as a result of the application of confocal microscopy (white light confocal microscopy and Laser Scanning Confocal Microscopy). It produces highly accurate 3D topographies and 2D profiles (Álvarez-Fernández *et al.* 2020).

Microscopic studying methods hold significant promise in enriching and advancing the burgeoning field of lithic use-wear analysis. This potential arises from the capacity of microscopy techniques to unveil nuanced wear features, residues, and edge modifications that might remain imperceptible to the naked eye or conventional macroscopic analysis (Pedergnana & Ollé 2018). Moreover, these microscopic methods have the potential to transcend the constraints of traditional use-wear classification systems. By uncovering micro-fractures, micro-polish, and subtle modifications, microscopy techniques contribute to the creation of refined typologies that correlate more closely with specific tool-use actions. This finer granularity in classification allows for a deeper exploration of prehistoric activities, including cutting, scraping, sawing, drilling, and more, fostering a richer narrative of past behaviors.

2.2.1 Low and High Power Approach, and Importance of Blind Test

Research works that followed recognized various areas of application of use-wear studies. During the 1970s and 1980s series of experiments involving high and low-powered microscopes were carried out simultaneously by several researchers. The resolution of LPA (stereomicroscope) and HPA (reflected microscopy) within the realm of use-wear analysis exemplifies a nuanced spectrum of methodologies that have evolved over time (Evans 2014). The LPA, which traces its origins back to pioneer researchers, centers on the utilization of microscopy at lower magnifications (Odell & Odell-Vereecken 1980). This method has several advantages, including ease and speed of analysis and the availability of equipment. In contrast, the HPA at its core, the high-power approach accentuates the investigation of polishes, and discernible alterations on stone surfaces that amplify reflectivity when subjected to microscopic observation (Keeley 1980). For example, a similar experiment by George H. Odell and Keeley set out with aspects such as the determination of use motion and hardness of

contact materials from striations on chipped stone tools and the nature of polishes produced as a result of diverse actions and contact materials (Odell 2004; Stemp 2014). The principal way of proving the accuracy of the techniques employed in these kinds of research was through a blind test, which involves individuals who independently utilize the objects of interest and others who carry out analysis based on certain parameters (Odell 2004). Utilizing blind testing methodologies became essential for conducting comprehensive assessments, establishing standards, and precisely calibrating techniques (Moss 1987; Rots *et al.* 2006).

Furthermore, the 1980s saw a fierce debate over the accuracy of the techniques used in the identification of worked materials (Pedergnana *et al.* 2020a; Rodriguez *et al.* 2021; Ibáñez & Mazzucco 2021). On the flip side, during this period an analytical procedure was built to overcome previously contentious low vs. high power approaches by gathering a reliable set of available evidence for functional diagnosis (Ibáñez *et al.* 2019). Significant information has been collected during blind tests of microwear polishing experiments conducted between 1986-1988 years, which were made by M. Newcomer, R. Grace, R. Unger-Hamilton, and E.H. by Moss (Moss 1987; Wadley *et al.* 2004). It was an outstanding experiment because it was concrete, factual, clear, and with important details of the variables extracted, including tool type, duration of use, interpret motion, etc. Information from blind-test results was collated in a database for statistical evaluation (Moss 1987).

One of the significant issues in use-wear analysis remains the quantitative description of polished surfaces. Even though many use-wear traces are relatively easy to categorize and quantify, quantitative descriptions of polished surfaces proved to be challenging. However, headways were made in the past two decades with the help of confocal microscopy (Evans & Donahue 2008b). Initially utilized to analyze wear on tooth surfaces, recent works in the area of lithic materials are thought to be promising (Calandra et al. 2019). Texture analysis of polishes (due to antler, wood, dry hide, fresh hide, and greasy hide processing) showed quantitative differences (Ibáñez *et al.* 2019).

In the last quarter of the 20th century, significant conferences were held to address major concerns regarding micro-wear analysis. These conferences facilitated discussions on wear mechanisms, post-depositional modifications of stone tools, and the reliability of lithic micro-wear analysis, often informed by the outcomes of blind tests. An important turning point occurred at the 1989 Uppsala conference, where the Low Power and High Power Approaches were discussed extensively. Previously seen as separate, competing methodologies, researchers at this conference recognized the complementarity of these

approaches, agreeing that their combined use yielded better results compared to their individual applications (Grace 1996; Marreiros *et al.* 2015).

2.2.3 Research Gap and Contribution of the discipline

The domain of use-wear analysis has rapidly progressed within a concise timeframe, undergoing numerous trials and experimental phases during its inception. Consequently, it has evolved into a distinct discipline, yielding significant outcomes, particularly in the investigation of epochs such as prehistoric archaeology. The meticulous scrutiny of minute details has proven to be a conduit for substantial revelations. Initial stages were characterized by diverse methodological approaches, punctuated by experimental endeavors. These foundational efforts have critically contributed to method refinement. However, the imperative for a unified methodological framework has arisen to mitigate potential errors. Notwithstanding the remarkable strides achieved, this realm necessitates continued advancement, but there are still research gaps and opportunities for further contributions within this discipline. Here are some crucial areas where researchers still can make significant contributions:

-Enhancement of quantitative approaches: While quantitative methods have advanced the field, there is still room for refining these techniques. Developing more sophisticated methods for analyzing wear patterns and alterations, such as using machine learning algorithms to classify and identify wear features, could enhance the accuracy and objectivity of interpretations.

- Integration of multidisciplinary approaches: Collaborations between archaeologists, material scientists, engineers, and experts from related fields can lead to a more holistic understanding of artifact use. Combining expertise in microscopy, materials analysis, and experimental archaeology can provide new insights into wear patterns and their causes.

- Standardization and Reproducibility: Establishing standardized protocols for wear analysis and sharing datasets can enhance the reproducibility of studies and allow for better cross-comparisons between different archaeological sites and collections.

- Statistical Approaches: Applying advanced statistical methods to wear analysis data can help in quantifying the level of certainty associated with interpretations. This could involve developing probabilistic models that consider multiple factors affecting wear patterns.

- Environmental Factors: Exploring how environmental factors such as humidity, temperature, and exposure to different elements affect wear patterns can contribute to more nuanced interpretations.

- Digital and Computational Methods: Leveraging digital technologies like 3D scanning and computational modeling can aid in simulating wear patterns and understanding how they develop over time.

- Digital, software, and Computational Methods: Leveraging digital technologies like 3D scanning and computational modeling can aid in simulating wear patterns and understanding how they develop over time.

Chapter III. Materials and Method

3.1 The Procedure of Experimental Protocol

The master's thesis is bifurcated into two distinct components, with each contributing significantly to the exhaustive exploration of the research objective. The primary emphasis is placed upon the execution of experimental investigation, followed by assiduous laboratory analysis. These dual segments operate synergistically to establish the bedrock for the overarching research pursuit.

Part I: Experimental work

The first portion of the master's thesis is centered on the implementation of a stringent experiment. This phase is characterized by the deployment of experimental stones as investigative instruments on a diverse array of contact materials. The central aim pertains to the scrutiny of resultant interactions transpiring between the stones and the respective contact materials. The dimensions of each experimental stone tool were also measured, including length, width, and thickness. Measurements were taken for all, allowing an assessment of whether the examined objects were effectively utilized and their morpho-potentiality to be evaluated. The experimental parameters encompass a selection of contact materials, the application of specific actions, and the quantification of these interactions via precisely controlled strokes, each flake was used during. The experimental protocol encompasses distinct stages: the selection of raw materials, the determination of actions, the quantification of strokes, and the documentation of samples (Table 1). This empirical inquiry serves as the foundational framework for amassing primary data, thereby enabling subsequent analysis.

Part II: Laboratory Appraisal

The subsequent phase of the master's thesis entails an all-encompassing laboratory analysis. This stage leverages the data procured from the experimental phase and employs two distinct microscopes operating at variable magnifications. The utilization of laser scanning confocal microscopy (Olympus LEXT OLS5100) and Microdisplay scanning confocal microscopyopy (Sensofar S neox) at specified magnifications constitutes the pivotal cornerstone of this analysis.

Information was acquired from both microscopes, encompassing details such as stone number, microscope type, objective specifications, zoom level, type of measurement (3D-stitching), size of the measured area (3x3; corresponding to a suitable fraction of the objective), XYZ coordinates, measurement duration, and parameters, along with upper and lower parameter bounds, color and laser brightness. Interesting surfaces were captured by implementing a 10% overlap. Additionally, data pertaining to temperature, and humidity were gathered to facilitate monitoring of the ambient conditions and their potential influences. All measurements were numbered and subsequently stored in their respective files.

The surface measurements of the experimental stones were conducted in three stages. In the first stage, measurements were taken before use, wherein points were selected that were situated close to the edges and were more likely to exhibit increased use-wear during interactions with the contact material. From each of the eight pieces, three points were chosen from the dorsal surface and three from the ventral side. Subsequently, measurements were captured at magnifications of 10x/0.3NA, 20x/0.45NA, and 100x/0.8NA using a Sensofar s neox microscope. The second measurements were taken after use, using the same points and magnification levels as in the initial measurement phase, by the same microscope. Finally, in the third stage, measurements were performed on the same points, but using an Olympus microscope.

Following the microscopic scrutiny, integration with the MountainsMap ® 9 system is enlisted to extract, scrutinize, and construe the acquired outcomes. The calculation of additional parameters according to 3D surface texture analysis using standardized ISO parameters and subsequent analyses is enabled by the MountainsMap® software. This software facilitates the quantification and characterization of textural attributes, ultimately contributing to the formulation of meaningful inferences drawn from the outcomes of the experimental phase.

Part III: Development of an Effective Workflow

Throughout this thesis work, an extensive exploration was undertaken to identify comparable studies. However, the exclusive finding up to the present juncture pertains to authored by Arman S.D., entitled 'Minimizing Inter-Microscope Variability in Dental Microwear Texture Analysis' (Arman *et al.* 2016). The focus of this article revolves around the application of the DMTA methodology to enhance the comprehension of dietary patterns in extinct mammals. A notable attribute of DMTA resides in its inherent capability for the

objective collection of data. Nevertheless, the challenge of discordant outcomes arising from diverse microscopy instruments presents an impediment to achieving result reproducibility. To address this, automated techniques are introduced to diminish measurement noise across microscopes during the scanning of identical surfaces using varied microscopes. These discrepancies persist even in scenarios where scans are slightly displaced or executed sequentially under standardized parameters. The principal origins of this variability are attributed to instrument measurement noise, further compounded by the inherent sensitivity of the SSFA-based DMTA technique.

During our experiment, an earnest effort was exerted to adhere to the protocol and procedural steps delineated in the aforementioned work. However, as the research progressed, a realization emerged that the prescribed methodology was not suitably congruent with our specific case. Consequently, an alternative protocol, thoughtfully aligned with the distinct exigencies inherent to our research context, was formulated. This revised protocol underwent comprehensive testing and validation procedures.

Exp. Tool number	ELTE_IAS_000093	ELTE_IAS_000094	ELTE_IAS_000096	ELTE_IAS_000200	ELTE_IAS_000201	ELTE_IAS_000202	ELTE_IAS_000203	ELTE_IAS_000204
Production_technique	Direct_percussion	Direct_percussion	Direct_percussion	Direct_percussion	Direct_percussion	Direct_percussion	Direct_percussion	Direct_percussion
Hammer_type	Hard	Hard	Hard	Hard	Hard	Hard	Hard	Hard
Hammer_RawMat	Stone	Stone	Stone	Stone	Stone	Stone	Stone	Stone
Task	Sawing	Sawing	Sawing	Scraping	Scraping	Sawing	Sawing	Sawing
TaskSpecDirection	Bidirectional	Bidirectional	Bidirectional	Unidirectional	Unidirectional	Bidirectional	Bidirectional	Bidirectional
ToolRawMat	Flint	Flint	Flint	Flint	Flint	Flint	Flint	Flint
ToolRawMatReg	Kremenets'	Kremenets'	Kremenets'	Kremenets'	Kremenets'	Kremenets'	Kremenets'	Kremenets'
ToolRawMatCountry	Ukraine	Ukraine	Ukraine	Ukraine	Ukraine	Ukraine	Ukraine	Ukraine
WorkedMat	Reed	Wood	Wood	Leather	Leather	Reed	Antler	Antler
WorkedMatState	Soaked in water	Fresh	Fresh	Fresh	Fresh	Fresh	Soaked in water	Soaked in water
WorkedMatSpec	Arundo domax	Quercus Ilex	Quercus Ilex	Cervus elaphus	Cervus elaphus	Arundo donax	Cervus elaphus	Cervus elaphus
DorFacePos	Internal	Internal	External	Lead	Follow	Internal	Internal	Internal
UseDuration	2h04min45s	1h07min36s	2h10min57s	2h20min58s	1h01min03s	1h15min54s	1h09min06s	2h22min32s
StrokeNb	10000	5000	10000	10000	5000	5000	5000	10000
HandHold	R	R	R	R	R	R	R	R
ContactAngle	80-90°	80-90°	80-90°	30-40°	30-40°	80-90°	80-90°	80-90°
Cleaning	20min 2% Derquim ultra-sound (before use) 10min 5% H2O2 ultra-sound 10min 2% Derquim ultra-sound 5min Aceton ultra-sound (before measurement) 20min Distilled Water ultra-sound	20min 2% Derquim ultra-sound (before use) 10min 5% H2O2 ultra-sound 10min 2% Derquim ultra-sound 5min Aceton ultra-sound (before measurement) 20min Distilled Water ultra-sound	20min 2% Derquim ultra-sound (before use) 10min 5% H2O2 ultra-sound 10min 2% Derquim ultra-sound 5min Aceton ultra-sound (before measurement)	20min 2% Derquim ultra-sound (before use) 10min 5% H2O2 ultra-sound 10min 2% Derquim ultra-sound 5min Aceton ultra-sound (before measurement) 10min 5% H2O2 ultra-sound 10min 2% Derquim ultra-sound 5min Aceton ultra-sound	20min 2% Derquim ultra-sound (before use) 10min 5% H2O2 ultra-sound 10min 2% Derquim ultra-sound 5min Aceton ultra-sound (before measurement) 10min 5% H2O2 ultra-sound 10min 2% Derquim ultra-sound 5min Aceton ultra-sound 20min Distilled Water ultra-sound	20min 2% Derquim ultra-sound (before use) 10min 5% H2O2 ultra-sound 10min 2% Derquim ultra-sound 5min Aceton ultra-sound (before measurement)	20min 2% Derquim ultra-sound (before use) 10min 5% H2O2 ultra-sound 10min 2% Derquim ultra-sound 5min Aceton ultra-sound (before measurement)	20min 2% Derquim ultra-sound (before use) 10min 5% H2O2 ultra-sound 10min 2% Derquim ultra-sound 5min Aceton ultra-sound (before measurement)

Table 1: Presents a detailing dataset detailing various attributes of multiple tools used in a specific context, including reference numbers (e.g., ELTE_IAS_000093, ELTE_IAS_000094, etc.), production techniques, tasks (Sawing and Scraping), contact materials, use durations, and more. This information provides a full overview of the tools and their usage characteristics.

Taken as a whole, these two segments collectively encapsulate an essential narrative, encompassing the entire trajectory of the research endeavor. The experimental inquiry in Part I establishes the empirical foundation, thus yielding tangible data for subsequent analysis. Conversely, the laboratory analysis in Part II harnesses advanced microscopy techniques and specialized software tools to unveil profound insights into the interactions discerned during the experimental phase (Table 2). This methodically structured and well-coordinated approach underscores the meticulous nature of the research, ensuring a comprehensive comprehension of the research question, and culminating in the generation of valuable contributions to the pertinent academic domain.

3.2 Material used during the experiment

To conduct the experimentation, eight different flakes, all crafted from flint originating in the Kremenets region of Western Ukraine, were chosen. Each of these tools was assigned alphanumeric identifiers: ELTE_IAS_000093, ELTE_IAS_000094, ELTE_IAS_000096, ELTE_IAS_000200, ELTE_IAS_000201, ELTE_IAS_000202, ELTE_IAS_000203, and ELTE_IAS_000204 (Figure 2).

Stone tool use-wear analysis involves studying microscopic traces like polish, striations, and fractures on tools to determine how they were utilized. By identifying distinct marks produced by various materials and motions, such as sawing or scraping. Because of this, we carefully selected both the stone material and the contact material, movement, etc.

Four contact materials were involved, including: 1. Fresh reed (*Arundo donax*), commonly known as giant reed or carrizo, is a tall perennial grass-like plant that grows in wetland areas and along water bodies. The sawing of this contact material, which is notably hard and in a fresh state, is separated by nodes that are harder than the interior of the stems; 2. Fresh wood (*Quercus ilex*) commonly known as the holm oak. Sawing on the wood can cause more significant edge damage, polish, striation micro-fractures, compared to reed due to its density and fibrous structure. ; 3. Soaked antler (*Cervus elaphus*), commonly known as the red deer, is one of the largest and most iconic deer species. Antler is a bony structure, which is composed mainly of calcium and phosphorus, and it provides the antlers with their sturdy and rigid form. Soaked antlers can create a polished surface on flint tools due to their smooth and dense texture.; and 4. Hide (*Cervus elaphus*), distinctive wear patterns can be observed on stone tools when employed on soft leather. Six flakes (2 per contact material) were

employed in a sawing motion, accumulating 5000 and 10000 strokes, across the three distinct contact materials, namely fresh reed *(Arundo donax*), soaked antler (*Cervus elaphus*), and wood (*Quercus Ilex*). Additionally, two stones were utilized to perform scraping on leather (Cervus elaphus), while one flake underwent 5000 strokes and another underwent 10000 strokes (Figure 1). The pliable nature of soft leather enables it to engage with the stone tools, resulting in the development of polish abrasion and potential smoothing of the tool edges. Moreover, the comparatively milder texture of the leather may lead to subtle rounding of the edges of the stone tools.

Figure 1: Contact material- A. Soaked antler (Cervus elaphus); B. Fresh wood (Quercus ilex); C. Fresh reed (Arundo donax); D. Leather (Cervus elaphus); E. Fresh wood (Quercus ilex);

This selection was motivated by a range of underlying considerations that contribute to the experiment's validity and its potential to yield meaningful insights into the functional attributes of the tools. The inherent variations in hardness, texture, and abrasiveness among the chosen materials introduce a degree of complexity that mirrors the challenges that tools of antiquity may have encountered. By subjecting the stone tools to interactions with materials of varying properties, we could discern nuanced wear patterns and responses that encapsulate a broader spectrum of potential usage scenarios. Incorporating diverse contact materials facilitates the cross-validation of experimental outcomes. By observing consistent wear patterns across different materials when subjected to similar actions, the experiment's

reliability and the reliability of its findings are reinforced. This comparative approach bolsters the credibility of the experiment's conclusions and their potential implications for this master thesis.

Some experimental stone tools (ELTE_IAS_000093, ELTE_IAS_000094, and ELTE_IAS_000096), have been documented through the silicone molds capturing their pristine surfaces, encompassing the edges as well as the ventral and dorsal facets. This measure has been taken to safeguard against unforeseen contingencies and to facilitate potential future analyses and measurements as required.

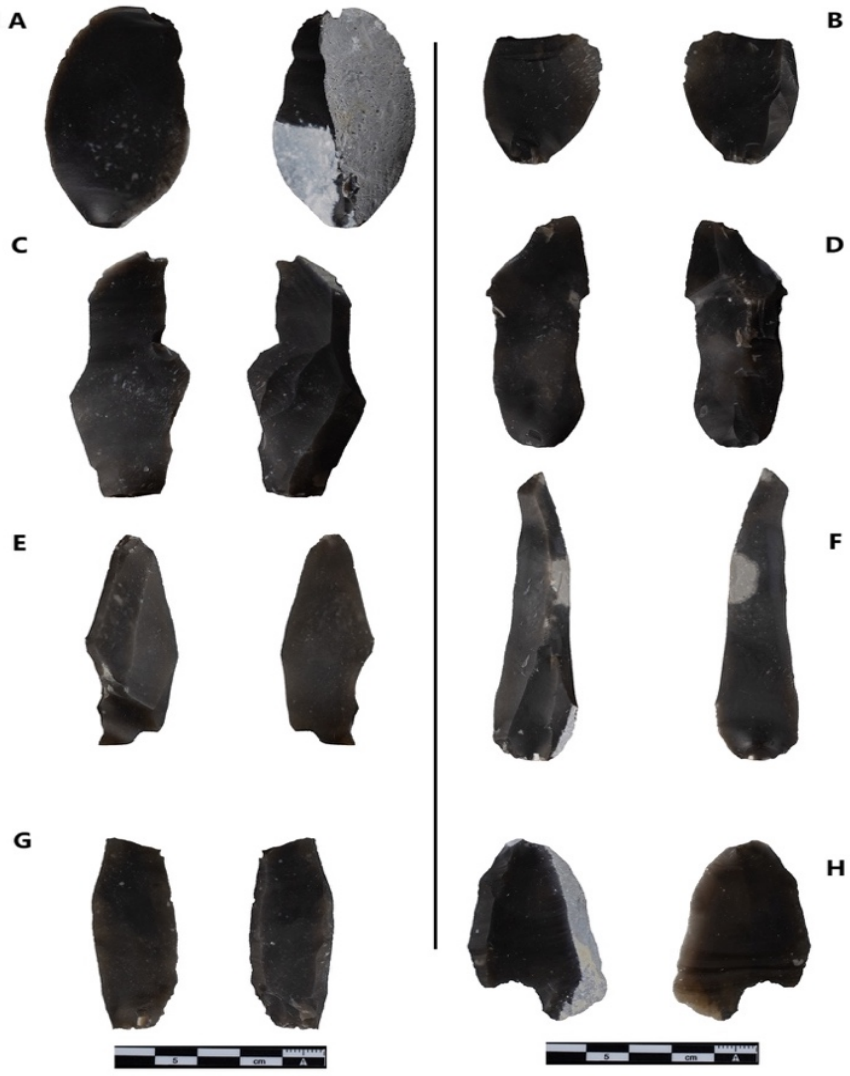

Figure 2: Exp. stone tools during the experiment: A. ELTE_IAS_000093; B. ELTE_IAS_000202; C. ELTE_IAS_000096; D. ELTE_IAS_000094; E.ELTE_IAS_000203 F. ELTE_IAS_000204; G. ELTE_IAS_000200; H. ELTE_IAS_000201

3.3 Preparing, conducting experiments, and cleaning procedure

The cleaning procedure encompassed a dual-phase approach. Prior to the begenning of experimentation, the preparatory phase consisted of sequential actions. Initially, the flakes were subjected to a thorough cleansing process involving immersion in a warm solution composed of a 2% concentration of the soapy substance (Derquim LM02) within an ultrasonic bath, with a duration of 20 minutes allocated for this treatment. Subsequently, each measurement iteration underwent a cleansing regimen employing acetone for a duration of 5 minutes. Furthermore, following the ultrasonic bath treatment, the experimental flints underwent a process of gentle cleansing and drying utilizing pressurized air, aimed at eradicating any residual debris and minute deposits originating from the manipulation process. A post-experiment cleaning approach was adopted following the experimental phase. This discernment stemmed from the observation that the preceding cleaning protocols exhibited limitations in effectively removing certain residues, particularly those arising subsequent to usage and contingent upon the nature of the contact material employed. Consequently, a choice was made to introduce chemical cleaning during the culminating phase of the analysis. To this end, the stone tools underwent further cleansing measures employing specific solutions. Notably, hydrogen peroxide (H2O2) at a concentration of 5% and distilled water were enlisted for a duration of 10 minutes within the ultrasonic bath. This strategic employment of chemical cleaning served to address residues that persisted after the prior cleaning procedures.

Nevertheless, there existed an exceptional, as instances of residues were observed on the two experimental stones, with leather being the contact material. In response to this circumstance, an additional round of chemical cleaning was undertaken (Figure 3).

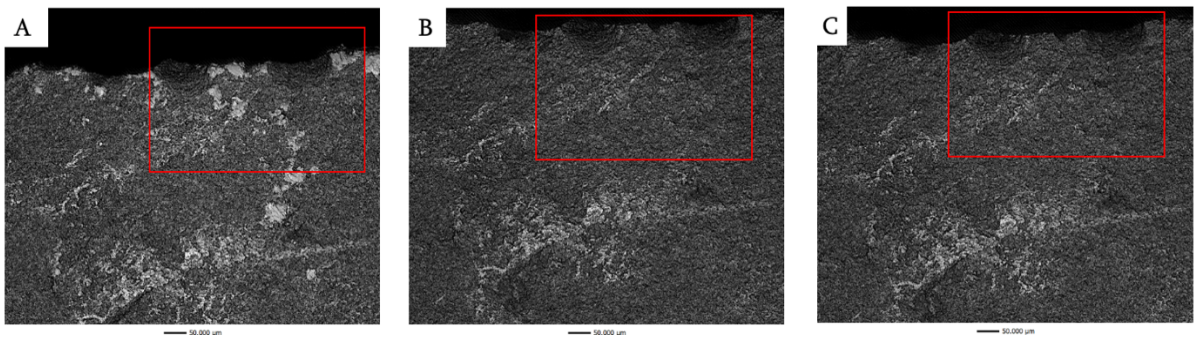

Figure 3: A. Residues are present after the implementation of the H2O2, soap, and acetone cleaning procedure; B. Following the repetition of the chemical cleaning process, H2O2, 10 min; C. A further cleaning procedure involving solely acetone for a duration of 5 minutes results;; ELTE_IAS_000201; VENTRAL; Taken with the 20x/0.45NA the objective of the Sensofar S neox.

It is noteworthy that across all phases of the cleaning regimen, consistency was upheld. After each cleaning procedure, a concluding step was recurrently enacted. Specifically, the application of acetone followed by the utilization of pressurized air facilitated the attainment of a uniformly cleaned and died state for the stone tools. This approach was consistently maintained to ensure that the tools were devoid of extraneous substances and impeccably prepared for the subsequent stages of analysis.

The cleaning procedure's dual-phase framework, coupled with the incorporation of specific cleansing agents and meticulous supplementary steps, elucidates a comprehensive strategy to attain optimal cleanliness of the experimental stone tools. This methodological endeavor underscores the rigorousness inherent in the pursuit of precise and credible use-wear analysis outcomes.

3.4 Laser Scanning Confocal Microscopy (Olympus LEXT OLS5100)

In this work has been used Laser Scanning Confocal Microscopy (Olympus LEXT OLS5100), developed by Olympus Corporation, renowned for its pioneering contributions to optical and imaging technologies, which is designed for metrology in material science.

Measurements were taken with this microscope at the Institute of Archaeological Sciences of Eötvös Loránd University (ELTE).

This instrument operates at the intersection of confocal microscopy and laser scanning methodologies, yielding a sophisticated platform for high-resolution surface profiling and comprehensive analysis of diverse materials. Central to the LEXT OLS5100's functionality is its adept utilization of confocal microscopy principles, wherein light control facilitates the acquisition of focused images. This systematic elimination of extraneous out-of-focus light components culminates in augmented image resolution and enhanced contrast, thereby affording a profound level of fidelity in the visual representation of the examined specimens.

The microscope's operational mechanism is deeply rooted in the precision-driven technique of laser scanning. This underlying mechanism orchestrates the incremental acquisition of imagery through a point-by-point scanning process, a methodology that engenders a paradigm of meticulous measurement and intricate analysis of the specimen's topographical attributes. Notably, the paramount capability of the LEXT OLS5100 resides in its aptitude to confer comprehensive three-dimensional profiles of the specimen's surface morphology. This intricate profiling not only furnishes discernment into the nuances of

surface roughness but also facilitates an exhaustive comprehension of height variations and related surface characteristics. The LSCM optics have been designed to best accommodate incident light with an optimal wavelength of 405 nm. This particular wavelength is chosen to ensure the highest level of performance and accuracy within the imaging process (Table 2).

	MPLFLN10XLEXT	*LMPLFLN20XLEXT*	*MPLAPON100XLEXT*
NA	0.3	0.45	0.8
WD (mm)	10.4	6.5	3.4
Focusing spot diameter (Units: µm)	1.6	1.1	0.52
FOV (um)	1280 x 1280	640 x 640	128 x 128

Table 3: Displays the Laser Scanning Confocal Microscopy (Olympus LEXT OLS5100) objective lenses, identified by codes like MPLFLN10XLEXT, LMPLFLN20XLEXT, and MPLAPON100XLEXT along with their numerical aperture (NA), working distance (WD), focusing spot diameter, and field of view (FOV)

The LEXT OLS5100 is a non-contact measurement system, which means it doesn't physically interact with the specimen during imaging and analysis. This feature is especially useful when dealing with delicate or sensitive samples, as it helps preserve their integrity without any invasive procedures.

During this study, three distinct magnifications were employed in the Laser Scanning Confocal Microscopy analysis, each serving specific purposes. Initially, a 10x/0.3NA objective was employed, enabling the capture of large fields of view while maintaining a reasonable level of detail. It's worth noting that the numerical aperture (NA) of 0.3, while suitable for preliminary sample overview and navigation, may not provide the precision required for reliable surface roughness analysis. Subsequently, we employed a long working distance objective with a 20x/0.45NA magnification. It's worth noting that, despite the increased magnification, the numerical aperture (NA) of 0.45 still is not appropriate for precise roughness analysis. This configuration offered heightened magnification compared to the aforementioned 10x/0.3NA objective, thereby enabling more intricate imaging of samples. The incorporation of a "long working distance" attribute indicates the presence of increased

space between the objective lens and the sample. This characteristic proved particularly advantageous when examining delicate samples, such as the stone surface investigated in this study. Moreover, a magnification of 100x was implemented, concomitant with an objective lens characterized by a notably high numerical aperture (NA=0.8). The deployment of a 100x magnification objective aimed at capturing exceedingly high-resolution images of minute structures, encompassing individual cells or subcellular constituents. The elevated NA inherent to this objective facilitated enhanced resolution and light-capturing capabilities. It is essential to acknowledge that this enhancement in imaging prowess comes at the expense of a diminished depth of field, an inherent trade-off in utilizing such high numerical apertures.

Accompanying the instrument is a suite of software that serves as the analytical bedrock for visualizing and interpreting the three-dimensional data gleaned from the imaging process. This software milieu encompasses a spectrum of analytical tools tailored to address surface roughness quantification, feature measurement, volumetric computations, and other pertinent facets.

Noteworthy in its applicability, the LEXT OLS5100 finds resonance in an array of disciplines including materials science, engineering, semiconductor manufacturing, and the life sciences. Its utility is particularly accentuated in quality assurance protocols, research and development endeavors, and the realm of failure analysis. Central to its prowess is the caliber of resolution it affords, signifying the microscope's capacity to discern intricate features and structures at a minute scale. Furthermore, the reconfigurability of scanning parameters, such as scan area, velocity, and laser intensity, endows users with a realm of customization in consonance with the distinct demands posed by individual samples.

During this work, comprehensive measurement by LSCM of various image attributes, including intensity, color, and height, was useful for visualization as well as for surface analysis. Intensity imaging- capturing intensity images by scanning a focused laser beam over the sample's surface. These images reveal details about the sample's structure and features. Color imaging- This allows researchers to not only study the topography but also analyze the color variations across the surface. Height imaging- One of the primary applications of the LEXT series microscopes is the precise measurement of surface heights. By scanning the sample at different focal planes, the microscope can construct a 3D topographic map of the sample's surface.

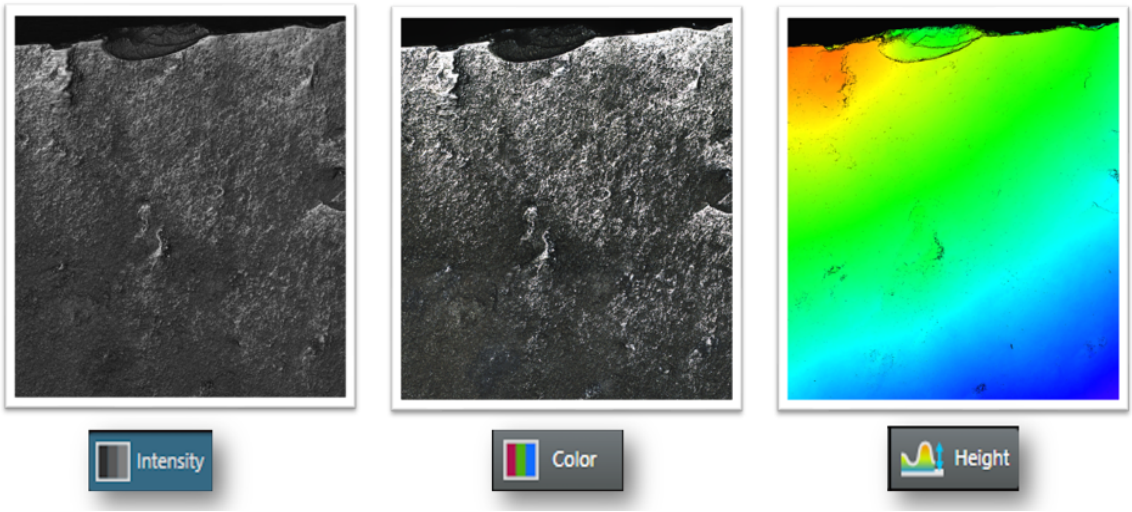

Figure 4: the surface of the experimental stone labeled as "ELTE_IAS_000096," subjected to 20x/0.45NA magnification, was used on fresh wood, involving 10,000 stocks. The acquired image, captured through the Olympus microscope, showcases discernible image characteristics, including intensity, color, and height, rendering it a valuable asset for both visualization and surface analysis

3.5 Microdisplay scanning confocal microscopy (Sensofar S neox)

The second technique employed during the studies involves the utilization of Microdisplay scanning confocal microscopy, the Sensofar S neox. Measurements with this microscope were carried out at IPHES. Initially, the exact same points and protocol were employed both before and after use.

Within this instrument, a sophisticated optical system is embodied, facilitating advanced imaging capabilities. Through the implementation of light-emitting diodes (LEDs) as the illumination source, the achievement of confocal imaging is realized by the microscope, thereby enabling the acquisition of high-resolution three-dimensional (3D) data from specimens. The optical design integrated into the Sensofar S neox involves the implementation of premium Nikon objective lenses that have been meticulously designed to rectify chromatic aberrations, resulting in the production of sharply defined images characterized by elevated contrast and resolution. These objectives contribute to the mitigation of optical artifacts and the enhancement of image clarity across a range of magnifications including 10x, 20x, and 100x, which were utilized during the measurements (Table 3).

	Nikon - EPI 10X	*Nikon - EPI 20X*	*Nikon - ELWD 100X*
NA	0.30	0.45	0.8
WD (mm)	15.5	4.5	4.5
Spatial sampling (um)	0.69	0.34	0.07
Optical resolution (um)	0.47	0.31	0.18
System noise (nm)	30	8	3
Maximum slope (°)	17	27	53
FOV (um)	1689 x 1413	845 x 707	169 x 141

Table 4: The table presents essential optical parameters for the Microdisplay scanning confocal microscopy (Sensofar S neox) system, using different Nikon objectives. These parameters include numerical aperture (NA), working distance (WD), spatial sampling, optical resolution, system noise, maximum slope, and field of view (FOV).

Central to the instrumental capabilities of the Sensofar S neox is its confocal imaging modality, which employs a pinhole aperture to selectively capture emitted light emanating exclusively from the focal plane of interest. By means of this methodology, the microscope adeptly confines the excitation light to the specific focal volume, effectively negating the influence of out-of-focus light that could otherwise contribute to image degradation. The resultant effect of this approach is improved depth discrimination and heightened lateral resolution, thereby engendering the production of 3D reconstructions with heightened fidelity.

The incorporation of LED-based illumination in the Sensofar S neox emerges as a pivotal determinant of its operational framework. The utilization of LEDs ensures a consistent and stable light source, thereby alleviating concerns regarding potential photobleaching and phototoxicity that are conventionally associated with traditional light sources. This stability serves to sustain the integrity of the specimen under scrutiny. This confocal microscopy instrument's proficiency is accentuated by its capacity to yield optical sections from diverse material compositions, spanning reflective, transparent, and rough surfaces, such as experimental stone surfaces. Through judicious manipulation of the optical pathway, the microscope seamlessly transitions between imaging modalities, thereby accommodating a spectrum of applications encompassing topographical analyses, roughness assessments, and morphological characterizations. The adaptability of the instrument is indicative of its versatility in addressing a wide array of research and industrial imperatives.

The Sensofar S neox's integration of confocal principles, reflective of its design and operational tenets, manifests in the enhancement of axial resolution, and the suppression of out-of-focus light, which, in turn, amplifies the precision and clarity of topographical visualizations. The intricate amalgamation of technological facets, including the aforementioned LED-based illumination, resonates cohesively to underscore the instrument's capabilities.

In the realm of performance, the Sensofar S neox deploys a high-resolution camera sensor with dimensions up to 2448x2048 pixels, in conjunction with a high-resolution display boasting dimensions of 3840x2160 pixels. The outcome of this synergy is the acquisition of images that obviate the necessity for up- or downscaling, thereby consistently presenting as sharp, vibrant, and true-to-life renditions on-screen.

To optimize the illumination for distinct applications, the S neox integrates four LED light sources within its optical core, spanning the red (632 nm), green (532 nm), blue (460 nm), and white (580 nm) spectra, however, during this measurement, the optical core operating at green (532 nm) was utilized.

This strategic utilization of LEDs with varying wavelengths corresponds to the application's specific requirements, with shorter wavelengths tailored for scenarios necessitating exceptional lateral resolution, while longer wavelengths are leveraged to accommodate phase-shifting interferometry on expansive, smooth surfaces. Sequential color illumination, another salient aspect of the Sensofar S neox, entails the sequential activation of red, green, and blue LEDs to illuminate the specimen's surface under observation. The resulting triad of monochromatic images is then amalgamated to form a high-resolution color image. This methodological approach confers benefits encompassing elevated color fidelity, vivid saturation, and precise pixel-to-pixel color depiction. Notably, this obviates the need for interpixel color interpolation, which can compromise the integrity of color information.

In different LEXT, only two types of visual images are captured by the Sensofar microscope, which are intensity and height images.

3.6 Integration with the MountainsMap® 9 System

After collecting the information from both microscopes, MountainsMap®9 (version 9.0, 9.0.10203) was used for the final result. Digital Surf (Besançon, France) has developed this powerful software for surface analysis and metrology suite. It is designed to process, analyze, and visualize data derived from various types of microscopy and metrology,

including both comparable confocal microscopes. By employing surface metrology, insights into the characteristics of use-wear marks, such as their morphology, dimensions, orientation, and distribution, can be gained by analysts. The software is equipped to provide advanced tools for characterizing surfaces and extracting valuable information from microscopy data.

The software facilitates Surface visualization, allowing the manipulation and observation of 2D and 3D surface data, thereby enabling the observation of surface structures, textures, and features. A wide array of surface analysis tools is offered by this software, allowing for the quantification of surface roughness, texture, and other characteristics. The application of diverse filters and processing techniques to enhance the visibility of specific features in the surface data is made possible. For datasets or images of substantial size, the software can assist in their stitching or cutting to create a more comprehensive perspective. It makes it possible for one can opt for pre-defined lighting configurations. Furthermore, the option to save, import, or export customized lighting setups is available for reuse.

The software supports advanced analyses, including wear analysis. These tools hold particular value in use-wear analysis. The generation of comprehensive reports and the exportation of data in various formats for further analysis or sharing are functions that can be carried out using the software. The data produced by the LSCM, and Sensofar S neox, encompass surface profiles and pictures, and were subjected to processing and analysis using MountainsMap®9 software to extract quantitative insights concerning surface properties.

Prior to commencing the analysis within the Mountain software, meticulous verification was conducted to ensure the organization and accuracy of all files and measurements. The names attributed to the files from both the Sensofar and Olympus microscopes served as indicators linking their respective information. Consequently, these files were meticulously organized in accordance with their designated sequence. Following the verification process, the Sensofar and Olympus files, including the PLUX and LEXT files, were subjected to the 'TEMPLATE Identity card' feature in MountainsMap 9. This procedure facilitated the extraction of data pertaining to the acquisition settings.

3.6.1 Files preprocessing and Types

We initiated the initial phase of the comparison between the two microscope systems within the MountainsMap software by examining their respective files. For the Sensofar microscope, file formats such as .plux .dat, .stl, .x3p, .pcd were scrutinized, whereas, for the

Olympus microscope, .lext .rep, .sdf, .raw, .csv, .stl formats were considered. Meticulous consideration was given to selecting a file format that would be compatible with both microscopes. The choice of .plux and .lext files from the respective systems ensured a meaningful basis for comparison.

The profilers employed in this study generate raw surface files comprising both topography and intensity layers. To implement filters or modifications on the surface, it becomes essential to exclusively extract the topography layer, thereby producing a surface file in .lext or .plux format. Our objective was to investigate whether this procedure yields discernible variations in the resulting surfaces.

3.6.2 Preparation of Templates

Confronted with an extensive dataset necessitating comprehensive analysis, we undertook a systematic approach to process each scan in groups. This involved the creation of seven unique templates within the MountainsMap® software. We strategically designed these templates to apply various operations and filters to individual datasets, allowing us to subsequently compute 3D surface texture parameters, specifically the surface texture parameters defined by the ISO 25178 standard. The deliberate integration of these templates notably accelerated the procedural workflow, resulting in a marked enhancement of the study's overall efficiency.

For the purpose of our research endeavors, we will employ magnifications of 100x/0.8NA objective lenses, utilizing measurements acquired from both microscopy instruments. We have successfully uploaded the corresponding PLUX and LEXT files into the MountainsMap® system, in preparation for the forthcoming templates analyses.

Template 1a:

1. When creating template 1a, settings were chosen to follow the Arman et al. (2016) workflow and started the template with the leveling of the surface (Figure 5). We employed the Least-square plane (LS-plane method) to level surfaces, as it is the recommended approach for handling random surface textures, that aligns with the present case. This method ensures that the process of leveling maintains a constant XY spacing of data points, thereby preserving the digital lateral resolution. The

least-squares plane operator effectively removes the overall slope that is present on a surface. This slope might result from measurements that were not conducted under strictly horizontal conditions. (For instance, during measurements at a magnification of 100x/0.8NA, achieving precise alignment at the same location with exact points and rotation proved to be quite challenging). The process of removing the least-squares plane involves the determination of the equation of the plane (P plane) that minimizes the sum of the squared basic distances between points on the surface (x,y,z) and their corresponding points on the plane (x,y,z). The LS-Plane method is used as an operator in the microscope comparison study.

2. Remove of the nominal form- For the second step, we proceeded to eliminate the nominal form using a least squares polynomial of degree 2. This function was applied to ensure that the surface's shape didn't result in data loss during thresholding, particularly in the context of the microscope comparison study. Mathematically, the "Remove form" operator entails the elimination of a surface's general form. This allows the subsequent separate study of waviness and roughness components. The process involves approximating the surface's general form using a slowly varying mathematical function. This approximation is then treated as the "form," and the removal process entails subtracting this function from the measured surface.

3. Remove outliers- the primary purpose of the "Remove outliers" operation is to enhance the accuracy and reliability of data obtained from optical profilers, particularly in the context of surface measurement and analysis. The outliers can arise due to various factors such as measurement noise, instrument limitations, or irregularities in the sample being measured. By removing outliers, the goal is to improve the quality of the collected data by eliminating erroneous or misleading data points that do not accurately represent the true characteristics of the surface being measured. This operator was applied to remove features with a slope greater than 80°, which were considered to be random differences typical of measurement noise. Strong strength is chosen during the correction, which means non-measured points are dilated.

4. Threshold- we used the threshold operator to eliminate the upper and lower 0.1% of the data, a range commonly associated with measurement noise. This action was taken to eliminate random disparities that predominantly stem from measurement noise, ensuring that the subsequent analysis is based on pertinent data. This operator proves particularly valuable in the removal of peak values. The process of setting the thresholds, which determine the heights of the horizontal planes used to segment the surface, offers flexibility.

5. Fill non-measured points- the "Fill non-measured points (Use a smooth shape calculated from the neighbors)" operator was used, which holds significance when the surface contains non-measured points. These points can either originate from the measurement process itself or can be designated as such using a different operator. This operator becomes particularly relevant when there's a presence of numerous and dispersed non-measured points across the surface. Its purpose is to reconstruct these non-measured points, ultimately enhancing the overall completeness and quality of the data. The operation of "Fill non-measured points" involves substituting each non-measured point with a calculated value derived from its neighboring valid points. By doing so, the non-measured areas are seamlessly filled in, and the resultant effect is both imperceptible and highly effective in terms of data integrity and accuracy.

6. Extract area- the process of extracting area involves cropping scans to equalize the scan region size between microscopes. This tool facilitates the extraction of specific areas of interest. As a result of the dissimilarity in dimensions between field of view at a comparable magnification of 100x—specifically (NA: 0,8), LEXT - 128 x 128 μm, and Sensofar S neox 169 x 141 μm, extract areas were uesd to precisely section the surfaces at congruent locations. The intention was to ensure uniformity in size, with each section measuring 340 x 340 μm (totally comprising nine squares).
7. Retouch- This function was not needed to be used all the time, it was employed only in specific individual cases. This operator serves the purpose of replacing specific flawed points within the surface. Examples of defects include dust particles. It also offers the capability to transform an area comprising non-measured points into a valid region. The significance of the "Retouch Surface"

operation lies in its ability to enhance data integrity and the quality of the surface model by rectifying or converting flawed or incomplete regions. By employing mathematical constructs like smooth shapes or oblique planes, the operator ensures that corrections blend seamlessly with the surrounding surface, minimizing visual discrepancies.

8. Export studiable- the final action entailed exporting the studiable and preserving it within the suitable folder, accompanied by the relevant description.

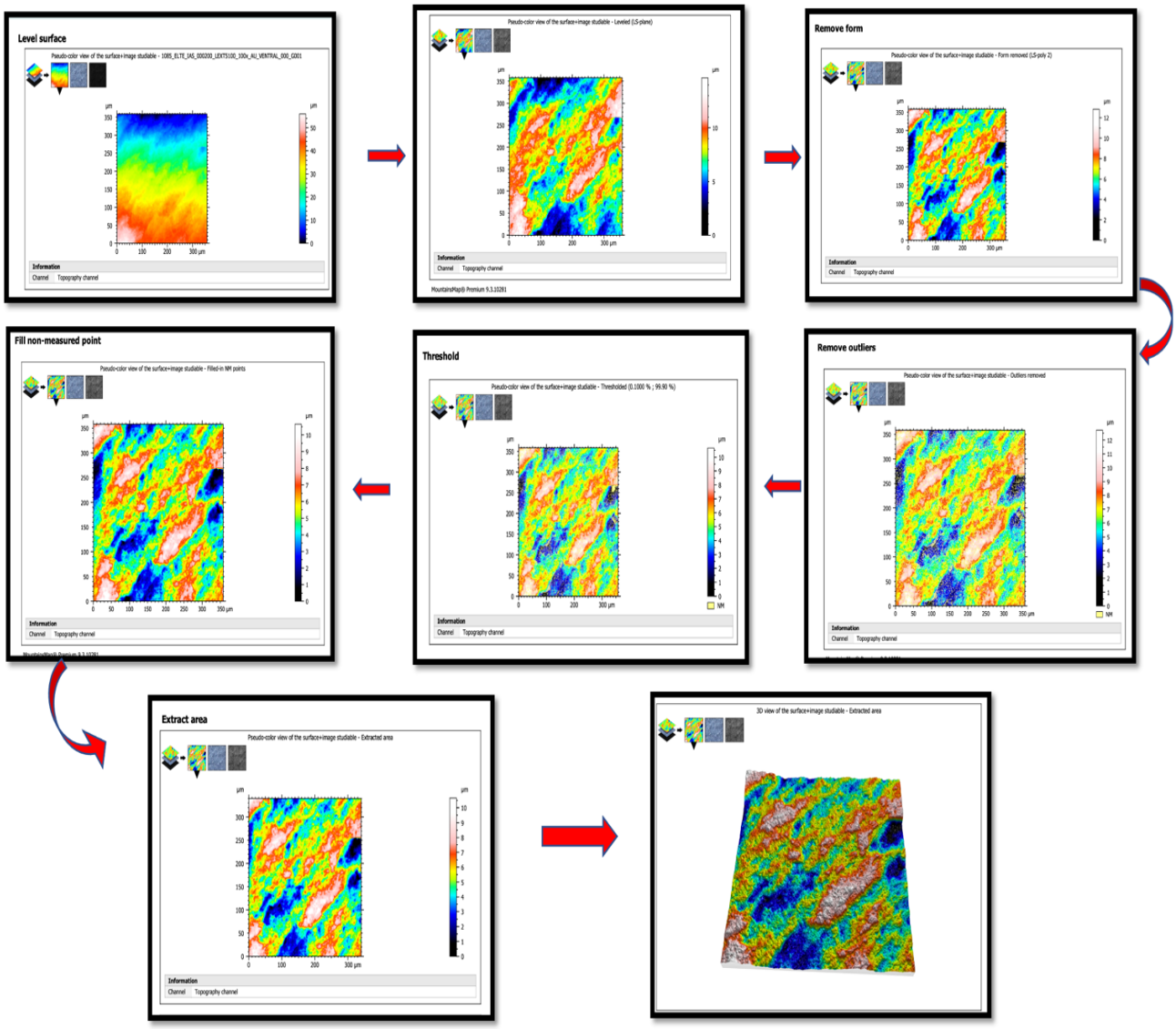

Figure 5: Figure visually summarizes the sequential processing steps detailed in Template 1a, in MountainsMap®.

Template1b:

After working on Template 1a, as discussed in Arman et al. (2016) article, it was observed that in our case specific even topographical images in various research areas exhibited visual discrepancies (Figure 6).

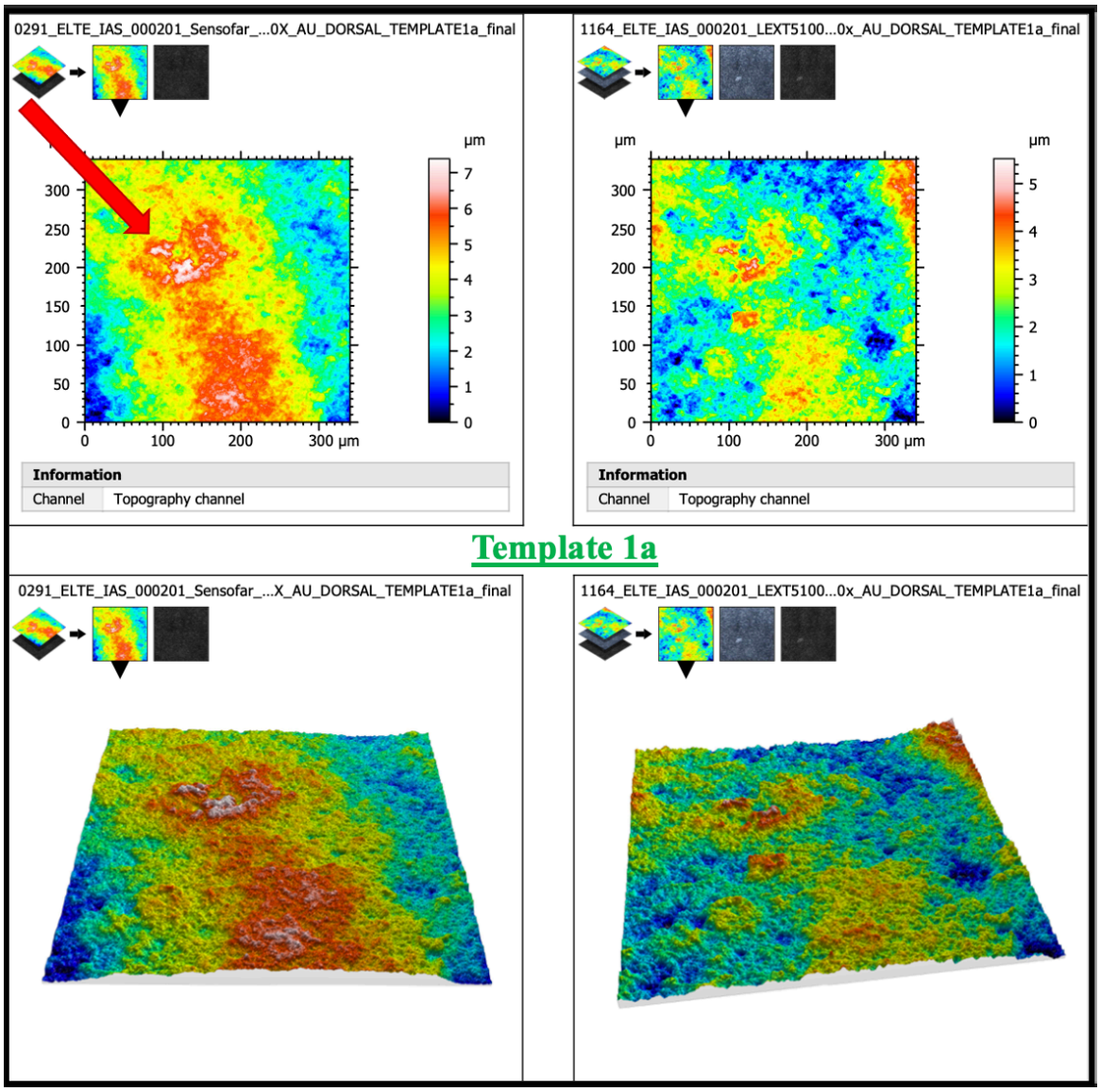

Figure 6: Visualization of the same surface of the tool ELTE_IAS_000201 acquired with the Sensofar Sneox (left) and Olympus LEXT OLS5100 (right) after applying Template 1a. This postprocessing yields different surface topography.

Consequently, efforts were made to modify the protocol that had been previously tested and effect changes to enhance it. To achieve this, adjustments were made to the sequence of steps. The Extract Area operation was positioned at the forefront, enabling the sectioning and normalization of the surface to a consistent size of 340 x 340 µm. Various settings were employed during its application. As a result of these modifications, all processes

were initiated by first extracting the surface data from both measurements. Subsequently, all parameters were applied anew through each process step (Figure 7).

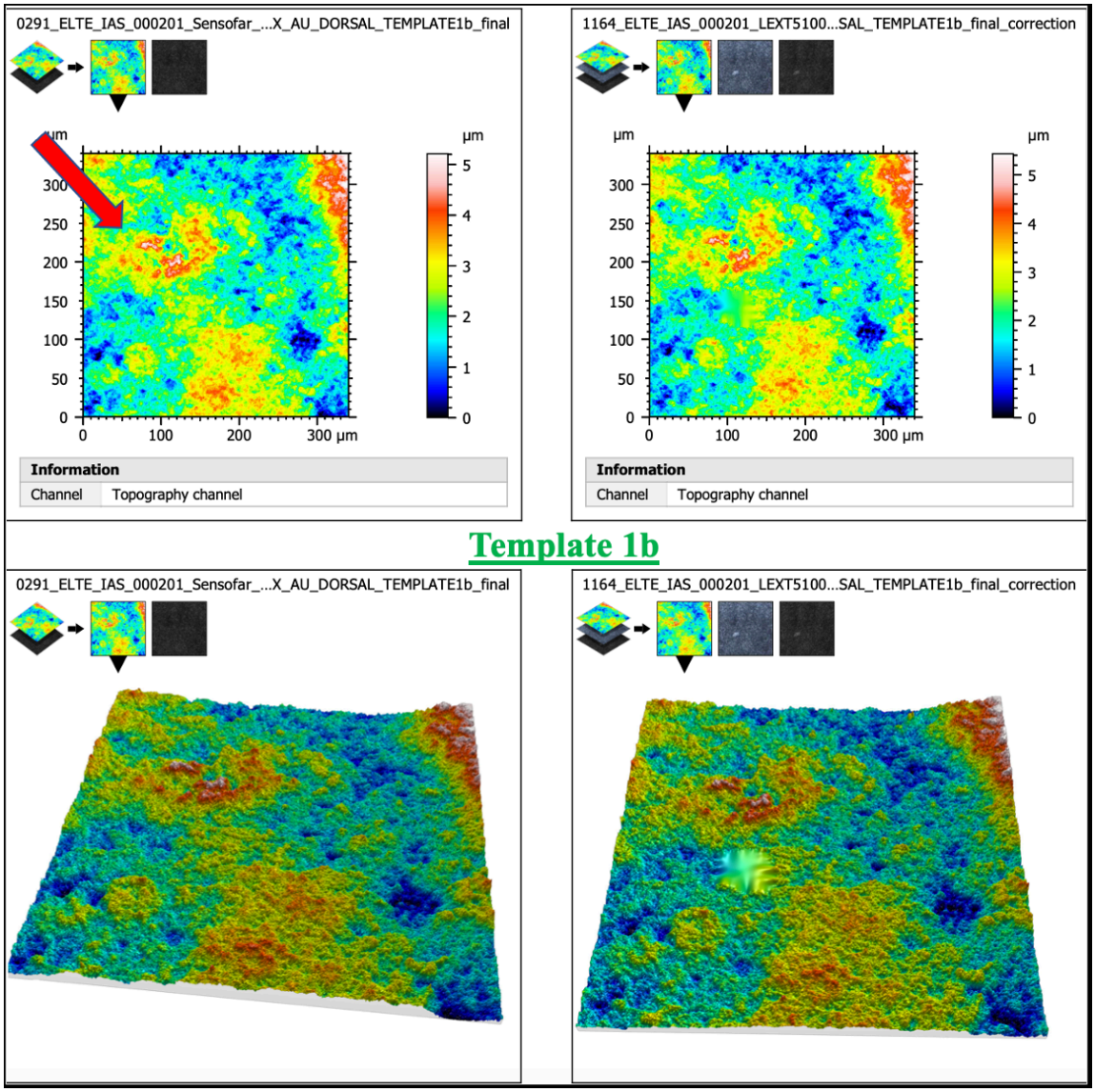

Figure 7: Visualization of the same surface of the tool ELTE_IAS_000201 acquired with the Sensofar Sneox (left) and Olympus LEXT OLS5100 (right) after applying Template 1b. The resulting surfaces are now very similar (the smooth part on the surface of the right is due to a correction of a particle detected after measurement).

Template 2a:

Resampling is a technique employed within this study to align the spatial sampling of scans captured by distinct microscopes. In the mentioned research, the scans were resampled in both the x and y directions to achieve a spatial sampling of 0.130 µm (2616 points), exceeding the typical sampling interval of most utilized microscopes (Figure 8). This

resampling procedure serves to standardize the data and mitigate variations in surface roughness between different microscopes.

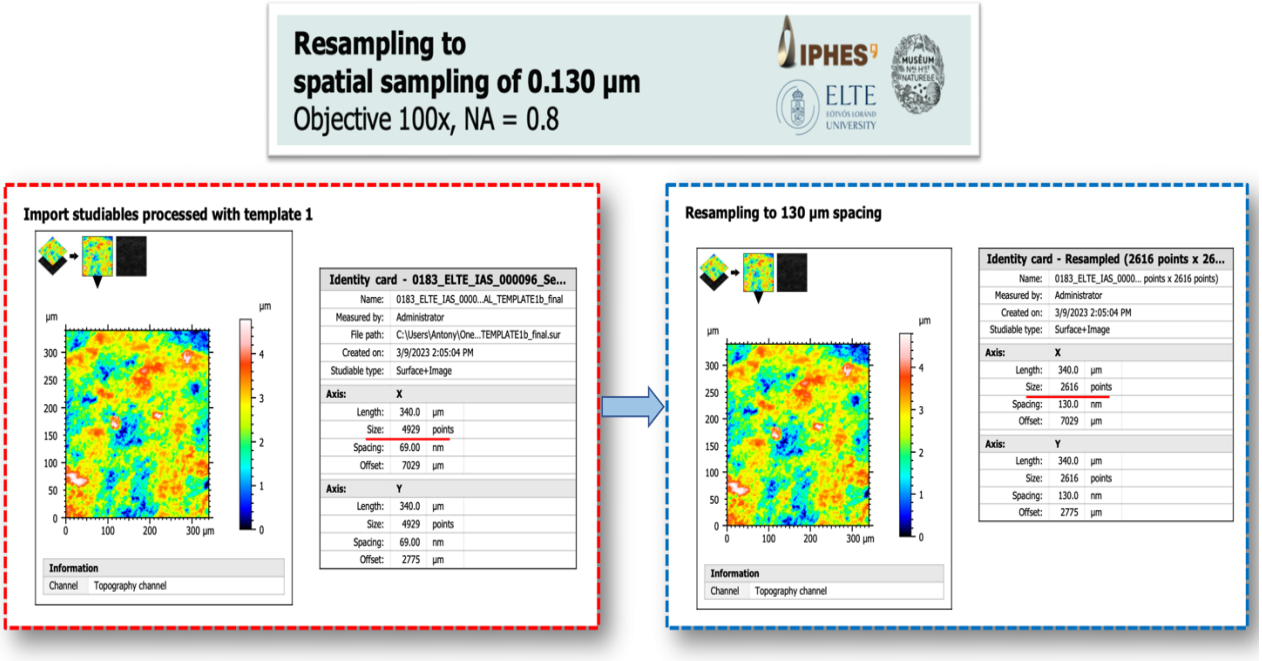

Figure 8: Picture illustrating the process of resampling to achieve a spatial sampling of 0.130 µm. The original data has been transformed to ensure that data points are evenly spaced at intervals of 0.130 µm, allowing for precise analysis and alignment with measurement standards.

Template 3:

Template 3 was formulated through the use of applied studiables with various filter types and cut-off values. The most contemporary form of filtering involves the division of data frequencies, also known as wavelengths, into two distinct categories. The first category encompasses long wavelengths or low frequencies, referred to as "waviness," while the second category comprises short wavelengths or high frequencies, known as "roughness." This separation is achieved through mathematical means, where a wavelength threshold, called a cut-off, is utilized as the separation criterion. The filter allocates wavelengths above the cut-off to waviness and those below the cut-off to roughness. The effectiveness of this separation hinges on the chosen filter type and the specific cut-off value applied (Figure 9).

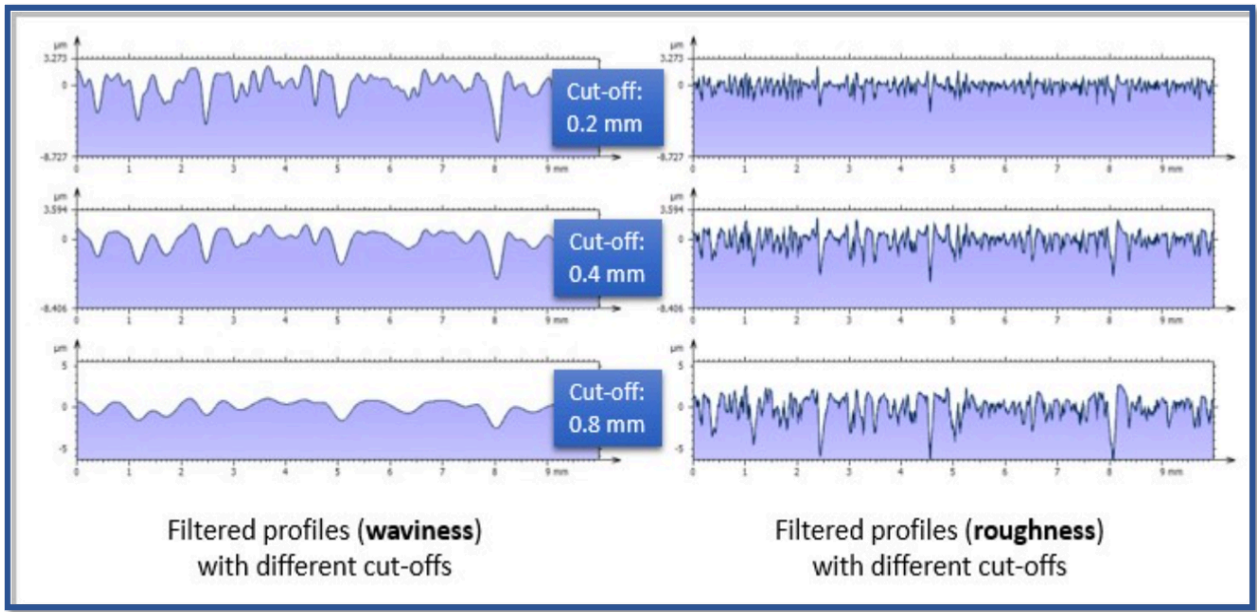

Figure 9: waviness and roughness filters, with different cut-offs (via www.digitalsurf.com)

Template 3, consisting of variations 3a; 3b; 3c; and 3d; involves the application of filters to extract roughness components. After the formulation of Template 3, we proceed to apply filters, including the Gaussian filter, Robust Gaussian filter of order 2, and Spline filter. Various cut-off values are employed in conjunction with the application of end-effect correction (ISO 16610-31).

- Gaussian filter- For a wavelength equal to the cutoff, the filter attenuates (or transmits) 50% of the wavelength amplitude. The Gaussian filter is frequently used but it does not behave correctly around discontinuities such as outliers, steps, or in the presence of shape. Therefore, robust filters have been developed (Figure 10).
- Robust Gaussian filter of order 2- this filter has a mean line (a mean plane) that correctly follows the natural trend of the profile (surface) without being disturbed by breaks in the profile contrary to the Gaussian filter. It is thus preferred for structured or layered surfaces, or where shapes, grooves, or pores are present such as our surfaces (Figure 10).
- Spline filter- The main idea of the spline filter is to provide a smooth and continuous representation of data points by using splines, which are geometric curves that link a series of data points. This filter is an alternative to techniques like the Gaussian filter for mitigating noise and irregularities in data, particularly on surfaces. By introducing suspended points connected to data points through spring-like linkages, the cubic spline filter aims to create a curve that passes through these suspended points,

achieving a balance between preserving the essential features of the data and providing a smoother, more continuous profile (Figure 10).

All parameters were computed and subsequently exported.

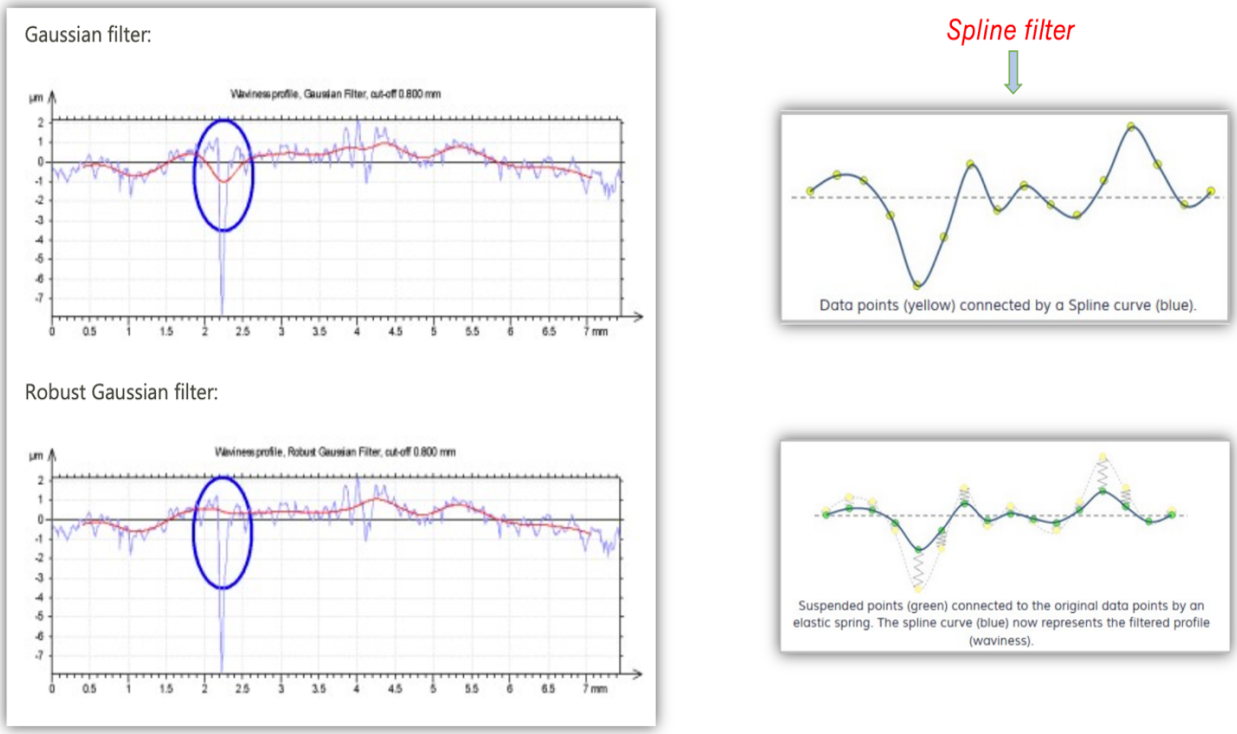

Figure 10:Examples showcasing the visualization of the Gaussian filter, Robust Gaussian filter of order 2, and Spline filter are provided (via www.digitalsurf.com)

Template 3a:

Applying filters to extract roughness, including the Gaussian filter, Robust Gaussian filter of order 2, and Spline filter, with a cut-off value of 0.025 mm and the implementation of end-effect correction.

Template 3b:

Applying filters to extract roughness, including the Gaussian filter, Robust Gaussian filter of order 2, and Spline filter, with a cut-off value of 0.01225 mm and the implementation of end-effect correction.

Template 3c:

Applying filters to extract roughness, including the Gaussian filter, Robust Gaussian filter of order 2, and Spline filter, with a cut-off value of 0.050 mm and the implementation of end-effect correction.

Template 3d:

1. Particle analysis- following the method presented in Borel et al. 2021b, particle analysis is used here to extract the most altered (polished) area of each surface. This allows the later computation of the parameters on the polished area only, therefore on part of the surface which was actually in contact with the worked material (Figure 11).
2. Applying filters to extract roughness, including the Gaussian filter, Robust Gaussian filter of order 2, and Spline filter, with a cut-off value of 0.025 mm and the implementation of end-effect correction.

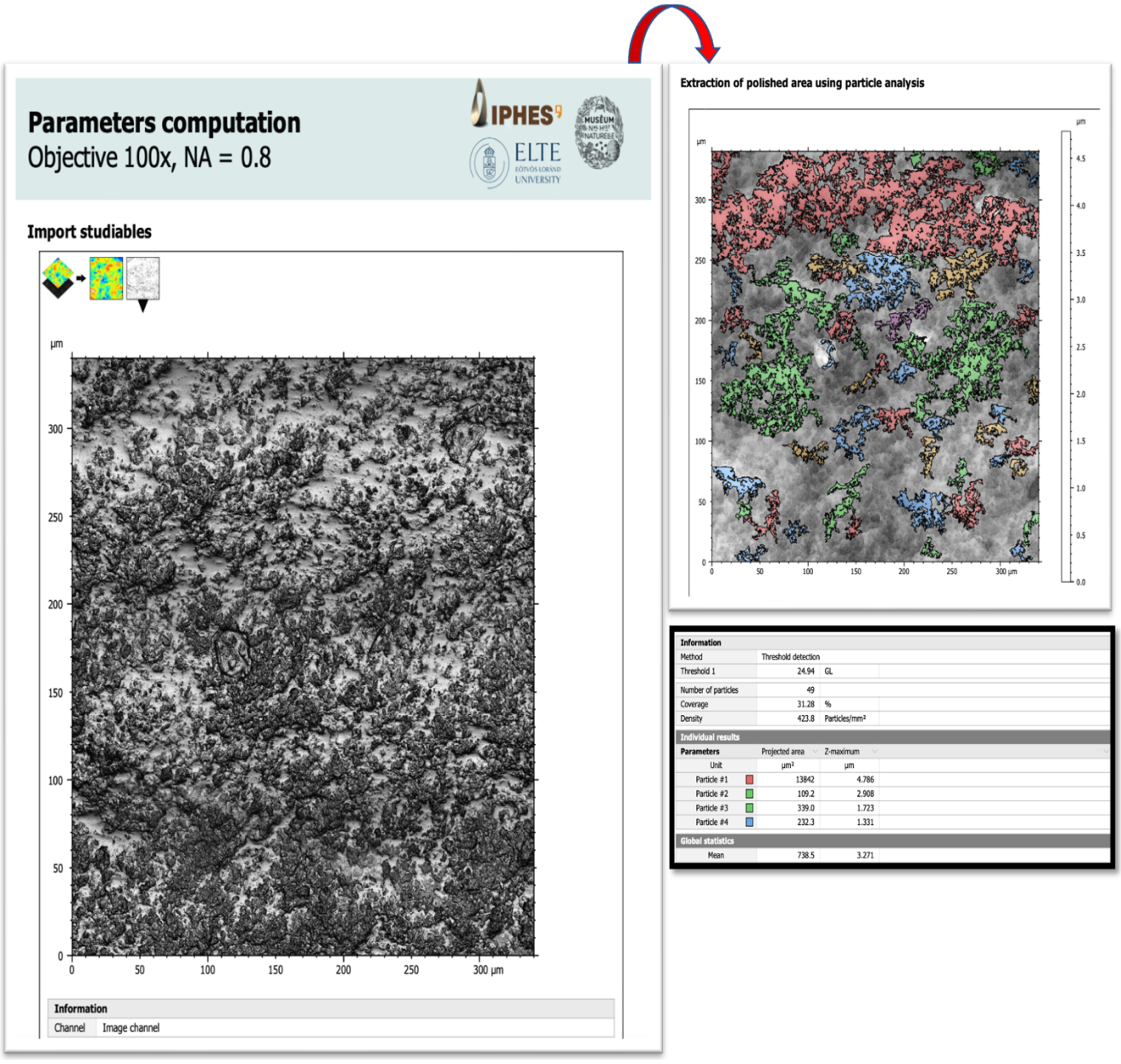

Figure 11: Particle analysis to extract the most altered (polished) area of the surface; Objective 100x/ NA=0.8

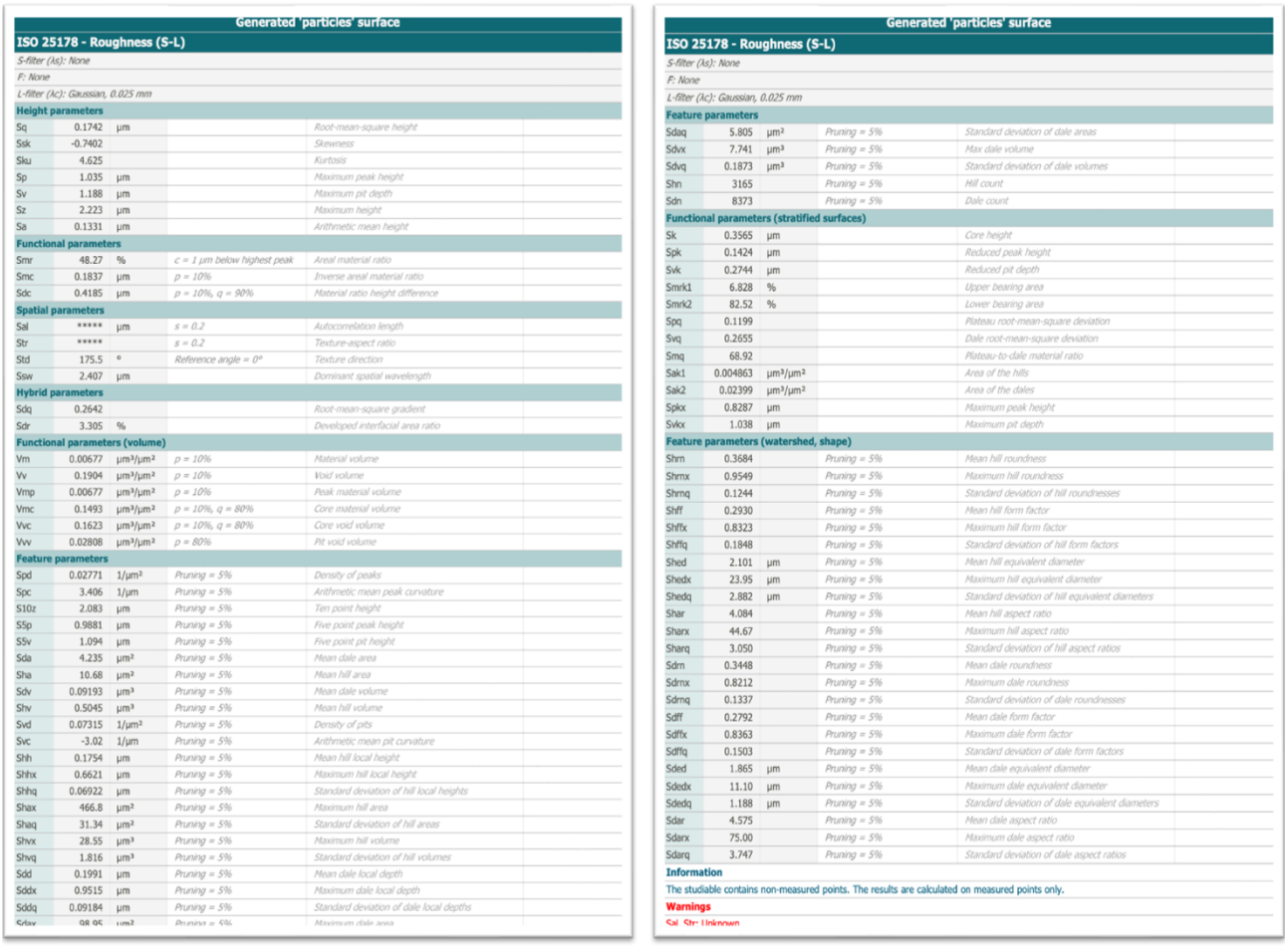

Generated 'particles' surface

ISO 25178 - Roughness (S-L)

S-filter (As): None

F: None

L-filter (Ac): Gaussian, 0.025 mm

Height parameters				
Sq	0.1742	µm		Root-mean-square height
Ssk	-0.7402			Skewness
Sku	4.625			Kurtosis
Sp	1.035	µm		Maximum peak height
Sv	1.188	µm		Maximum pit depth
Sz	2.223	µm		Maximum height
Sa	0.1331	µm		Arithmetic mean height
Functional parameters				
Smr	48.27	%	c = 1 µm below highest peak	Areal material ratio
Smc	0.1837	µm	p = 10%	Inverse areal material ratio
Sdc	0.4185	µm	p = 10%, q = 90%	Material ratio height difference
Spatial parameters				
Sal	*****	µm	s = 0.2	Autocorrelation length
Str	*****		s = 0.2	Texture-aspect ratio
Std	175.5	°	Reference angle = 0°	Texture direction
Ssw	2.407	µm		Dominant spatial wavelength
Hybrid parameters				
Sdq	0.2642			Root-mean-square gradient
Sdr	3.305	%		Developed interfacial area ratio
Functional parameters (volume)				
Vm	0.00677	µm³/µm²	p = 10%	Material volume
Vv	0.1904	µm³/µm²	p = 10%	Void volume
Vmp	0.00677	µm³/µm²	p = 10%	Peak material volume
Vmc	0.1493	µm³/µm²	p = 10%, q = 80%	Core material volume
Vvc	0.1623	µm³/µm²	p = 10%, q = 80%	Core void volume
Vvv	0.02808	µm³/µm²	p = 80%	Pit void volume
Feature parameters				
Spd	0.02771	1/µm²	Pruning = 5%	Density of peaks
Spc	3.406	1/µm	Pruning = 5%	Arithmetic mean peak curvature
S10z	2.083	µm	Pruning = 5%	Ten point height
S5p	0.9881	µm	Pruning = 5%	Five point peak height
S5v	1.094	µm	Pruning = 5%	Five point pit height
Sda	4.235	µm²	Pruning = 5%	Mean dale area
Sha	10.68	µm²	Pruning = 5%	Mean hill area
Sdv	0.09193	µm³	Pruning = 5%	Mean dale volume
Shv	0.5045	µm³	Pruning = 5%	Mean hill volume
Svd	0.07315	1/µm²	Pruning = 5%	Density of pits
Svc	-3.02	1/µm	Pruning = 5%	Arithmetic mean pit curvature
Shh	0.1754	µm	Pruning = 5%	Mean hill local height
Shhx	0.6621	µm	Pruning = 5%	Maximum hill local height
Shhq	0.06922	µm	Pruning = 5%	Standard deviation of hill local heights
Shax	466.8	µm²	Pruning = 5%	Maximum hill area
Shaq	31.34	µm²	Pruning = 5%	Standard deviation of hill areas
Shvx	28.55	µm³	Pruning = 5%	Maximum hill volume
Shvq	1.816	µm³	Pruning = 5%	Standard deviation of hill volumes
Sdd	0.1991	µm	Pruning = 5%	Mean dale local depth
Sddx	0.9515	µm	Pruning = 5%	Maximum dale local depth
Sddq	0.09184	µm	Pruning = 5%	Standard deviation of dale local depths

Generated 'particles' surface

ISO 25178 - Roughness (S-L)

S-filter (As): None

F: None

L-filter (Ac): Gaussian, 0.025 mm

Feature parameters				
Sdaq	5.805	µm²	Pruning = 5%	Standard deviation of dale areas
Sdvx	7.741	µm³	Pruning = 5%	Max dale volume
Sdvq	0.1873	µm³	Pruning = 5%	Standard deviation of dale volumes
Shn	3165		Pruning = 5%	Hill count
Sdn	8373		Pruning = 5%	Dale count
Functional parameters (stratified surfaces)				
Sk	0.3565	µm		Core height
Spk	0.1424	µm		Reduced peak height
Svk	0.2744	µm		Reduced pit depth
Smrk1	6.828	%		Upper bearing area
Smrk2	82.52	%		Lower bearing area
Spq	0.1199			Plateau root-mean-square deviation
Svq	0.2655			Dale root-mean-square deviation
Smq	68.92			Plateau-to-dale material ratio
Sak1	0.004863	µm³/µm²		Area of the hills
Sak2	0.02399	µm³/µm²		Area of the dales
Spkx	0.8287	µm		Maximum peak height
Svkx	1.038	µm		Maximum pit depth
Feature parameters (watershed, shape)				
Shm	0.3684		Pruning = 5%	Mean hill roundness
Shmx	0.9549		Pruning = 5%	Maximum hill roundness
Shmq	0.1244		Pruning = 5%	Standard deviation of hill roundnesses
Shff	0.2930		Pruning = 5%	Mean hill form factor
Shffx	0.8323		Pruning = 5%	Maximum hill form factor
Shffq	0.1848		Pruning = 5%	Standard deviation of hill form factors
Shed	2.101	µm	Pruning = 5%	Mean hill equivalent diameter
Shedx	23.95	µm	Pruning = 5%	Maximum hill equivalent diameter
Shedq	2.882	µm	Pruning = 5%	Standard deviation of hill equivalent diameters
Shar	4.084		Pruning = 5%	Mean hill aspect ratio
Sharx	44.67		Pruning = 5%	Maximum hill aspect ratio
Sharq	3.050		Pruning = 5%	Standard deviation of hill aspect ratios
Sdm	0.3448		Pruning = 5%	Mean dale roundness
Sdmx	0.8212		Pruning = 5%	Maximum dale roundness
Sdmq	0.1337		Pruning = 5%	Standard deviation of dale roundnesses
Sdff	0.2792		Pruning = 5%	Mean dale form factor
Sdffx	0.8363		Pruning = 5%	Maximum dale form factor
Sdffq	0.1503		Pruning = 5%	Standard deviation of dale form factors
Sded	1.865	µm	Pruning = 5%	Mean dale equivalent diameter
Sdedx	11.10	µm	Pruning = 5%	Maximum dale equivalent diameter
Sdedq	1.188	µm	Pruning = 5%	Standard deviation of dale equivalent diameters
Sdar	4.575		Pruning = 5%	Mean dale aspect ratio
Sdarx	75.00		Pruning = 5%	Maximum dale aspect ratio
Sdarq	3.747		Pruning = 5%	Standard deviation of dale aspect ratios

Information

The studiable contains non-measured points. The results are calculated on measured points only.

Warnings

Sal Str Unknown

Figure 12: containing 85 metrological parameters and their corresponding values, after parameters computation; 100x/0.8NA

3.7 Data analysis

After the computation of all parameters using MountainsMap 9 software, summary statistics, scatter plots, box plots, and principal component analysis, (PCA) were generated using open-source software in R v4.1.038 within RStudio 2022.07.2 Build 576. A selection of parameters and variables was made to facilitate the application of the methodology. The total of seven distinct workflows described above were subsequently utilized for further analysis.

The 85 parameters of the ISO 25178 were formerly computed (Figure 12). In order to reduce the number of parameters and identify the most relevant ones we computed Pearson's correlation between each pair of parameters. We tested correlation significance correcting p-values for multiple testing using the Holm method and with an alpha of 0.05. In instances where the p-value fell below the pre-defined significance level ($\alpha = 0.05$), the null hypothesis was rejected in favor of the alternative hypothesis, indicating the presence of statistically significant correlations. By removing one parameter from each pair where significant

correlation was identified and where the value of the correlation was above 0.7, a total of 38 parameters were initially retained (Table 4). After a second round of the same process, we identified 10 more parameters that were redundant and we kept a final set of 28 parameters (Table 5).

Our dataset contained as well 14 categorical variables for subsequent testing: 1. The reference number of the measurements; 2. Tool reference number; 3. Surface reference; 4. Microscope type 5. Objective magnification; 6. Objective numerical aperture (NA); 7. Usage status; 8.Contact material; 9. Motion characteristics; 10. Task specification; 11. Number of stocks; 12. Utilization duration; 13. Applied workflow; 14. Filters;

Applied workflow

Workflow 1: template 1a / template 2a / template 3a
Workflow 2: template 1b / template 2a / template 3a
Workflow 3: template 1a / template 3a
Workflow 4: template 1b / template 3a
Workflow 5: template 1b / template 2a / template 3b
Workflow 6: template 1b / template 2a / template 3c
Workflow 7: template 1b / template 2a / template 3d

First tested parameters	Second tested parameters	Correlation value	P	P.adjusted
Sa_¬µm	Smc_p10Perc_¬µm	0.990798621	0	0
Sa_¬µm	Vm_p10Perc_¬µm¬≥/¬µm¬≤	0.840579484	0	0
Sp_¬µm	Vm_p10Perc_¬µm¬≥/¬µm¬≤	0.704177192	0	0
Smc_p10Perc_¬µm	Vm_p10Perc_¬µm¬≥/¬µm¬≤	0.818113415	0	0
Sp_¬µm	S10z_Pruning5Perc_¬µm	0.88641916	0	0
Sv_¬µm	S10z_Pruning5Perc_¬µm	0.906927497	0	0
Vm_p10Perc_¬µm¬≥/¬µm¬≤	S10z_Pruning5Perc_¬µm	0.740716774	0	0
Sa_¬µm	Sk_¬µm	0.973759037	0	0
Smc_p10Perc_¬µm	Sk_¬µm	0.989068305	0	0
Vm_p10Perc_¬µm¬≥/¬µm¬≤	Sk_¬µm	0.750405484	0	0
Sa_¬µm	Svk_¬µm	0.809084197	0	0
Sv_¬µm	Svk_¬µm	0.725892656	0	0
Smc_p10Perc_¬µm	Svk_¬µm	0.735811085	0	0
Vm_p10Perc_¬µm¬≥/¬µm¬≤	Svk_¬µm	0.79251698	0	0
S10z_Pruning5Perc_¬µm	Svk_¬µm	0.74044078	0	0
Sp_¬µm	Spkx_¬µm	0.992271795	0	0
S10z_Pruning5Perc_¬µm	Spkx_¬µm	0.862706938	0	0
Sv_¬µm	Svkx_¬µm	0.994401095	0	0
S10z_Pruning5Perc_¬µm	Svkx_¬µm	0.884085877	0	0
Sda_Pruning5Perc_¬µm¬≤	Shed_Pruning5Perc_NoUnit	0.889940304	0	0
Shax_Pruning5Perc_¬µm¬≤	Shedx_Pruning5Perc_NoUn	0.953107536	0	0

Table 5: The table lists the 38 parameters initially retained after rejecting the null hypothesis in favor of statistically significant correlations at the α = 0.05 significance level.

Height parameters	Sa	*µm*	*Arithmetical mean height*
	Sku	*µm*	*Curtosis*
	Ssk	*µm*	*Skewness*
	Sp	*µm*	*Max. peak height*
	Sv	*µm*	*Max. pit depth*
Functional Parameters	Smr	C= 1 *µm below heights peak*	*Areal material ratio*
Spatial Parameters	Sal	*µm*	*Autocorrelation length*
	Ssw	*µm*	*Dominant spatial wavelength*
	Std		*Texture direction*
	Str		*Texture-aspect ration*
Hybrid Parameters	Sdq		*Root-mean square gradient*
Feature Parameters	Sda	*µm2*	*Mean dale are*
	Sddx	*µm*	*Max. dale local depth*
	Shax	*µm2*	*Max. hill area*
	Spc	*1/µm2*	*Arithmetic means peak curvature*
	Spd	*1/ µm*	*Density of peaks*
	Svc	*1/ µm*	*Arithmetic mean pit curvature*
Functional Parameters (stratified surface)	$Smrk_1$	%	*Upper bearing area*
	$Smrk_2$	%	*Lower bearing area*
	Smq		*Plateau-to-dale material ration*
Functional Parameters (watershed, shape)	Shar		*Mean hill aspect ratio*
	Sharx	*µm*	*Max. hill aspect ratio*
	Shff		*Mean hill from factor*
	Shffx		*Max. hill from factor*
	Shrn		*Mean hill roundness*
	Shrnx		*Max. hill roundness*
	Shrnq	*µm*	*Standard deviation of hill aspect ratio*
	Sdrnx		*Max. dale aspect ratio*

ISO 25178

Table 6: The table presents the set of final, 28 metrology parameters utilized for subsequent analyses

Chapter IV. Results

4.1 Interpretation of Use-Wear on the Experimental Stone Tools

In the confines of this chapter, we present the accumulated data that emerged as a consequence of the usage of the previously mentioned methods and techniques. Initially, the outcomes stemming from the qualitative analysis of use-wear are addressed (Table 6).

Derived from the outcomes of the microscopic analysis, the discernibility of traces on all experimental stone tools subsequent to their use is evident. Consequently, a differentiation becomes achievable between the surfaces before and after use. However, After use, it is noticeable that the polish did not develop to the same extent on all the flint working edges. In this regard, using four distinct contact materials will be expounded sequentially.

	OLYMPUS LEXT OLS5100	**Sensofar S neox**	**Number of measurement**
Objective -10x/0.30NA	106	108	214
Objective -20x/0.45NA	106	108	214
Objective -100x/0.8NA	106	108	214
		Total measurements: Total number of strokes: Total hour of the experiment on contact material	= 642 = 60,000 = 13:06:30

Table 7: The table encompasses data regarding measurements conducted employing both microscopes.

Reed (*Arundo donax*)

ELTE_IAS_000093 (10000 stocks) and ELTE_IAS_000202 (5000 stocks) stones were employed for the bidirectional sawing of reed *(Arundo donax*), utilizing flakes featuring an edge angle of 80°-90°. As a result, one of the most extensive wear patterns on the surface was generated. This was partly attributed to the highly abrasive nature of the contact material. Notably, our experimental tools exhibited a well-developed polish on both stone surfaces,

encompassing both edges, naturally, a more pronounced polish was evident after 10,000 stocks had been executed (Figure 13).

The polishing process closely followed the trajectory of the edge, actively engaging with the contact material, and coinciding with points of our prior measurements by microscopes. The post-usage polish displayed a smoother and more reflective texture compared to the adjacent untreated surface. This phenomenon is attributed to the abrasive action and smoothing effect of the tool's edge against the fibers of the reed. During the active sawing process, tiny flakes were detached from the edge of ELTE_IAS_000202. This presented a certain issue, given that a measurement had been taken at a compromised point prior to use.

Also, edge rounding was observable on both stone tools, although the progression of this feature differed between the two surfaces. Substantial edge rounding was discernible after 10,000 strocks, contributing to a slight thickening of the working edge on the same stone. Consequently, sawing efficiency was compromised due to this marginal increase in thickness.

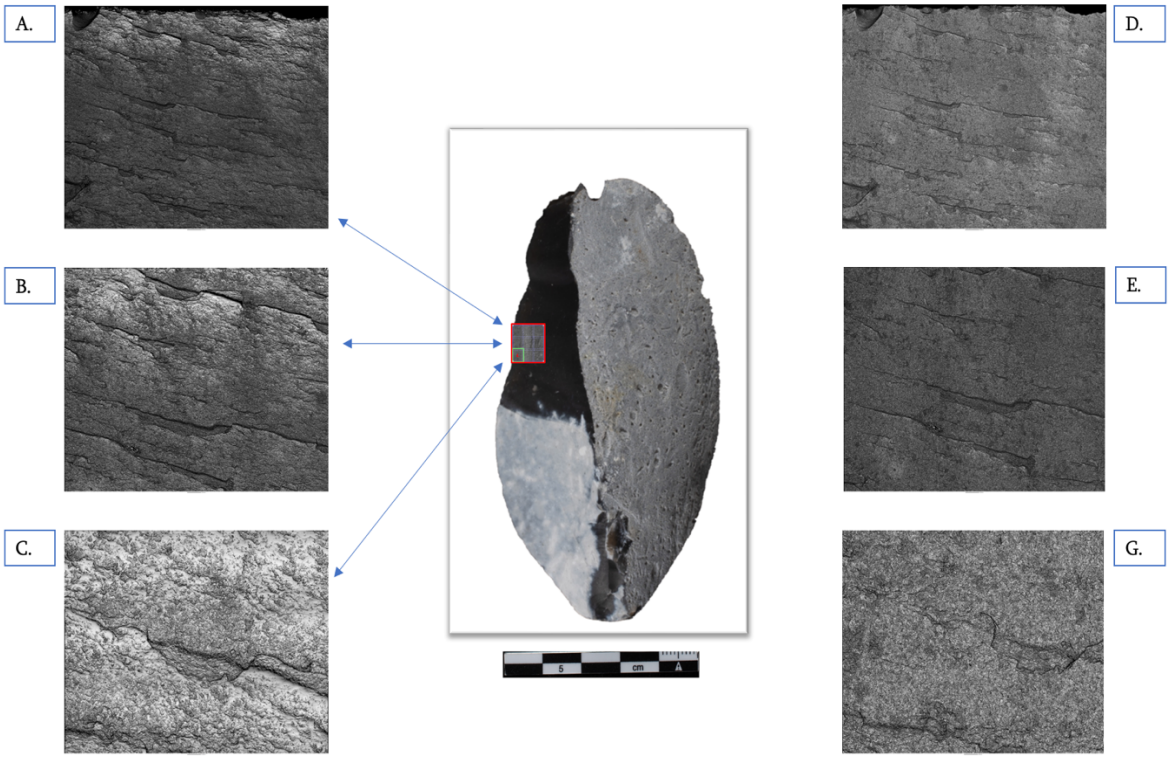

Figure 13: Experimental Analysis of Stone Surface Before and After Reed Contact Material Application (10000 stocks). A. after use, D. Before use,-10x/0.3NA ; B. After use, E. Before use- 20x/0.45NA; C. After use, G. Before use -100x/0.8NA; By Sensofar

Fresh wood (*Quercus ilex*)

ELTE_IAS_000096 (10000 stocks) and ELTE_IAS_000094 (5000 stocks) stones were employed for the bidirectional sawing of Fresh wood (*Quercus ilex*), worked angle of 80°-90°. After the implementation of transversal sawing actions, a notable prevalence of polish and micro-fractures, characterized by step and conchoidal patterns, became apparent, with their distribution varying by the specific movement type applied, also rarely but still striations were identified. The manifestation of edge rounding was primarily confined to proximal proximity to the edge itself and occurred infrequently. The emergence of highly lustrous polishes, characterized by impeccably smooth surfaces exhibiting a domed microtopography, exhibited a gradual process of expansion and eventual interconnection.

Disparities were observed in the development of polishing and usage indicators across the stones's surface between the dorsal and ventral aspects (Figure 14). A measurement conducted on a segment of the stone, situated proximate to the distal edge, revealed comparatively less pronounced polishing on the ventral surface. This observation can be attributed to the inherent topographical characteristics of the stone. Conversely, the dorsal aspect exhibited a consistent and uninterrupted presence of polished surfaces along all functional areas.

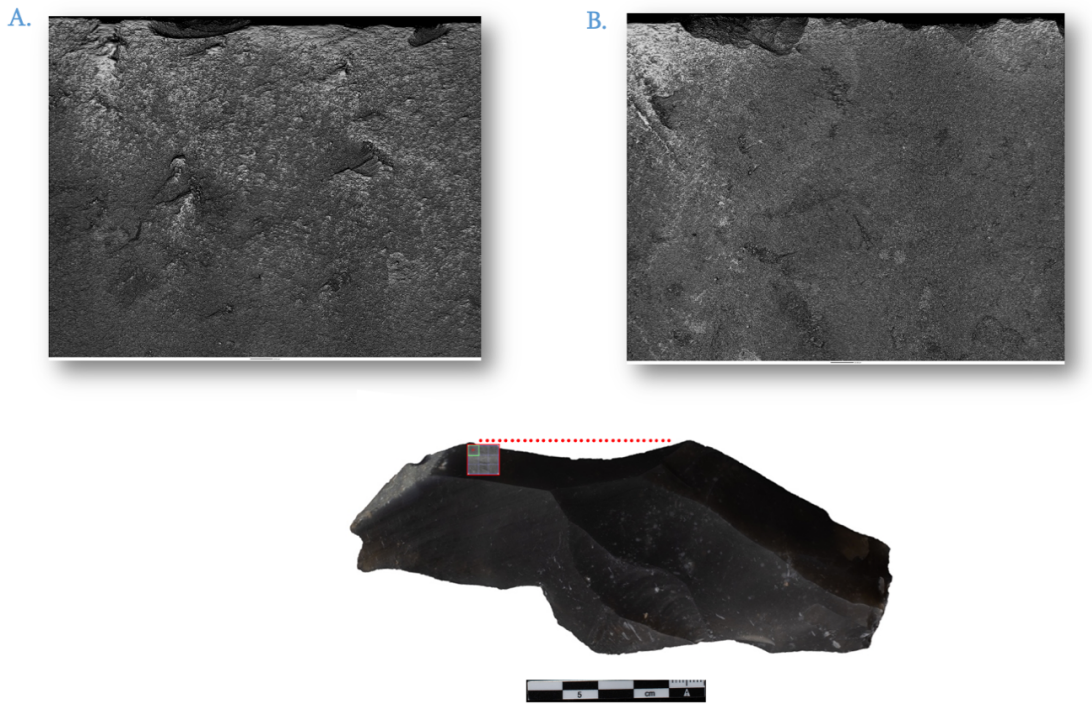

Figure 14: This figure presents the A. dorsal and B. ventral sides of the stone's surface at 20x magnification and 0.45 numerical aperture, revealing differences in polishing and usage indicators. By Sensofar

Soaked antler (*Cervus elaphus*)

The stones, designated by their catalog numbers as ELTE_IAS_000204 (10000 stocks) and ELTE_IAS_000203 (5000 stocks) , were utilized to undertake bidirectional sawing on soaked antler (*Cervus elaphus*). This sawing procedure was executed while maintaining a worked angle ranging between 80° and 90°. Upon meticulous examination of the surfaces of both experimental lithic tools, it was discerned that, up to the point of 5,000 sawing repetitions, the presence of polish remained infrequent and primarily appeared on irregular surface areas. However, beyond the threshold of 10,000 sawing repetitions, a more pronounced development of polish was observed. The process of sawing, as applied to the soaked antler material, yielded a diverse array of matte-finished polish remnants, which extended continuously over a substantial portion of the contact areas on the stone surfaces. Particularly noteworthy was the heightened luminosity and conspicuousness displayed by the working edge on the ventral side, when contrasted with the dorsal side of the same experimental lithic tool. Notably absent within the polished region were striations, which were conspicuously lacking on both sides.

Throughout the course of working the antler material, notable instances of step fractures and conchoidal micro-fractures became evident (Figure 15). This prominent fracturing phenomenon hindered the progression of edge rounding. The distribution of polish, furthermore, remained confined to a highly delimited area adjacent to the active edge.

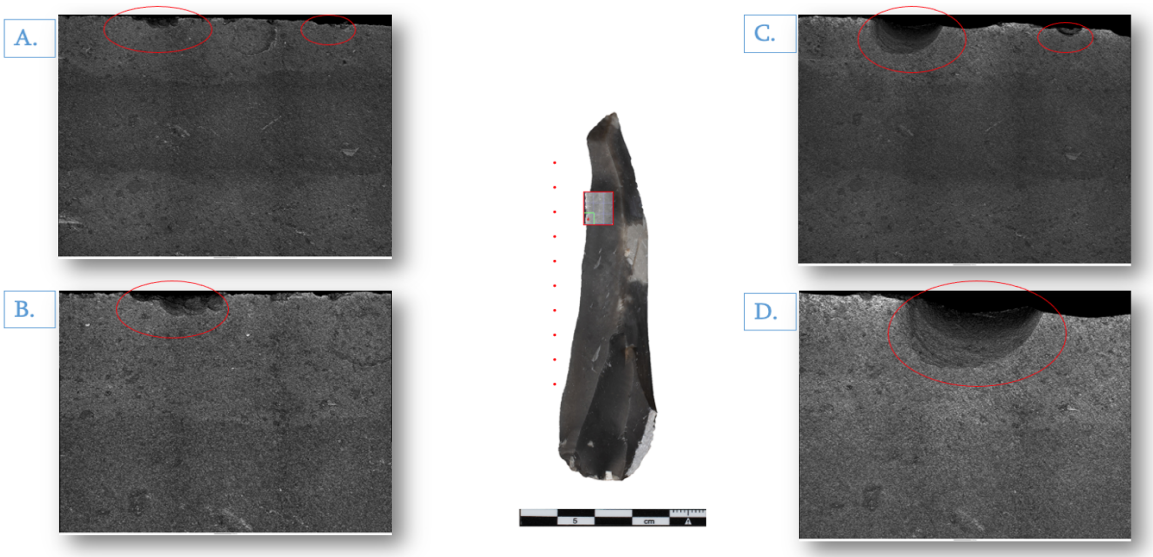

Figure 15: ELTE_IAS_000204- A. Before using; C. After used - 10x/0.3NA; B. Before used; D. After used - 20x/0.45NA; (Dorsal). Throughout the course of working on the antler material, notable instances of micro-fractures became visible. By Sensofar

Hide (*Cervus elaphus*)

The stones, identified through their respective catalog designations as ELTE_IAS_000200 (10000 stocks) and ELTE_IAS_000201 (5000 stocks), were engaged in the experimental work of unidirectional scraping on hides (*Cervus elaphus*). In this instance, the scraping protocol was enacted at a consistent worked angle ranging between 30° and 40°. This experimental phase represented a unique deviation from the established norm, as it involved the application of a softer contact material and a transition from the conventional sawing motion to a scraping technique. The primary aim of employing the unidirectional scraping approach was to meticulously cleanse the internal surfaces of the acquired hides, thereby eradicating residual remnants of flesh and subcutaneous layers.

In the context of microscopic investigations conducted on the stone subject to 5,000 stockes of scraping movement, an insufficiency in the manifestation of micro-fractures associated with longitudinal activity was discerned. Remarkably, the presence of striations was notably absent in this context. The absence of striations was attributed to the absence of abrasive additives during the hide working experiments. The resultant polishes from working hide exhibited parallels with the greasy polish characteristic of meat processing (Figure 16).

Upon advancing to the stone surface subjected to 10,000 scraping cycles, a conspicuous bright polish was observed in close proximity to the tool's edge. This particular polish presented a disorderedly structured, smooth, and reflective surface. However, it is noteworthy that the development of polish was not uniformly distributed across the entirety of the contacting edge. Notably, only a few instances showcased minor degrees of rounding subsequent to longitudinal activity. In some cases, the longitudinal activity resulted in the emergence of micro-fractures on the stone's surface.

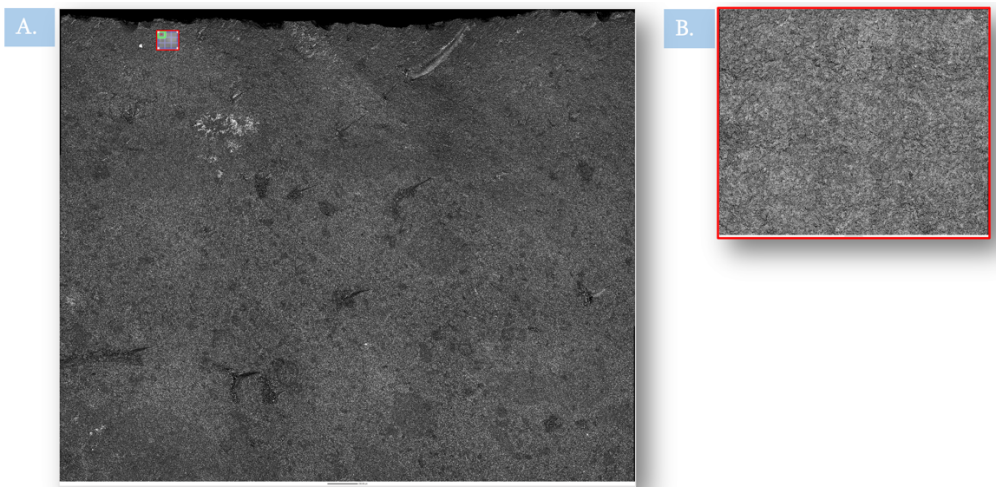

Figure 16: ELTE_IAS_000201-A. Measurement with 20x/0.45NA; B. Measurement with 100x/0.8NA; After using on hide.

4.2 Comparing Microscopy Techniques: Examining the Comparative Outcome

In the present study, an extensive comparative analysis was conducted to assess the effectiveness of two microscopy techniques, namely laser scanning confocal microscopy (Olympus LEXT OLS5100) and Microdisplay scanning confocal microscopy (Sensofar S neox), in the context of use wear research on stone tools. The objective of this investigation was to ascertain whether the measurements acquired from both microscopy instruments yielded congruent outcomes.

Aspect	OLYMPUS LEXT OLS5100 	Sensofar S neox 
Light Source	*Laser : violet (405 nm).*	*LEDs: red (630 nm), green (530 nm), blue (460 nm)*
Spectral Range	*Narrow*	*Broader*
Resolution	*Higher due to narrow spectrum and intensity*	*Advanced, but not as high as laser*
Max. magnification	*100x*	*150x*
Imaging Speed	*Slower due to point-by-point scanning*	*Faster with parallel illumination*
Best Lateral Resolution	*Up to 0.12 µm*	*Sub-nanometer (0.09 µm)*
Maximum Axial Resolution	*0.001 µm*	*-*
Sample Movement Sensitivity	*Sensitive to vibrations*	*Sensitive to vibrations*
Field of view	*16 µm–5,120 µm*	*(single shot) > 6.7 × 5.6 mm*
Display resolution	*0.5 nm*	*0.001 nm*
XY sample size	*up to 210 mm*	*up to 700 x 600 mm*
Measurement array	*4096 × 4096 pixels*	*1232 x 1028 pixels*
Dynamic range	*16 bits*	*64-bit*

Table 8: This table summarizes and compares various technical aspects and specifications of the OLYMPUS LEXT OLS5100 and Sensofar S neox microscopy systems, providing valuable insights into their respective capabilities and differences.

The microscopy techniques employed in this study were based on their potential to provide high-resolution images and 3D imaging capabilities. These techniques were applied to a set of stone tools with well-documented use wear patterns, allowing for a systematic evaluation of their respective capabilities.

The comparative analysis revealed notable similarities and differences between the two microscopy techniques. Laser scanning confocal microscopy using the Olympus LEXT OLS5100 consistently delivered images with exceptional clarity and depth. The 3D imaging capabilities of this technique facilitated the precise visualization of intricate use wear features, thereby enhancing the overall interpretability of the wear patterns. An intensity image was employed to distinctly define the boundaries of traces from polishing (Figure 17). This was primarily attributed to the laser's ability to measure all points on the surface, resulting in reduced occurrence of shadows and glare in the images. Additionally, the use of high resolution (100x) further improved the perceptibility of surface topography. Also important to say, the objectives had the same numerical aperture (NA=0.8), but their field of view, was not exactly the same (Table 7), (Figure 17).

Microdisplay scanning confocal microscopy utilizing the Sensofar S neox also furnished high-resolution and 3D imagings. However, the images acquired exhibited greater brightness, clarity, and detail when contrasted with those generated by laser scanning confocal microscopy. Unlike the Olympus instrument, the Sensofar device was optimized to record and encompass the entirety of the measuring surface. Consequently, the resultant images presented increased brightness, clarity, and stability in terms of both shadows and highlights. This approach heightened the sharpness of the composite image while a little concurrently diminishing the prominence of polishing marks and use traces.

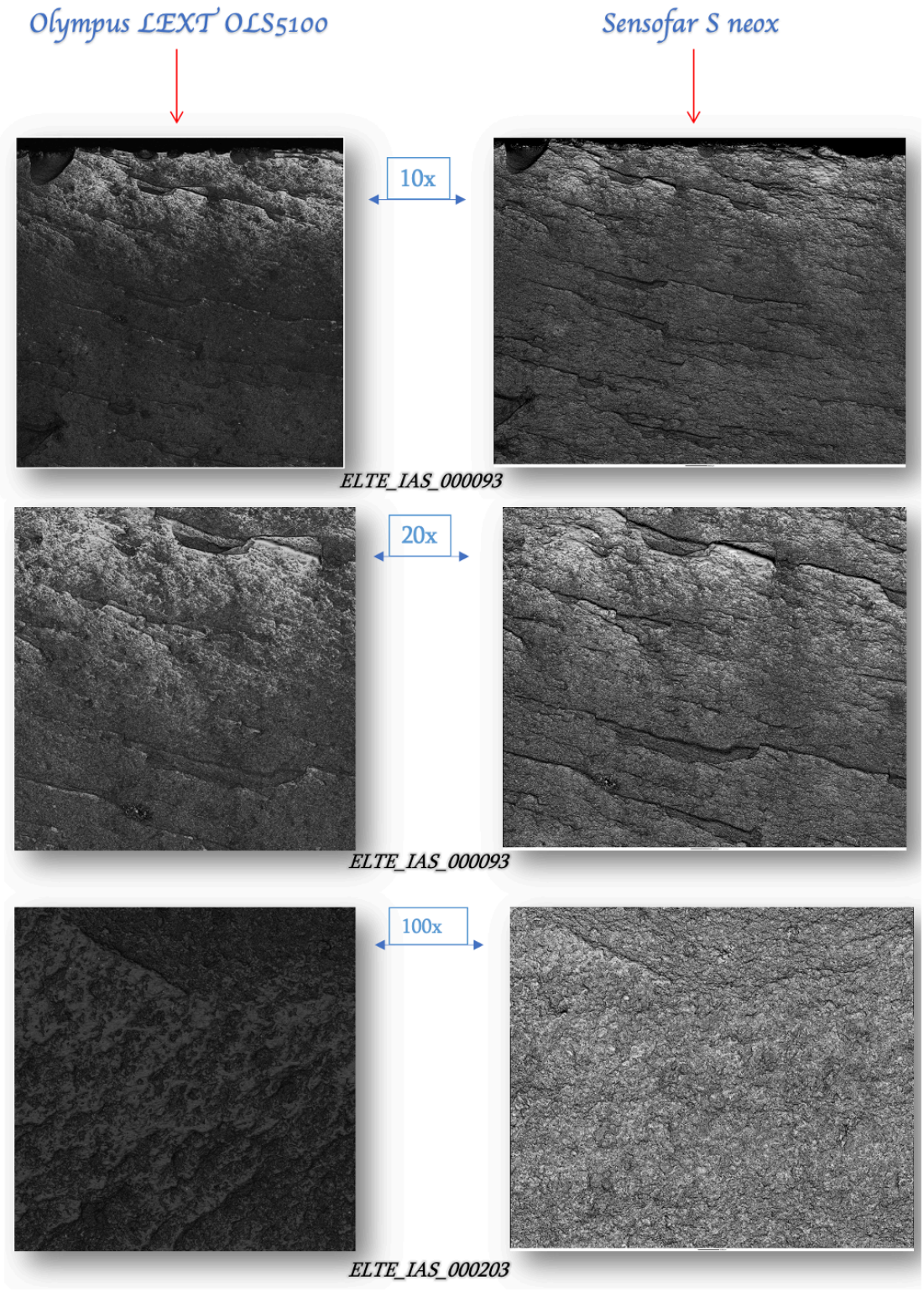

Figure 17: Figure presents measurements, taken at different magnifications 10x/0.30NA; 20x/0.45NA; , and 100x/0.8NA using both microscopes.

4.3 Quantitative Comparative Analysis of Applied Workflows 1 and Workflows 2: Results

In our study, we initially adopted the methodology outlined by Arman et al. (2016). However, as we progressed with our work, we encountered a visual inconsistency during studiables comparison that prompted us to adjust Template 1a (Figure 6; Figure 7). Our attention was directed toward influencing the impact of these modifications on the statistical outcomes and overall results in order to compare measurements from two microscopes. More specifically, we endeavored to comprehend the discrepancies in results between two closely related workflows: Workflow 1, involving surface leveling and after all subsequent steps that were discussed in the methodology part, and Workflow 2, where area extraction preceded before leveling. These workflows were devised to investigate the impact of minor adjustments in our methodology.

The findings revealed that the outcomes between the microscopes may have influenced the choice of workflows and applied filters. Particularly noteworthy was the parameter commonly used for height measurement (Sa), which exhibited a significant correlation between the microscopes when a robust Gaussian filter was applied within Workflow 2: template 1b / template 2a / template 3a (see Figure 18). The process initially involved area extraction (Template 1b), followed by resampling data from both microscopes to achieve a spatial sampling of 0.130 µm (Template 2a), and subsequently, the application of a cut-off value of 0.025 mm (Template 3a).

However, it is essential to note that when the same workflows were applied with a different filter, in this case, Spline, the outcomes exhibited slight variations. In this case, the correlation between the microscopes remained nearly identical medians, and the lower whisker without overlapping was observed within Workflow 1: template 1a / template 2a / template 3a (Figure 19).

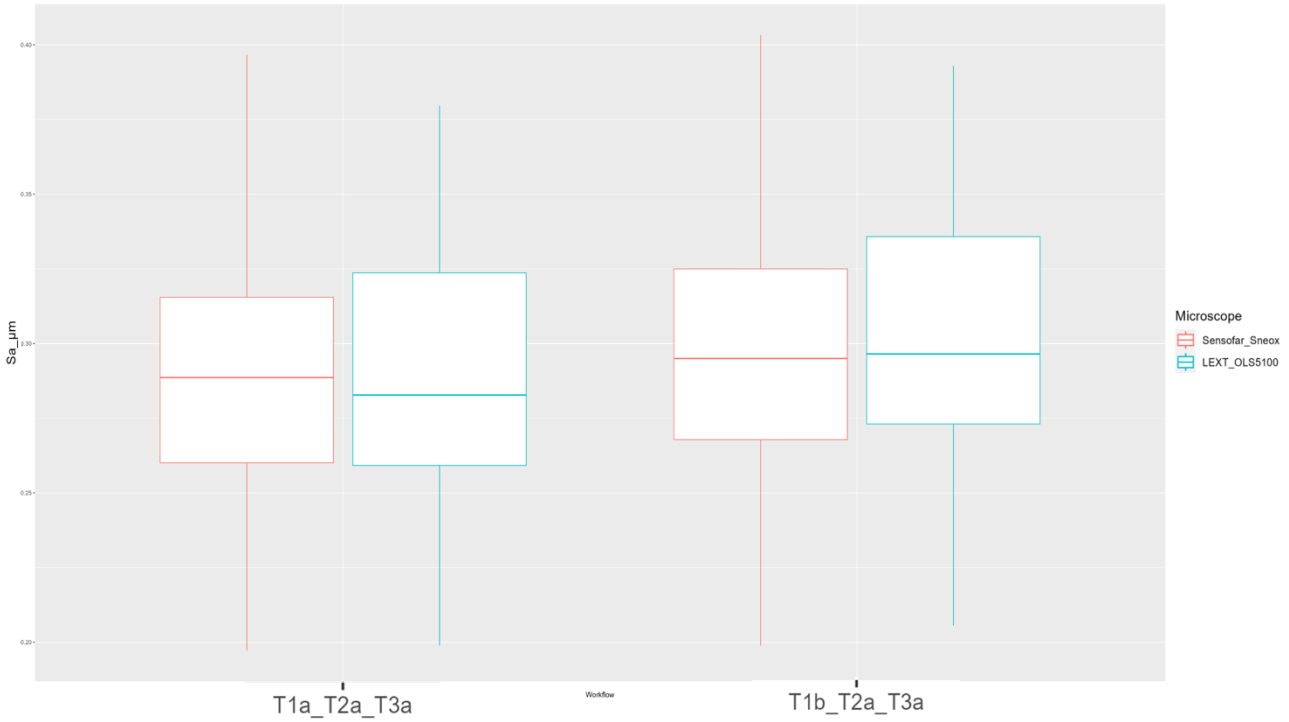

Figure 18: Box-plot displaying Sa values spread and mean from measurements using two microscopes, applying Workflow 1 and Workflow 2, both used for the Robust Gaussian filter

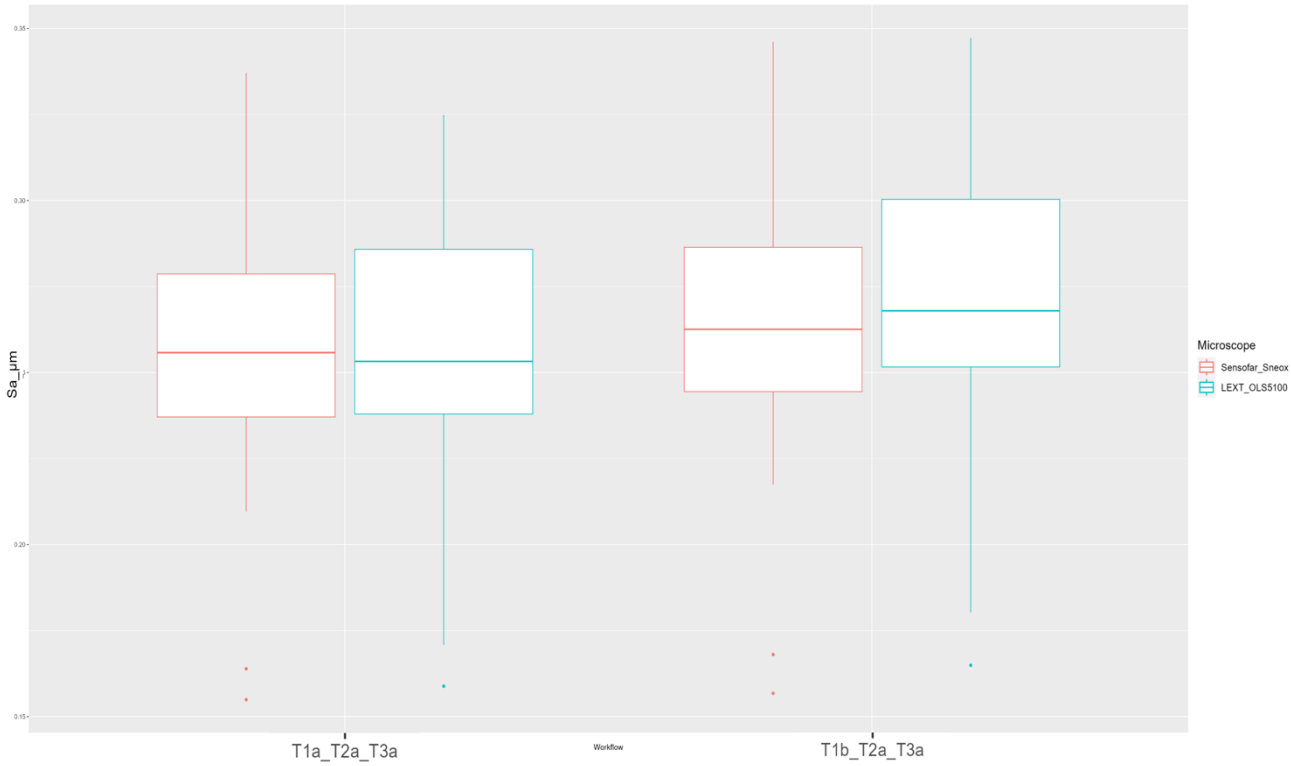

Figure 19: Box-plot displaying Sa values spread and mean from measurements using two microscopes, applying Workflow 1 and Workflow 2, both after Spline filtering

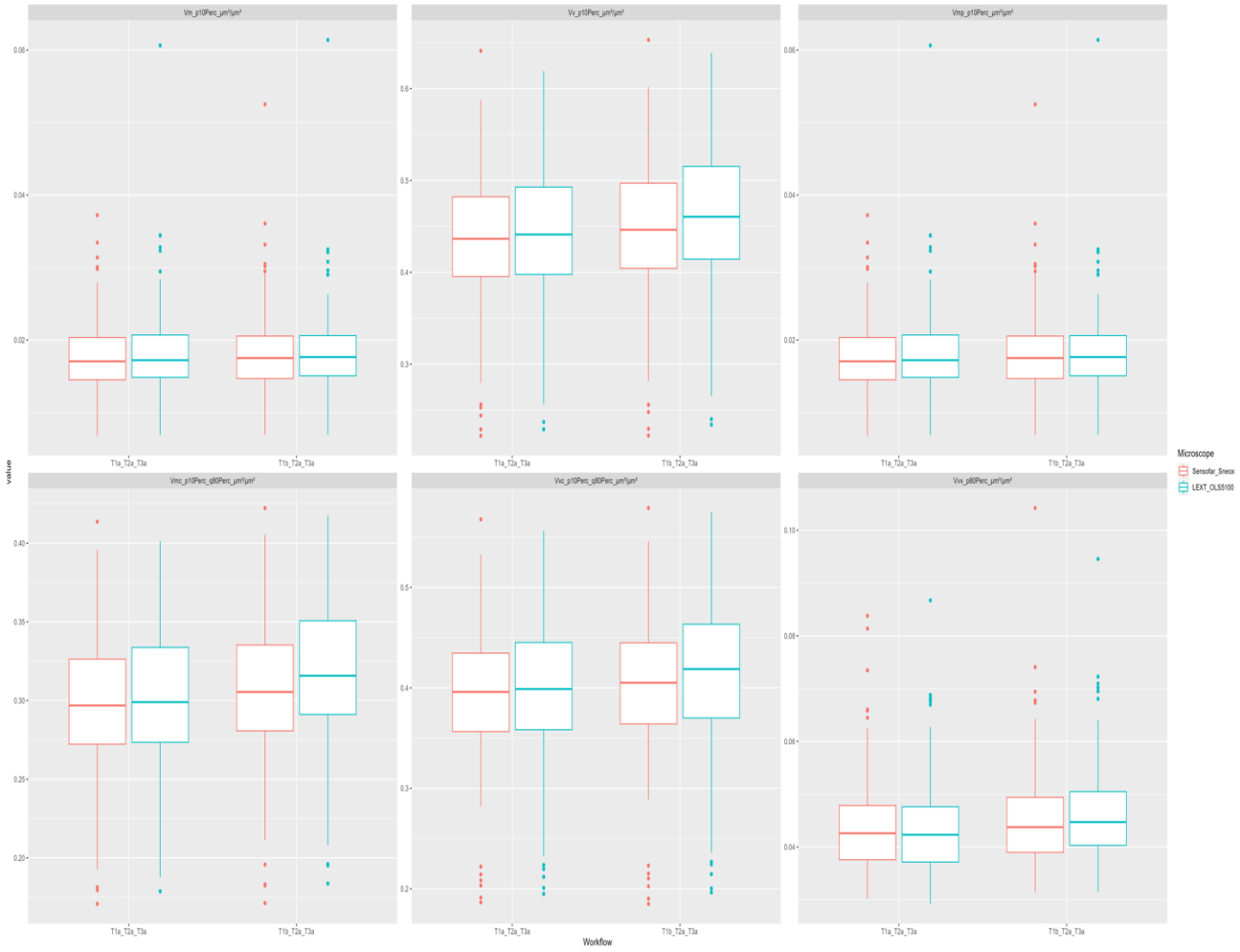

Figure 20: The box plot depicts the spread and mean values of the functional metrology parameters, along with a comparison of two workflows using distinct color representations. The red color represents the results obtained with Sensofar's neox, while the turquoise color corresponds to the data from LEXT.

To determine the relative effectiveness of the two workflows, they were applied to functional volume parameters (Figure 20). The results were interesting, as, in this instance, for some cases, the observed significant difference was less pronounced. Notably, both microscopes exhibited a median that was similar for Vm- material volume (p- 10%) and Vmp- peak material volume in both Workflow 1 and Workflow 2.

The disparities and similarities between Workflow 1 and Workflow 2 evolve with affected by the parameters. However, because of the most parameters and also the visual similarity observed in Template- 1b (through topographic images), our decision to use Template1b for further analysis was reinforced.

4.4 Filter Testing: Refining Surface Data Analysis and Roughness Extraction

To assess the efficacy of varying cut-off values, three scales were chosen. The first scale, represented by 0.01225 mm, employed a reduced cut-off value, allowing for greater inclusion of waviness in the measurements, potentially resulting in a reduction of roughness values as depicted in Workflow 5 (Figure 21). The second scale, at a middle value of 0.025 mm, struck a balance between filtering out waviness and retaining roughness in the surface profile as shown in Workflow 2 (Figure 21). Finally, the third scale adopted a higher cut-off value of 0.050 mm, signifying an increased cut-off value that filters out a greater portion of low-frequency waviness, thereby isolating high-frequency roughness components as presented in Workflow 6 (Figure 21). To assess the performance of the two microscopes, we applied each of these.

These testing cut-off values held an important role in our research, as they determined the level of detail and spatial frequencies considered when calculating different parameters. Furthermore, this analysis provided valuable insights into how each microscope performed in capturing various levels of detail in surface texture under different filtering and cut-off conditions.

Upon close examination, we found that the 0.025 mm cut-off scale, employed in Template 3a, offered a balanced and effective approach for evaluating surface roughness, neither excessively coarse nor overly fine. This specific cut-off value provided valuable insights into surface roughness characteristics and served as the preferred choice for our subsequent analyses and assessments of the microscopes' performance.

After experimenting with all cut-off values, we proceeded to apply different workflows with various filters, encompassing both soft filter (SF) Gaussian and Robust Gaussian and hard filters which for we used Spline (HF).

As previously mentioned, identical points were measured from the surfaces by both microscopes for the purpose of assessing the congruence between the acquired data and the measurements obtained from the microscopes. To determine how well the obtained result coincided with the surface measured by the microscopes, we compared both measurements with each other, one by one. For each point that was taken with both microscopes on 100x/0.8NA magnification, a single common identification number was given.

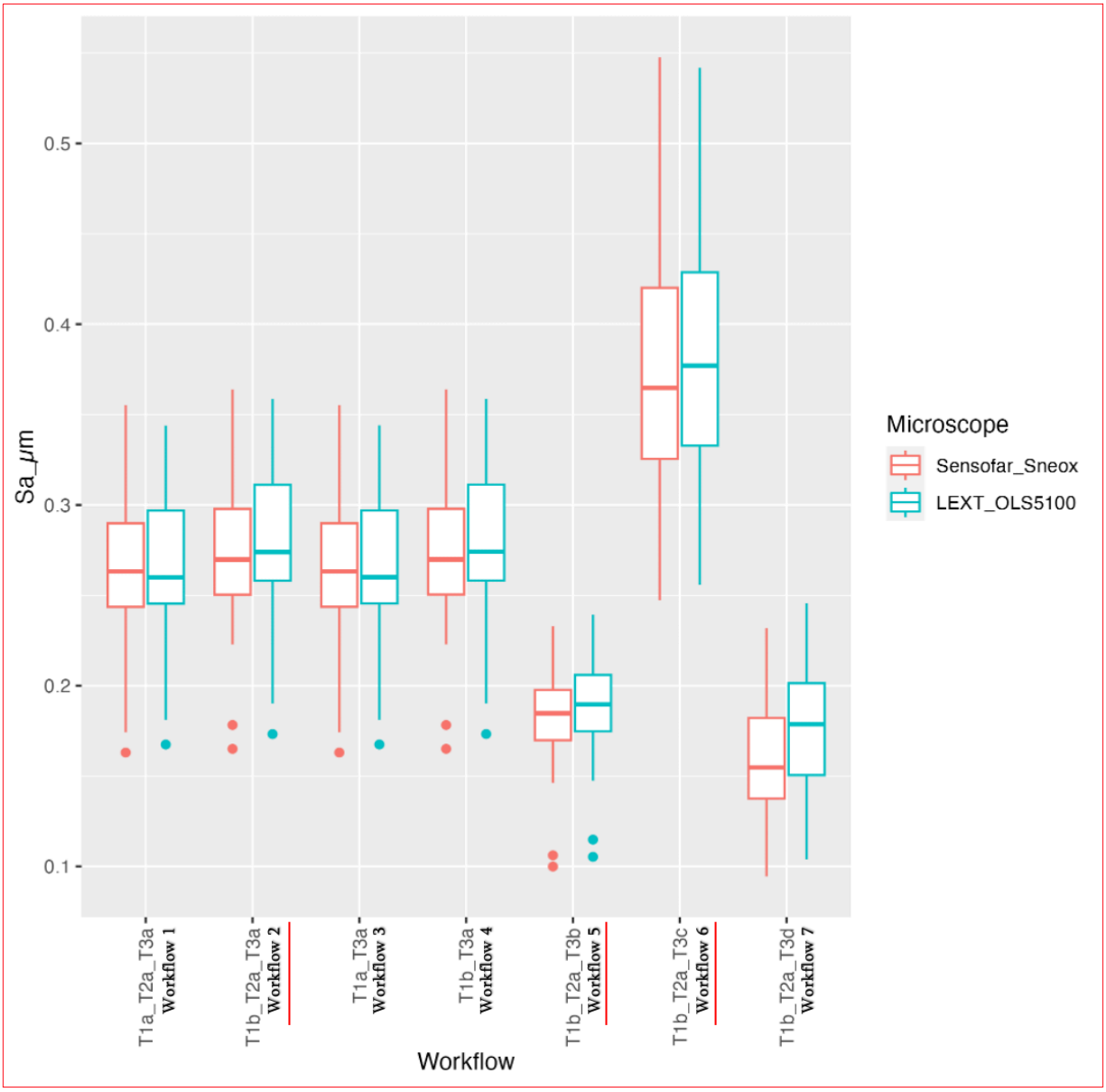

Figure 21: the box plot illustrates how different cut-off values (0.025 mm, 0.01225 mm, and 0.050 mm) and workflows affected the distribution of Sa values for both microscope, providing insights into its performance under various filtering conditions.

For instance, the measured point labeled as ELTE_IAS_000093, which was initially measured using a Sensofar S neox microscope at 100X magnification with a numerical aperture of 0.8 (denoted as '0243_ELTE_IAS_000093_Sensofar_Sneox_100X_AU_ DORSAL) , and the exact same point and information were measured using an Olympus microscope (hereafter referred to as *'1012_ELTE_IAS_000093_LEXT5100_100x_AU _DORSAL*'), shared the common identifier '93a.' (Annex Figures). This approach facilitated visual representation and streamlined the application of data processing workflows employing specific color filters, as illustrated (Figure 22). In this representation, the turquoise color corresponds to measurements obtained from the Olympus microscope, while the red color

represents data acquired using the Sensofar S neox microscope. These data were applied to the Sa_um parameter.

The value of the computed measurement of Sa is extremely similar in most of the measurements, implying that the measurements obtained from the sampled surface points using both microscopes were largely consistent in the majority of cases. However, our comparative analysis revealed an outlier within one of the graphs, specifically in graph 200e (Figure 22). To discern the underlying cause of this disparity, we revisited the visual representation of the sampled surface. Our observations indicated that the divergence stemmed from differences in the tilt angle of the surface during measurement. This finding reinforces the argument that erroneous information obtained from either microscope during surface measurements can be identified.

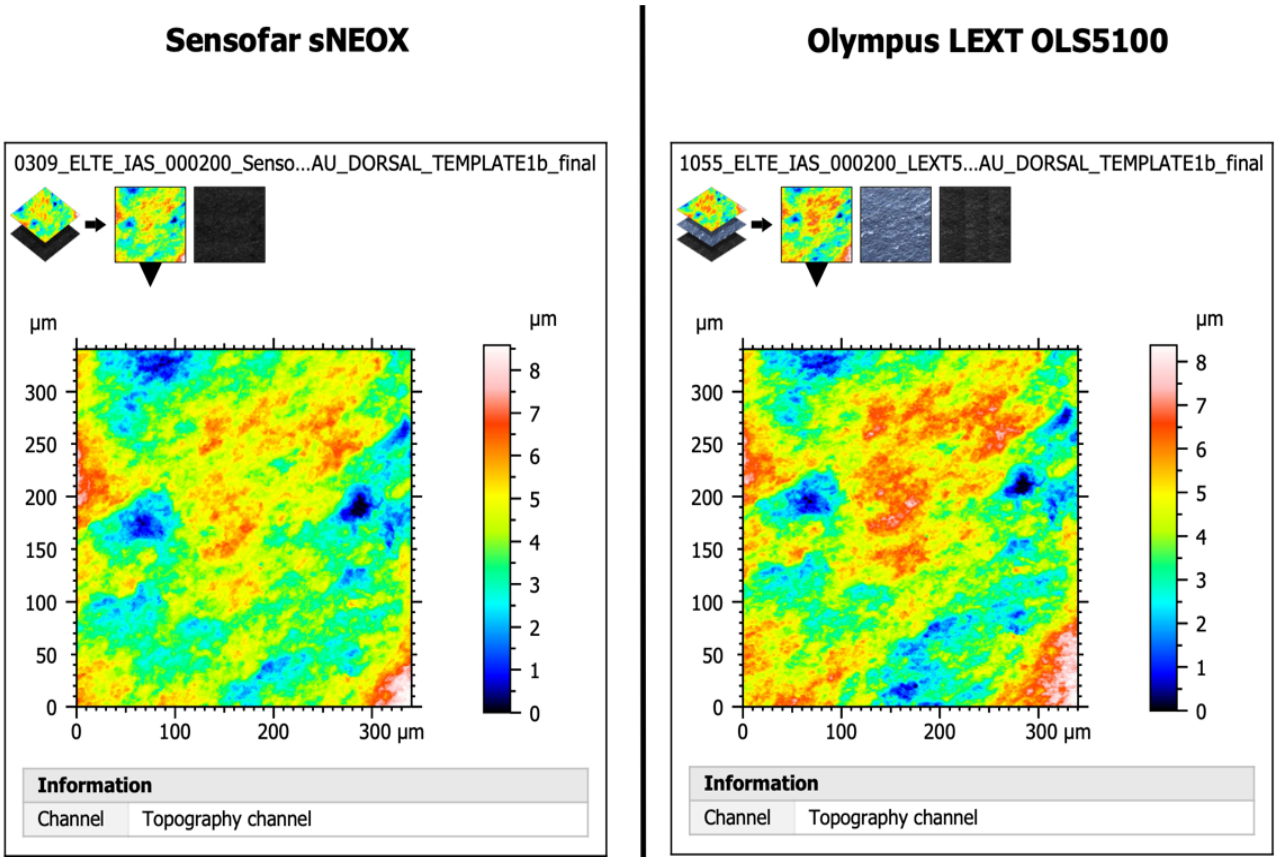

Figure 22: A single point was captured in photographs using two different microscopes, revealing disparities between the images, because of rotation; 100x/08NA77 (common identifier 200e)

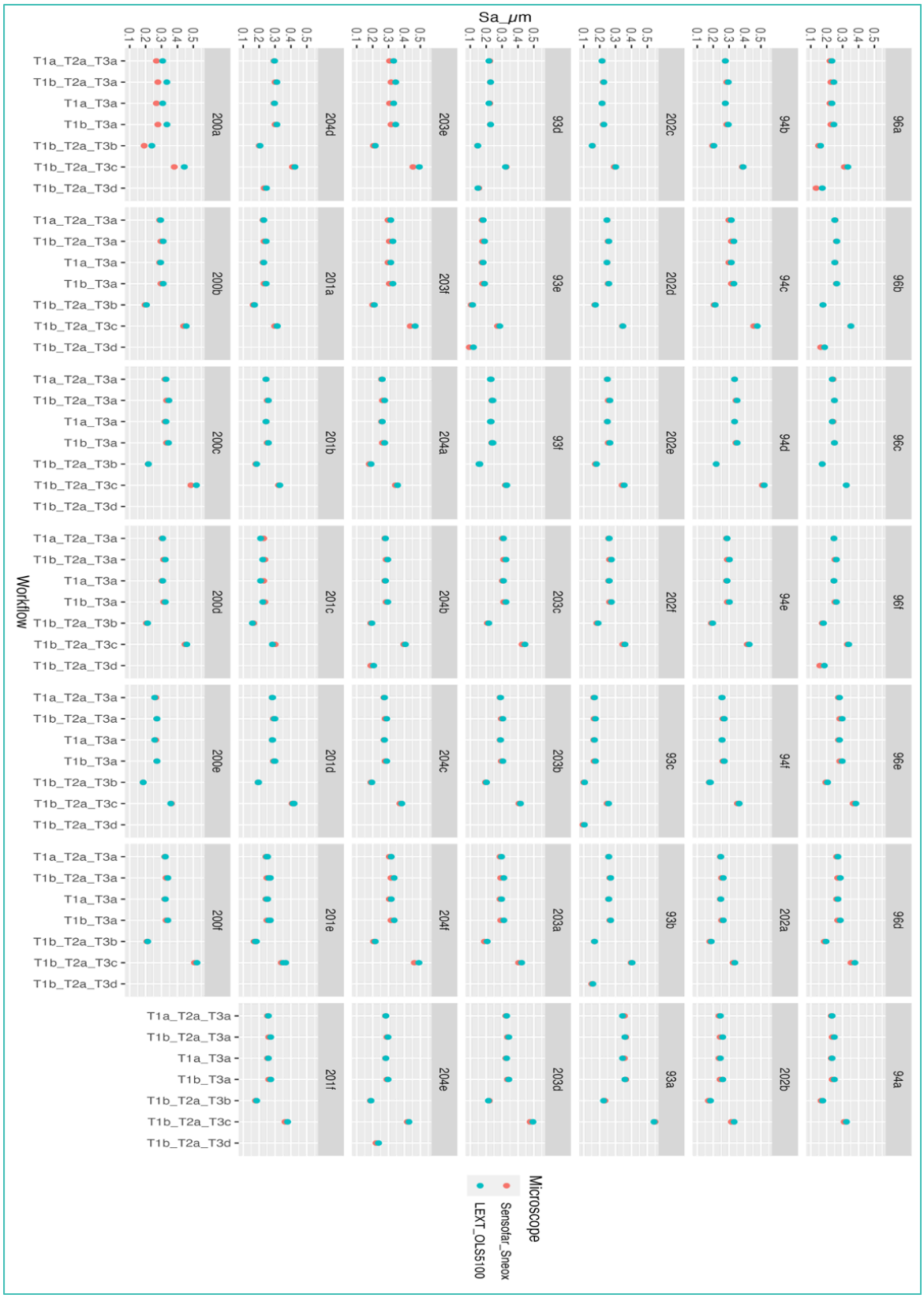

Figure 23: Mean Sa_um from measurements taken by both microscopes, which assigned unique identifiers to corresponding surface points. For example, "0243_ELTE_IAS_000093_Sensofar_Sneox_100X_AU_DORSAL" measured by Sensofar and "1012_ELTE_IAS_000093_LEXT5100_100x_AU_DORSAL" measured by Olympus shared the identifier '93a.'; 100x/0.8NA

4.5 Resampling, and Comparison of the Microscopes

Comparing data from two microscopes with and without resampling reveals differences due to inherent spatial sampling variations between the microscopes. Because comparing microscopes possess distinct specifications and imaging sensors, resulting in differences in spatial sampling—the distance between data points in x and y directions within an image.

Without resampling, data from Sensofar S neox and Olympus LEXT5100 the application of multivariate data analysis reveals the presence of two distinct and separate groups, leading to discrepancies in the comparison (Figure 24.A). But same dataset with the resampling procedure is addressing these issues. To address these issues, the scans were resampled in both the x and y directions to achieve a spatial sampling of 0.130 μm (2616 points). After resampling, it is ensured that both sets of data share the same grid, thereby making them more comparable (Figure 24.B).

The primary aim of comparing the two microscopes in our research involved an analysis of their performance in measuring surface texture parameters.

Most of the computed parameters showed comparative similarities with both of the systems.

This suggested that for these parameters, the microscopes produced consistent and comparable measurements. However, it was important to choose the right workflow, which needed to be adapted to the research topic and the information we wanted to analyze. After all the steps were completed, the measurements obtained from both microscopes reduced the differences and increased the accuracy of the interpretation.

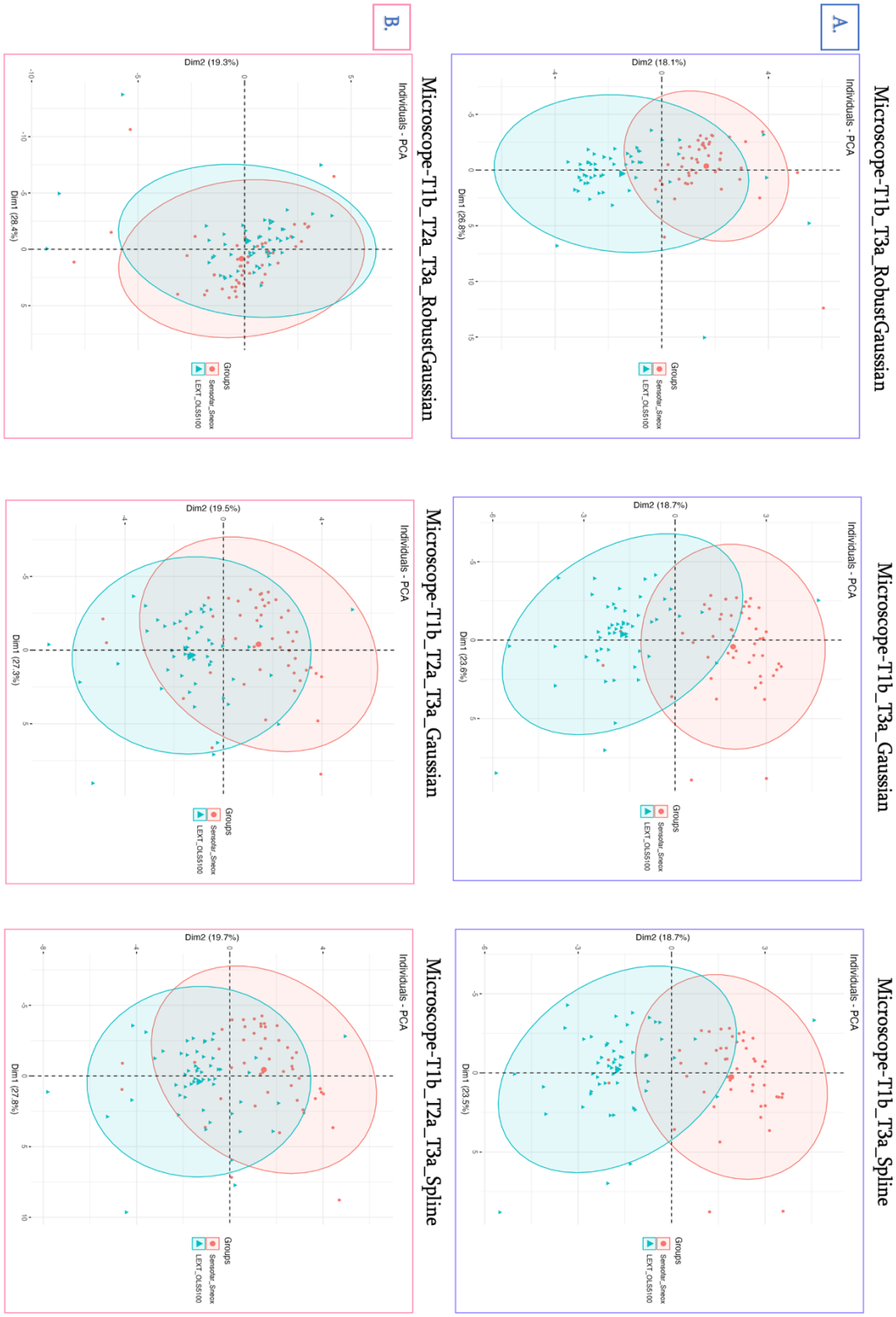

Figure 24: PCA represents the data visualization by applying three filters, using two different workflows: A. Workflow 4: applied template 1b and template 3a without resampling; B. Workflow 2: Applied template 1b, template 2a, and template 3a (cut-off 0.025 mm) with resampling

4.6 Quantitative Comparison of Microscopes on Contact Material

The primary objectives of this research were to assess the comparability of surface measurements within both microscopes and investigate the influence of workflow variations on the results. To achieve this, Principal Component Analysis (PCA) was employed to visualize the relationships among the preselected 28 metrological parameters (Table 5), considering different contact materials and microscopes under one of the tested was Workflow 2, encompassing template- 1b / template 2a / template 3a.

In the PCA plots, green was used to represent the experimental stone surface applied on antlers, blue denoted hide, red represented fresh wood, and the most prominent color, green, corresponded to reeds (Figure 25). These color codes were chosen for clarity and ease of interpretation. The evaluation of the acquired data from the six graphs used to analyze surface texture revealed significant similarities within all three filters and microscopes (Figure 24). But contact material is hard to differentiate. The results indicated that the four distinct groups of contact materials showed some overlap.

To better evaluate the possibility to discriminate contact materials with both microscopes we focused on surfaces where micropolishes were clearly identified and we applied the method of surface extraction proposed by Borel et al. (2021). This corresponds to Workflow 7- template 1b / template 2a / template 3d (Figure 26), which means Tb1, we applied for resampling (0.130 μm), and next, we used T3d, on which particle analysis is used here to extract the most altered (polished) area from each measured surface. However, it was clearly visible that the results obtained on hide did not provide a clear depiction. This was attributed to inaccuracies in the measurements within the active contact area (the most developed polished). Consequently, the decision was made to exclude this dataset and focus solely on three contact materials.

In this particular case, the dataset applied the Robust Gaussian Filter, when tested with measurements obtained from both microscopes, yielded notably almost accurate results. This clarity allowed for the distinct visibility of all three contact materials, each group of contact material is clearly identified based on the measurements by both microscopes.

To provide greater clarity regarding the differences that could be observed when each parameter is applied, Sa_um parameters were utilized, and the same information was employed for testing (Figure 27).

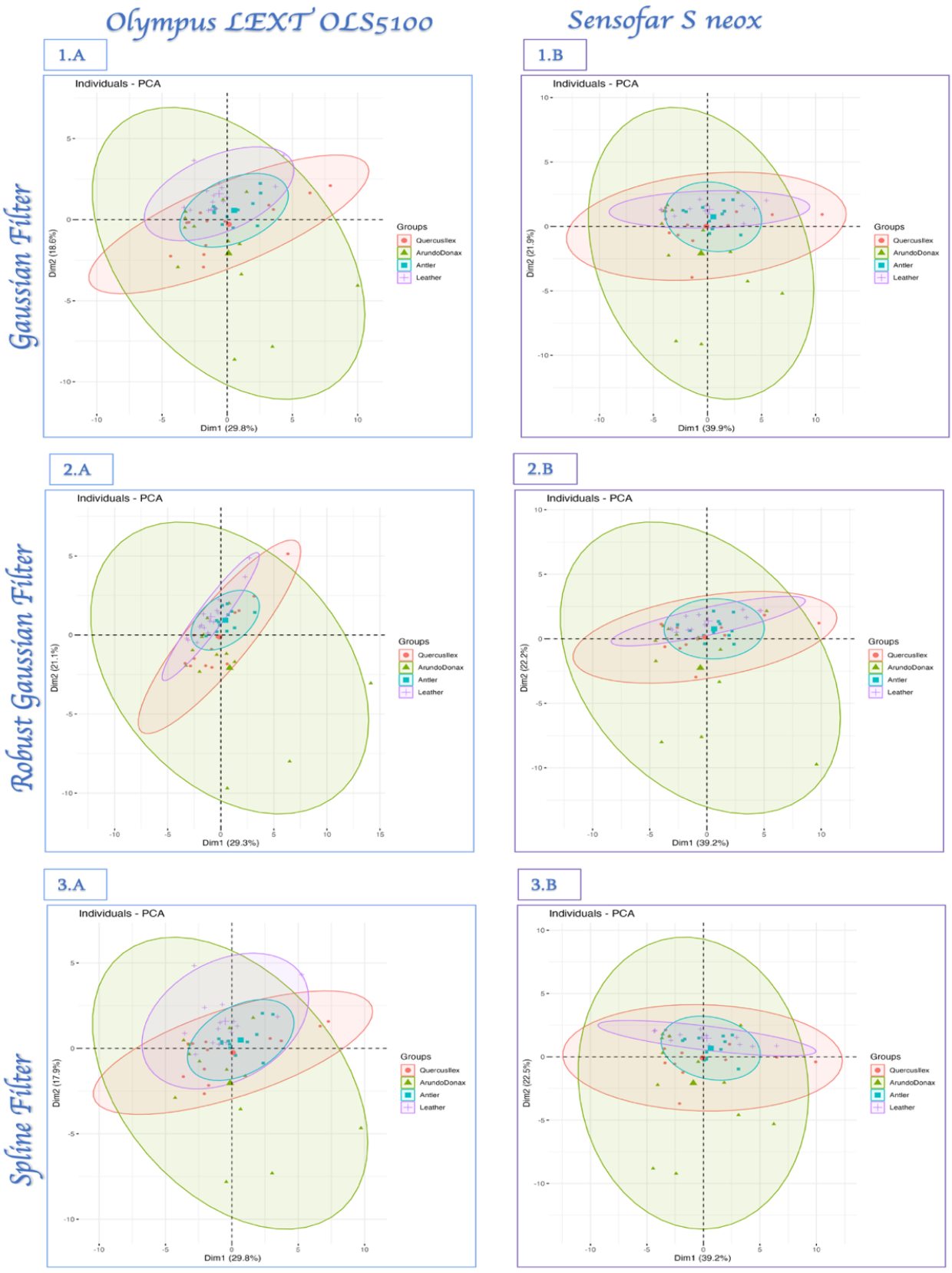

Figure 25: The two sections in the columns represent measurements obtained from two microscopes. Within the graphs, PCA depicts the characteristics of contact materials processed with different filters as follows: Gaussian Filter - denoted as '1. A' and '1. B,' Robust Gaussian Filter - denoted as '2. A' and '2. B,' and Spline Filter - denoted as '3. A' and '3. B.
Workflow 2: template 1b / template 2a / template 3a

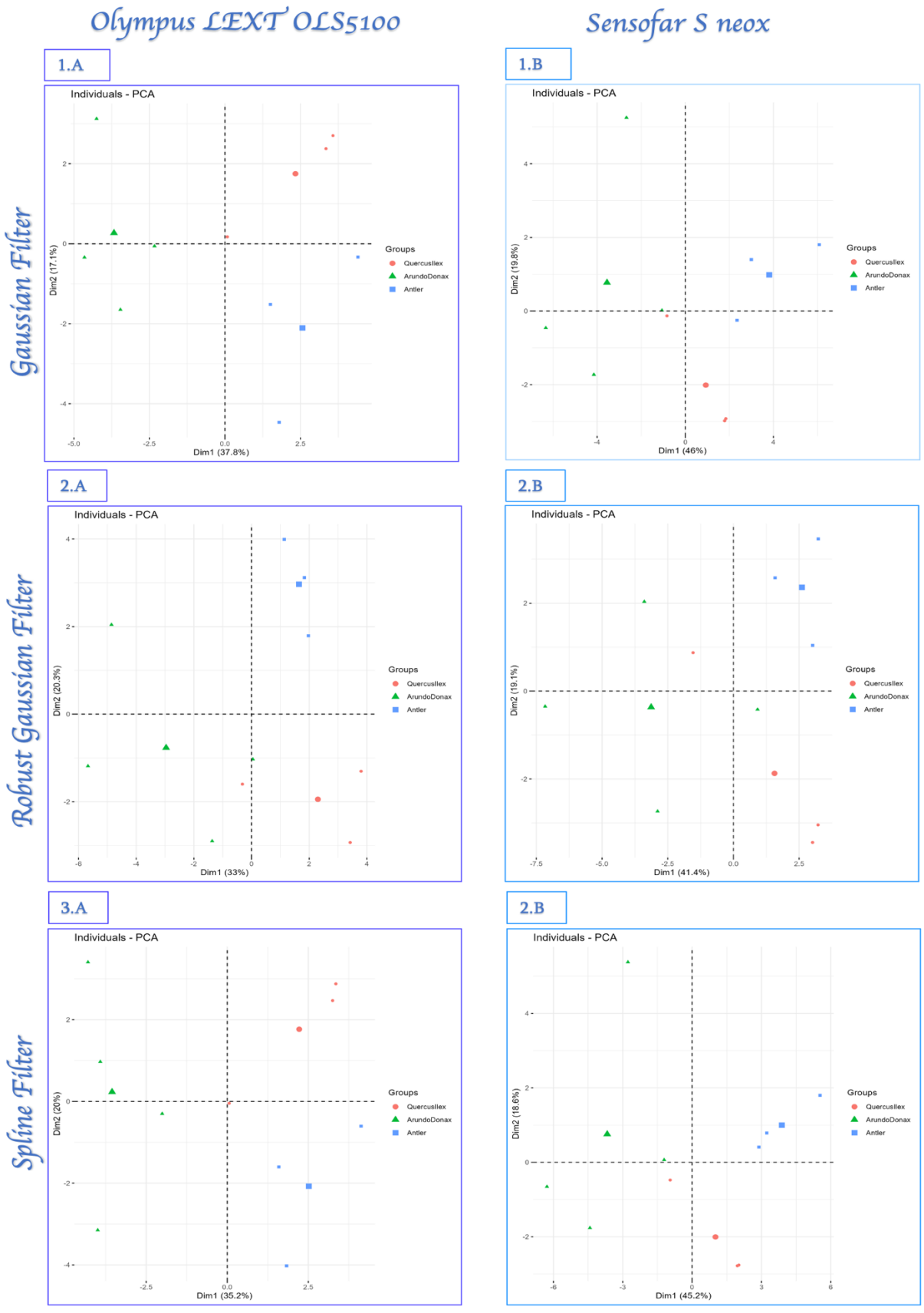

Figure 26: The two sections in the columns represent measurements obtained from two microscopes. Within the graphs, PCA depicts filters as follows: Gaussian Filter - denoted as '1. A' and '1. B,' Robust Gaussian Filter - denoted as '2. A' and '2. B,' and Spline Filter - denoted as '3. A' and '3. B. Workflow 7: template 1b / template 2a / template 3d

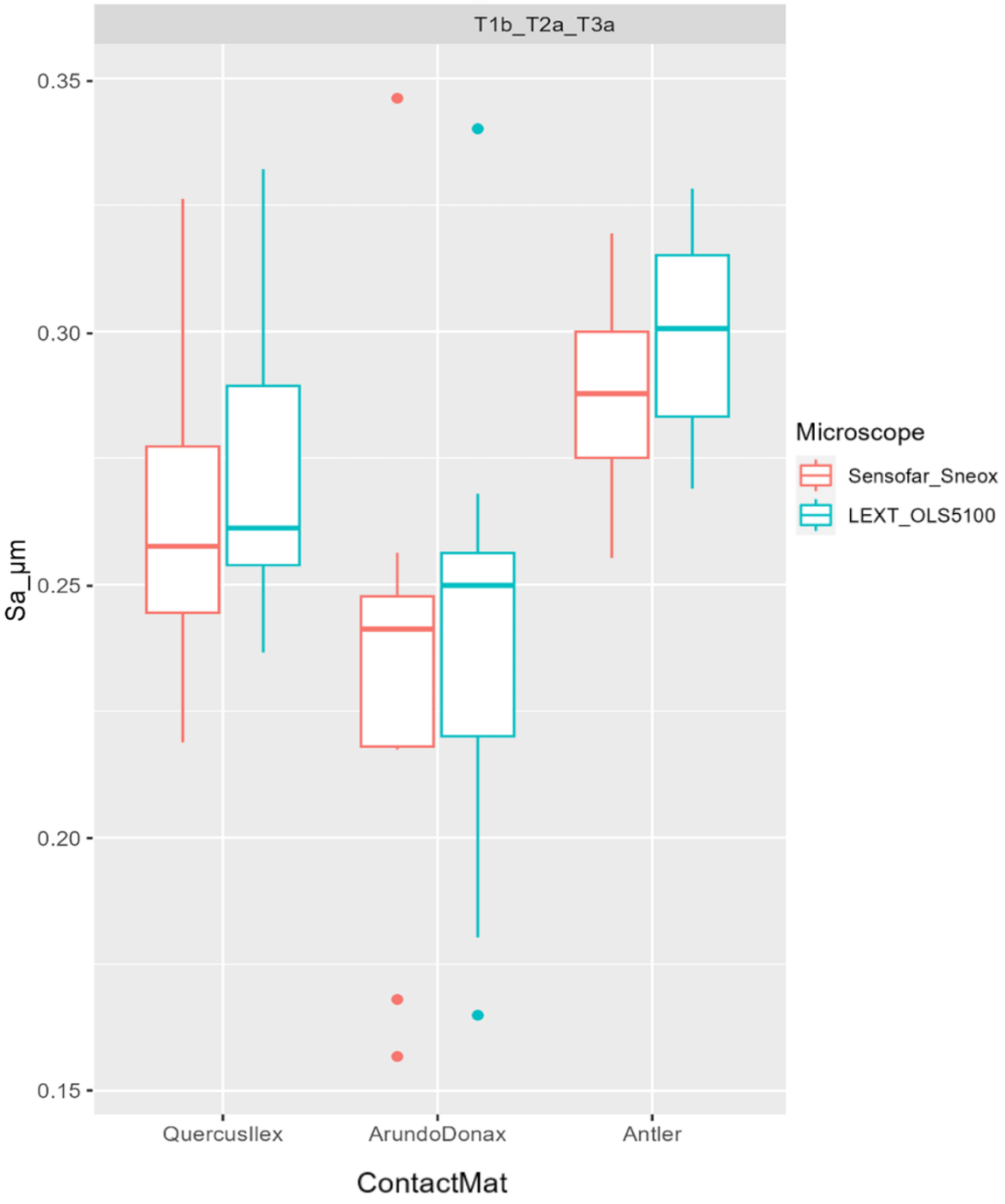

Figure 27:The box plot illustrates Sa_um parameters and the variation observed in contact materials using both microscopes.

The difference between the contact materials was clearly evident as they exhibited less overlap with each other, by one parameter, in this particular case Sa_um (Figure 27). However, when we compared each microscope separately with the contact materials, for instance, when we compared the two sets of data, one for reed (Arundo donax) and the other for antler, measured by Sensofar's neox, it was visible that the maximum value of reed was

smaller than the minimum values of antler. This pattern remained consistent when we checked the same measurements using Olympus. However, the maximum values for reed taken by Olympus overlapped with the minimum values of antler taken by Sensofar's neox. This observation shows that each microscope is capable of measuring surfaces in a way that allows good discrimination of these contact materials but that mixing data from the Sensofar with data from the Olympus can be misleading and lead to wrong interpretation of the used surfaces.

Chapter V. Discussion

In the pursuit of advancing scientific understanding and addressing the research of our objectives, this study leveraged advanced microscopy techniques, specifically laser scanning confocal microscopy (Olympus LEXT OLS5100) and microdisplay scanning confocal microscopy (Sensofar S neox). Despite both of our research microscopy being confocal in nature, our primary inquiry centered around whether they yield consistent results when utilized for stone surface texture quantification.

The utilization of these microscopy, enabled us to delve deeply into the intricacies of the subject, offering a high level of precision and detail in our observations. The measurement from both the Olympus LEXT OLS5100 and the Sensofar S neox, contributed to the richness and accuracy of our data. Throughout our analysis, it became clear that these microscopy techniques yielded complementary information and allowed us to explore different facets of the subject matter, in surface texture analysis. While each instrument possessed its own set of strengths and limitations, their combined use facilitated an integrated understanding of the microscopes under research.

Qualitative and quantitative analyses are both essential components of research, and they complement each other by providing informative insights.

The study of the surface texture analysis, and all parameters, applied to our dataset, which were used during the experiment plays a significant role in qualitative and quantitative analysis. The choice of the parameters is important and the qualitative documentation is essential because, sometimes, traces can be qualitatively evident but quantitatively undetectable with the wrong parameters (Borel *et al.* 2021a).

In order to evaluate the surface roughness analysis based on the data obtained from both microscopes, we devised 7 distinct workflows. However, it's worth noting that the total number of measurements acquired with both microscopes amounted to 624, encompassing three objectives: 10x/0.30NA, 20x/0.45NA, and 100x/0.8NA (Table 6). Given the considerable volume of measurements and considering practical constraints related to time and resources, it was unfeasible to process the entire dataset comprehensively. Consequently, we made the deliberate choice to focus exclusively on processing measurements captured at 100x magnification with a 0.8 numerical aperture (NA) in both microscopes, as previously mentioned (resulting in a total of 214 measured points with 100x/0.8NA magnification in both microscopes). The qualitative and quantitative results obtained from this focused analysis are presented below.

5.1 Qualitative Insights and Interpretations

The findings presented in this chapter represent a significant results of our first part of the experimental work, which is qualitative research. As we have conducted use-wear analyses on stone tools exposed to different movements, use duration, and contact material, which have taken an important stage in use-wear analysis and our experimental research. During this work recorded any traces, alterations, or wear patterns that have developed through use.

The findings further highlighted already implications, that suggest that surface modification on flint is influenced by the nature of the contact material, with material hardness playing a significant role in shaping the development of surface modifications (Pedergnana & Ollé 2017). These results suggest that softer contact materials, such as hide, are more likely to produce fewer surface modifications compared to harder materials, such as fresh wood, antler, and reed.

Qualitative analysis of use-wear has revealed that discernible traces consistently emerged on all experimental stone tools following their utilization, as expected. This observation underscores the effectiveness of the methods and techniques employed in this study, enabling a clear distinction between the surfaces before and after use. However, it is important to note that the development of polish on the experimental stons's working edges exhibited some variation among the different contact materials employed and of course, it was a better-developed surface that was used most time during the experimental work, which means that highly developed polished on the surfaces was a prominent observation in our study, after 5000 stocks. This high degree of polish indicated the extensive wear and abrasion contact material of these stones used during the experimental process. Also, alongside this polished appearance, micro-fractures were also detected on some stone surfaces, particularly on those where hard contact materials were employed. These micro-fractures were a consequence of the interaction between the stone tool and the hard nature of the contact material. The presence of these micro-fractures introduced a significant consideration for maintaining measurement consistency. Observed that there was a risk that the measurements we had taken before the experiment did not align precisely with the same points on the stone before and after the micro-fractures had formed.

In the case of ELTE_IAS_000093 and ELTE_IAS_000202 stones used for bidirectional sawing on a reed, we observed one of the most extensive wear patterns on the stone surfaces. This was attributed to the highly abrasive nature of reed as a contact material.

The post-usage polish displayed a smoother and more reflective texture, signifying the abrasive action and smoothing effect of the tool's edge against the reed fibers. Edge rounding was also noticeable, particularly after 10,000 stocks. The bidirectional sawing of fresh wood using ELTE_IAS_000096 and ELTE_IAS_000094 stones revealed notable polish and micro-fractures on the stone surfaces. The emergence of highly lustrous polishes, characterized by smooth surfaces with a domed microtopography, indicated a gradual process of expansion and interconnection. Interestingly, disparities were observed between the dorsal and ventral aspects of the stones, with the dorsal aspect consistently exhibiting polished surfaces along all functional areas. When sawing soaked antler with ELTE_IAS_000204 and ELTE_IAS_000203 stones, the development of polish was more pronounced after 10,000 sawing repetitions. Step fractures and conchoidal micro-fractures hindered the progression of edge rounding, and the distribution of polish was confined to a delimited area near the active edge. Striations were conspicuously absent on both sides of the tools. The use of ELTE_IAS_000200 and ELTE_IAS_000201 stones for unidirectional scraping on hides presented a departure from the established norm, involving a softer contact material and a scraping technique. Notably, the absence of abrasive additives during hide working experiments resulted in the absence of striations, with the resultant polishes resembling the greasy polish characteristic of meat processing. A bright and disorderedly structured polish was observed in close proximity to the tool's edge after 10,000 scraping cycles, though the development of polish was not uniform across the entire contacting edge.

In our study, we employed two microscopes, the Olympus LEXT OLS5100 and Sensofar S neox, for surface texture analysis. The Olympus microscope demonstrated remarkable resolution and advanced analytical capabilities, while the Sensofar S neox excelled in versatility and faster data throughput. Notably, the Sensofar S neox proved advantageous in scenarios involving a high volume of measurements and time constraints, thanks to its rapid data collection and processing capabilities. These microscope characteristics played a pivotal role in addressing specific research requirements and constraints, showcasing the importance of choosing the appropriate instrument for the task at hand.

5.2 Quantitative Analysis: Unveiling Workflows's Patterns and Implications

In the context of the experiments, the results from the quantitative surface texture roughness analysis show important findings within comparing both interesting microscopes. To understand these outcomes, various factors had to be considered, including the incorporation of filters and data manipulation techniques. The unique characteristics of the microscopes used and the specific variations observed could differ significantly, contingent upon the dataset under examination and the specific data processing methods employed.

The microscope comparison study demonstrated that, in the majority of cases, comparing the microscopes yielded similar results. It was observed that when both systems were systematically employed, the data produced could potentially yield consistent measurements. However, it is important to note that variations in filters and workflows had a comparable impact on the results obtained from both microscope measurements.

We endeavored to determine a suitable protocol that could effectively accommodate both microscope systems. As well as attempted to identify the optimal sequence within the order of steps for workflow.

Surface Leveling (Templates 1a and 1b)

Should we extract the area on which we computed the parameters before or after the leveling of the surface?! As for T-1a. we analyzed and noticed some inaccuracies in the topography, so we posed this question.

The key difference between the two templates lies in the order of operations. In Template 1a. Arman et al. (2016), the first step is to level surfaces, while in Template 1b. the first step is to extract a specific area of interest before leveling surfaces (Figures: 6 & 7).

When we leveled the entire surface first (LS-plane method), we ensured that the entire dataset was consistently processed. The LS-plane method was employed to ensure that the orientation of the specimen did not result in data loss during thresholding. This operator function was part of the editing process to achieve accurate and reliable measurements. Although, specifically, our analysis showed a different result.

However, Template 1b placed a strong emphasis on selecting and extracting a specific region of interest (340x340 µm) at the beginning of the process, as a first step. When we extracted that area first, the result was more efficient. We avoided processing unnecessary

data outside of the region of interest and reduced the inaccuracy of computational resources and time. It also reduced the risk of inadvertently including irrelevant data, and it ensured that only relevant information was processed and stored, simplifying subsequent analysis and storage.

In other steps, both templates followed identically for data processing and analysis. These steps involved the removal of the nominal form using a least squares polynomial of degree 2. The objective was to prevent data loss during thresholding and enable the separate analysis of waviness and roughness components. By eliminating the general form of the surface, the analysis could focus on specific surface characteristics. After removing outliers, we minimized the impact of measurement noise on the data analysis. Also, thresholding was employed to ensure that random differences, characteristic of measurement noise, did not affect the analysis. This process improved the quality of the scans by eliminating unwanted noise and artifacts. To enhance comparability between the surfaces, non-measured points on the surfaces were filled. This step aimed to alleviate differences between file types. The purpose of filling in these non-measured points was to ensure accurate analysis.

Even so, despite the application of a similar protocol, a different initial step in these two approaches altered the outcome. After we compared the results obtained with various filters and surface parameters, Template 1b proved to have been more efficiently suited to our research objective and significantly enhanced the similarity of the datasets acquired from the microscopes (Figure 19; Figure20).

Roughness Analysis

For the roughness analysis, we employed various filters, namely the Gaussian filter, the Robust Gaussian filter of order 2, and the Spline filter. The selection of these filters was made with the objective of minimizing intra-specimen variability while preserving the integrity of the relative area curve. These filters functioned by employing mathematical algorithms to identify and remove surface features that were smaller than a predefined threshold (Arman *et al.* 2016).

Different cut-off values, specifically 0.01225 mm, 0.025 mm, and 0.050 mm were tested in combination with the end-effect correction to identify the most optimal configuration within the workflow. The choice of these filters and the determination of the appropriate cut-off length were driven by their suitability in characterizing surface roughness, a pivotal component of surface analysis (Borel *et al.* 2021b).

We conducted a thorough evaluation of these filters using both laser scanning confocal microscopy and microarray scanning confocal microscopy. This comparative analysis allowed us to precisely gauge each microscope's performance in the context of characterizing surface roughness. The implication is that our roughness analysis consistently revealed that the choice of microscope had a negligible impact on the characterization of surface roughness. We consistently observed minimal variations in roughness parameters when employing different microscopes. This finding underscores the reliability and comparability of the two microscopy techniques within the realm of use-wear research.

However, it's important to note that the choice of cut-off length did have a discernible effect on our results. The box plot effectively illustrates how different cut-off values (0.025 mm, 0.01225 mm, and 0.050 mm) and workflows influenced the distribution of Sa values for both microscopes, showing their performance under testing filtering conditions.

Specifically, when employing a cut-off of 0.050 mm, the median of the box plot revealed more pronounced differences between the microscopes. In contrast, the 0.025 mm cut-off exhibited similarities and fewer outliers. Consequently, we opted to use the 0.025 mm cut-off length for subsequent computations, as it provided results that were more consistent and conducive to meaningful comparisons.

With PCA, the results of the filter and cut-off testing indicated that the filtering process applied in the study had a more pronounced effect on the comparability between microscopes than on the discrimination of contact materials. The use of filters played an important role in minimizing differences between microscopes while distinctions in contact materials through each metrology parameter, as demonstrated in Figure 26.

We employed PCA to compare microscopes across different cut-offs with filters, resulting in varying outcomes. Microscope similarity was more consistently maintained at a cut-off of 0.0025, with the Robust Gaussian filter displaying the most prominent results (Figure 28 -1B). Also, Gaussian and Spline filters yielded similar results with both microscopes. This trend persisted at a 0.01225 mm cut-off, albeit with weaker correlations. However, when employing a 0.050 mm cut-off, notably different results were obtained, leading to an increased disparity between the microscopes.

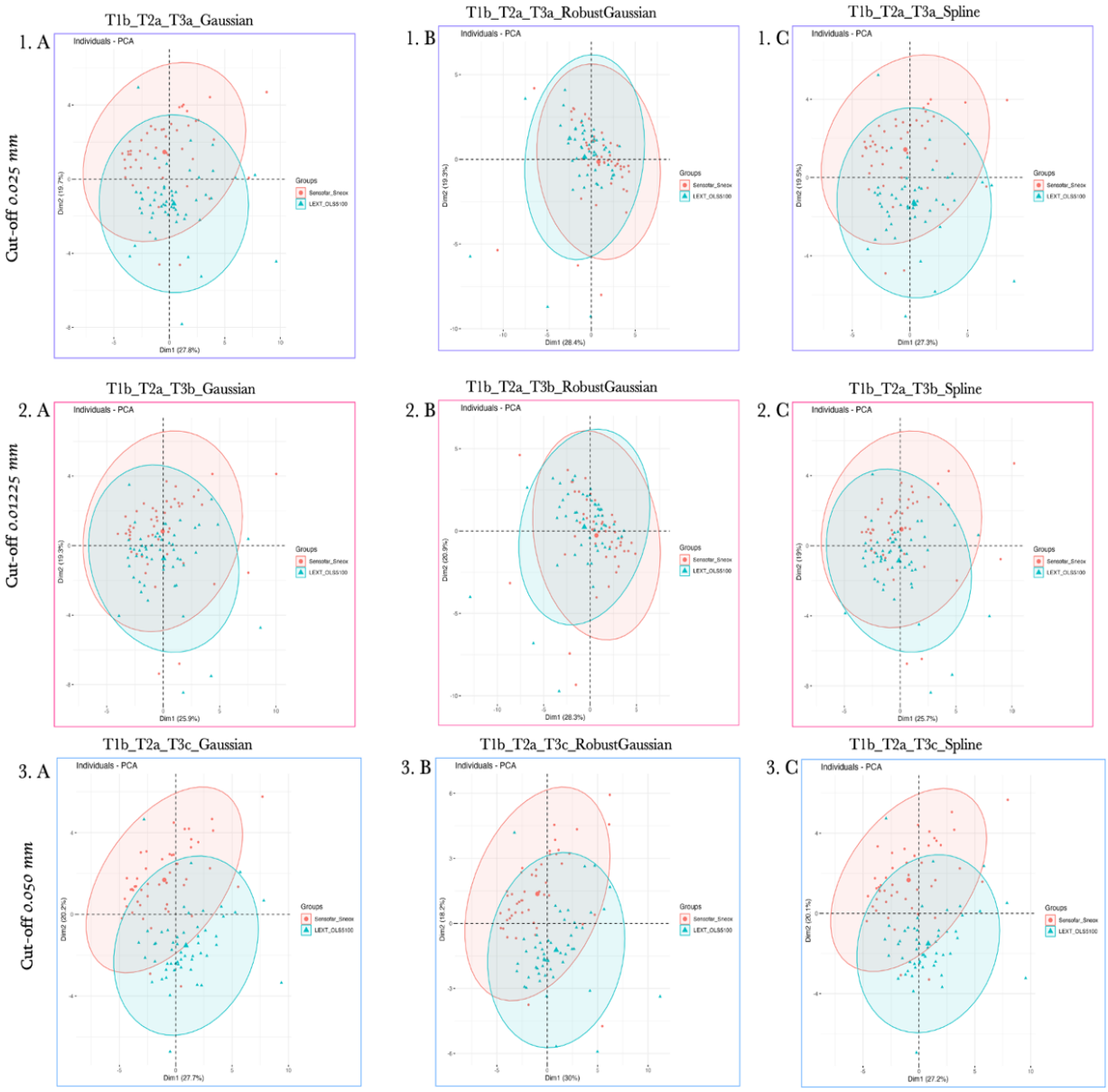

Figure 28: PCA was utilized to visualize the data with the application of three distinct filters, each employing different cut-off lengths: 1. A cut-off length of 0.025 mm; 2. A cut-off length of 0.01225 mm; 3. A cut-off length of 0.050 mm. The resulting visualizations were then compared between the two microscopes.

However, it is crucial to consider that the selection of the 28 parameters, primarily chosen for their low correlations, may not have been as effective in distinguishing between contact materials. It is worth noting that the individual impact of each parameter in isolation remains unknown, warranting further investigation in future studies. The lack of clarity in our PCA results may, in part, be attributed to this factor.

Additionally, another contributing factor could be the measurement conditions in sections with less polishing. Our use of high magnification, 100x/0.8NA, posed challenges in

capturing measurements near the extreme edges where the polishing quality was the highest. These factors collectively may have influenced the outcomes observed in our surface analysis.

For future research, it is imperative to explore and identify which specific metrology parameters are better suited for discriminating between different contact materials. This entails a more focused investigation into the individual contributions of each parameter and their relevance in the context of use-wear analysis.

Chapter VI. Conclusion and Perspective

Over the last decades, lithic use-wear analysis methods have been greatly refined, but there are still a few problems, which need to be fixed. Laboratory experiments provide ideal conditions for isolating specific variables to study. New microscopes, modern techniques, and more information from past experiments give us more information on use-wear analysis, and future possibilities of this discipline.

The use-wear analysis takes into account the fact that repeated actions performed with a stone tool leave microscopic and sometimes macroscopic evidence resulting from the type of activities carried out. Researchers have compared use-wear found on replicated tools used in experimental actions to use-wear found on archaeological artifacts. They have had success in classifying wear patterns found on artifacts. In this way, scientists can link a tool action (e.g., scraping or cutting) with a specific wear pattern.

In the pursuit of understanding surface roughness analysis and microscopy techniques, our research has made an important contribution. We have demonstrated that data obtained from the Olympus LEXT OLS5100 and the Sensofar S neox microscopes are indeed comparable but that they should not be mixed as this could lead to wrong interpretation of the contact material for example. This finding is a pivotal step forward in the field, where the assessment of data consistency has been a longstanding challenge.

Our study stands as one of the pioneering endeavors in this domain, shedding light on the comparability of two confocal microscopy techniques, in use-wear analysis. Beyond its immediate implications for our research, it offers a foundation for future investigations seeking to evaluate the reliability of different instruments in various scientific disciplines.

This experimental research has not only unveiled a comparative analysis of two advanced microscopy techniques but has also made a substantial methodological contribution with enduring implications for future investigations. The different workflows and templates employed in this research are of paramount significance, particularly in shaping the study's conclusion and broader scientific contributions. Firstly, they establish a standardized methodology that promotes reproducibility. This uniformity ensures that fellow researchers can readily adopt the same procedures, enhancing the credibility and reliability of this study.

Crucially, these templates highlight the comparability of data derived from distinct microscopy techniques. This validation not only solidifies the trustworthiness of these instruments for use-wear analysis but also lays the groundwork for future research that may rely on similar approaches. Moreover, the templates have contributed to the optimization of

surface roughness analysis. Through the exploration of various filters and cut-off values, they have refined these methods, resulting in more precise and meaningful outcomes.

Furthermore, the research signals future avenues, particularly in the fine-tuning of metrology parameters for material discrimination. This forward-looking perspective paves the way for ongoing advancements in microscopy techniques and surface analysis.

In conclusion, this master's thesis advances our understanding of microscopy and surface roughness analysis applied to stone tools wear analysis. It underscores the importance of data reliability and serves as a benchmark for future research. As scholars and scientists continue to explore the intricacies of these methodologies, our study provides a vital reference point in the pursuit of scientific knowledge

Bibliography

ÁLVAREZ-FERNÁNDEZ, A., R. GARCÍA-GONZÁLEZ, B. MÁRQUEZ, J.M. CARRETERO & J.L. ARSUAGA. 2020. Butchering or wood? A LSCM analysis to distinguish use-wear on stone tools. *Journal of Archaeological Science: Reports* 31: 102377. https://doi.org/10.1016/j.jasrep.2020.102377.

ANDERSON, P.C., L. ASTRUC, R. VARGIOLU & H. ZAHOUANI. 1998. Contribution of quantitative analysis of surface states to a multi-method approach for characterizing plant-processing traces on flint tools with gloss, in F. Alhaique (ed.) *Functional Analysis of Lithic Artefacts: Current State of Research, Proceedings of the XIII Congress of the International Union of Prehistoric and Protohistoric Sciences. Volume 6 - Tome II*: 1151–60. Forli, Italy: A.B.A.C.O.

ANDREFSKY, W. 1998. *Lithics*. Cambridge University Press.

ARMAN, S., P. UNGAR, C. BROWN, L. DESANTIS, C. SCHMIDT & G. PRIDEAUX. 2016. Minimizing inter-microscope variability in dental microwear texture analysis. *Surface Topography: Metrology and Properties* 4: 024007. https://doi.org/10.1088/2051-672X/4/2/024007.

BANNING, E.B. 2020. Bone and Shell Tools, in E.B. Banning (ed.) *The Archaeologist's Laboratory: The Analysis of Archaeological Evidence*: 231–40 (Interdisciplinary Contributions to Archaeology). Cham: Springer International Publishing. https://doi.org/10.1007/978-3-030-47992-3_14. https://doi.org/10.1007/978-3-030-47992-3_14.

BENCOMO, M., A. MAYOR, S. SOSSA-RÍOS, P. JARDÓN, B. GALVÁN, C. MALLOL & C.M. HERNÁNDEZ. 2023. Use-wear analysis applied in a dissected palimpsest at the Middle Palaeolithic site of El Salt (eastern Iberia): working with lithic tools in a narrow timescale. *Archaeological and Anthropological Sciences* 15: 92. https://doi.org/10.1007/s12520-023-01787-4.

BOREL, A., A. OLLÉ, J.M. VERGÉS & R. SALA. 2014. Scanning electron and optical light microscopy: two complementary approaches for the understanding and interpretation of usewear and residues on stone tools. *Journal of Archaeological Science* 48. Elsevier: 46–59.

BOREL, A., J. MARTEAU, L. COUSTENOBLE, T. INGICCO & C. BROWN. 2018. Studying wear marks with multiscale surface metrology. Poster presented at the UISPP conference, Session XII-1. New Technologies and Analytical Approaches in Traceology, June 4-9, June 4, Paris. 10.13140/RG.2.2.24413.72166.

BOREL, A., R. DELTOMBE, J. MARTEAU, P. MOREAU, M. BIGERELLE, G. LENGYEL & Z. MESTER. 2021a. Qualitative and Quantitative Analyses of Surface Alterations of Stone Tools Made of Raw Materials from the Carpathian Basin. *Hungarian Archaeology* 10: 1–11. https://doi.org/10.36338/ha.2021.3.4.

BOREL, A., R. DELTOMBE, P. MOREAU, T. INGICCO, M. BIGERELLE & J. MARTEAU. 2021b. Optimization of use-wear detection and characterization on stone tool surfaces. *Scientific Reports* 11. Nature Publishing Group: 24197. https://doi.org/10.1038/s41598-021-03663-4.

BRIUER, F.L. 1976. New Clues to Stone Tool Function: Plant and Animal Residues. *American Antiquity* 41. Cambridge University Press: 478–84. https://doi.org/10.2307/279013.

CALANDRA, I., L. SCHUNK, K. BOB, W. GNEISINGER, A. PEDERGNANA, E. PAIXAO, A. HILDEBRANDT & J. MARREIROS. 2019. The effect of numerical aperture on

quantitative use-wear studies and its implication on reproducibility. *Scientific Reports* 9: 1–10. https://doi.org/10.1038/s41598-019-42713-w.

CHOMKO, S.A. 1975. Bone "Awls" and Utilized Antler Tines From Arnold Research Cave, 23Cy64, Missouri. *Plains Anthropologist* 20: 27–40. https://doi.org/10.1080/2052546.1975.11908724.

CURWEN, E.C. 1930. Prehistoric Flint Sickles. https://www.cambridge.org/core/journals/antiquity/article/abs/prehistoric-flint-sickles/70C0F805048468379FCB906156677FD1.

DUMONT, J. 1982. The Quantification of Microwear Traces: A New Use for Interferometry. *World Archaeology* 14: 206–17.

EVANS, A.A. 2014. On the importance of blind testing in archaeological science: the example from lithic functional studies. *Journal of Archaeological Science* 48 (Lithic Microwear Method: Standardisation, Calibration and Innovation): 5–14. https://doi.org/10.1016/j.jas.2013.10.026.

EVANS, A.A. & R.E. DONAHUE. 2005. The elemental chemistry of lithic microwear: an experiment. *Journal of Archaeological Science* 32: 1733–40. https://doi.org/10.1016/j.jas.2005.06.010.

—. 2008a. Laser scanning confocal microscopy: a potential technique for the study of lithic microwear. *Journal of Archaeological Science* 35: 2223–30. https://doi.org/10.1016/j.jas.2008.02.006.

—. 2008b. Laser scanning confocal microscopy: a potential technique for the study of lithic microwear. *Journal of Archaeological Science* 35: 2223–30. https://doi.org/10.1016/j.jas.2008.02.006.

EVANS, J. 1897. *Ancient Stone Implements, Weapons, and Ornaments, of Great Britain* (Cambridge Library Collection - Archaeology). Cambridge: Cambridge University Press. https://www.cambridge.org/core/books/ancient-stone-implements-weapons-and-ornaments-of-great-britain/6D9763DB1DC0B4D28D74E60088D63AA3. https://doi.org/10.1017/CBO9781316155455.

FRAHM, E. 2014. Scanning Electron Microscopy (SEM): Applications in Archaeology, in C. Smith (ed.) *Encyclopedia of Global Archaeology*: 6487–95. New York, NY: Springer. https://doi.org/10.1007/978-1-4419-0465-2_341. https://doi.org/10.1007/978-1-4419-0465-2_341.

FUENTES, R. et al. 2019. Technological and behavioural complexity in expedient industries: The importance of use-wear analysis for understanding flake assemblages. *Journal of Archaeological Science* 112: 105031. https://doi.org/10.1016/j.jas.2019.105031.

FULLAGAR, R. 2004. Residues and Usewear. *Archaeology in Practice: A Student Guide to Archaeological Analyses*, 232–63.

FULLAGAR, R. & C. MATHESON. 2014. Stone Tool Usewear and Residue Analysis, in C. Smith (ed.) *Encyclopedia of Global Archaeology*: 7062–65. New York, NY: Springer. https://doi.org/10.1007/978-1-4419-0465-2_842. https://doi.org/10.1007/978-1-4419-0465-2_842.

GIBAJA, J.F. & B. GASSIN. 2015. Use-Wear Analysis on Flint Tools. Beyond the Methodological Issues, in J.M. Marreiros, J.F. Gibaja Bao & N. Ferreira Bicho (ed.) *Use-Wear and Residue Analysis in Archaeology*: 41–58 (Manuals in Archaeological Method, Theory and Technique). Cham: Springer International Publishing. https://doi.org/10.1007/978-3-319-08257-8_4. https://doi.org/10.1007/978-3-319-08257-8_4.

GIJN, A.L. van. 1990. The wear and tear of flint: principles of functional analysis applied to Dutch Neolithic assemblages. (Analecta Praehistorica Leidensia). Universiteit Leiden. https://hdl.handle.net/1887/15186.

GRACE, R. 1989. *Interpreting the Function of Stone Tools: The Quantification and Computerisation of Microwear Analysis* (BAR International Series 474). Archaeopress.
—. 1990. The Limitations and Applications of Use Wear Analysis. https://www.researchgate.net/publication/275333134_The_Limitations_and_Applications_of_Use_Wear_Analysis.
GRACE, R. 1996. Review Article Use-Wear Analysis: The State of the Art. *Archaeometry* 38: 209–29. https://doi.org/10.1111/j.1475-4754.1996.tb00771.x.
HALBRUCKER, É., G. FIERS, H. VANDENDRIESSCHE, T. DE KOCK, V. CNUDDE & P. CROMBÉ. 2021. Burning flint: An experimental approach to study the effect of fire on flint tools. *Journal of Archaeological Science: Reports* 36: 102854. https://doi.org/10.1016/j.jasrep.2021.102854.
IBÁÑEZ, J.J. & N. MAZZUCCO. 2021. Quantitative use-wear analysis of stone tools: Measuring how the intensity of use affects the identification of the worked material. *PLOS ONE* 16: e0257266. https://doi.org/10.1371/journal.pone.0257266.
IBÁÑEZ, J.J., J.E. GONZÁLEZ-URQUIJO & J. GIBAJA. 2014. Discriminating wild vs domestic cereal harvesting micropolish through laser confocal microscopy. *Journal of Archaeological Science* 48 (Lithic Microwear Method: Standardisation, Calibration and Innovation): 96–103. https://doi.org/10.1016/j.jas.2013.10.012.
IBÁÑEZ, J.J., T. LAZUEN & J. GONZÁLEZ-URQUIJO. 2019. Identifying Experimental Tool Use Through Confocal Microscopy. *Journal of Archaeological Method and Theory* 26: 1176–1215. https://doi.org/10.1007/s10816-018-9408-9.
KEALHOFER, L., R. TORRENCE & R. FULLAGAR. 1999. Integrating Phytoliths within Use-Wear/Residue Studies of Stone Tools. *Journal of Archaeological Science - J ARCHAEOL SCI* 26: 527–46. https://doi.org/10.1006/jasc.1998.0332.
KEELEY, L. 1982. Keeley L., Experimental determination of stone tool uses. A miorowear analysis, 1980. *Nouvelles de l'Archéologie* 8. Persée - Portail des revues scientifiques en SHS: 68–69.
KEELEY, L.H. 1974. Technique and methodology in microwear studies: A critical review. *World Archaeology* 5. Routledge: 323–36. https://doi.org/10.1080/00438243.1974.9979577.
—. 1980. *Experimental Determination of Stone Tool Uses: A Microwear Analysis*. University of Chicago Press.
KEELEY, L.H. & M.H. NEWCOMER. 1977. Microwear analysis of experimental flint tools: a test case. *Journal of Archaeological Science* 4: 29–62. https://doi.org/10.1016/0305-4403(77)90111-X.
KIMBALL, L.R., J.F. KIMBALL & P.E. ALLEN. 1995. Microwear polishes as viewed through the atomic force microscope. *Lithic Technology* 20. Maney Publishing: 6–28.
LERNER, H., X. DU, A. COSTOPOULOS & M. OSTOJA-STARZEWSKI. 2007. Lithic raw material physical properties and use-wear accrual. *Journal of Archaeological Science* 34: 711–22. https://doi.org/10.1016/j.jas.2006.07.009.
LEVI SALA, I. 1986. Use wear and post-depositional surface modification: A word of caution. *Journal of Archaeological Science* 13: 229–44. https://doi.org/10.1016/0305-4403(86)90061-0.
LIU, J., H. CHEN & Y. SHEN. Use-wear experimental studies for differentiating flint tools processing bamboo from wood., 14.
MACDONALD, D. 2014a. Evaluating Surface Cleaning Techniques of Stone Tools Using Laser Scanning Confocal Microscopy. *Microscopy today* 22: 22–26. https://doi.org/10.1017/S1551929514000364.

MACDONALD, D.A. 2014b. The application of focus variation microscopy for lithic use-wear quantification. *Journal of Archaeological Science* 48 (Lithic Microwear Method: Standardisation, Calibration and Innovation): 26–33. https://doi.org/10.1016/j.jas.2013.10.003.

MARREIROS, J., N. MAZZUCCO, J.F. GIBAJA & N. BICHO. 2015. Macro and Micro Evidences from the Past: The State of the Art of Archeological Use-Wear Studies, in J.M. Marreiros, J.F. Gibaja Bao & N. Ferreira Bicho (ed.) *Use-Wear and Residue Analysis in Archaeology*: 5–26 (Manuals in Archaeological Method, Theory and Technique). Cham: Springer International Publishing. https://doi.org/10.1007/978-3-319-08257-8_2. https://doi.org/10.1007/978-3-319-08257-8_2.

MARREIROS, J., I. CALANDRA, W. GNEISINGER, E. PAIXÃO, A. PEDERGNANA & L. SCHUNK. 2020. Rethinking use-wear analysis and experimentation as applied to the study of past hominin tool use. *Journal of Paleolithic Archaeology* 3. Springer: 475–502.

MOSS, E.H. 1987. A review of "Investigating microwear polishes with blind tests". *Journal of Archaeological Science* 14: 473–81. https://doi.org/10.1016/0305-4403(87)90033-1.

NUNZIANTE CESARO, S. & C. LEMORINI. 2012. The function of prehistoric lithic tools: A combined study of use-wear analysis and FTIR microspectroscopy. *Spectrochimica Acta Part A: Molecular and Biomolecular Spectroscopy* 86: 299–304. https://doi.org/10.1016/j.saa.2011.10.040.

ODELL, G.H. 1977. THE APPLICATION OF MICRO-WEAR ANALYSIS TO THE LITHIC COMPONENT OF AN ENTIRE PREHISTORIC SETTLEMENT: METHODS, PROBLEMS AND FUNCTIONAL RECONSTRUCTIONS. - ProQuest. https://www.proquest.com/openview/9b7f1e7dd1b2b3f52689012a3526e4d4/1?pq-origsite=gscholar&cbl=18750&diss=y.

—. 1981. The Mechanics of Use-Breakage of Stone Tools: Some Testable Hypotheses. *Journal of Field Archaeology* 8. Routledge: 197–209. https://doi.org/10.1179/009346981791505120.

—. 2004. *Lithic Analysis*. https://link.springer.com/book/10.1007/978-1-4419-9009-9.

ODELL, G.H. & F. ODELL-VEREECKEN. 1980. Verifying the Reliability of Lithic Use-Wear Assessments by 'Blind Tests': The Low-Power Approach. *Journal of Field Archaeology* 7. [Maney Publishing, Trustees of Boston University]: 87–120. https://doi.org/10.2307/529584.

OLLÉ, A. & J.M. VERGÈS. 2008. SEM functional analysis and the mechanism of microwear formation. *Prehistoric technology* 40: 39–49.

OLLÉ, A. & J.M. VERGÈS. 2014. The use of sequential experiments and SEM in documenting stone tool microwear. *Journal of Archaeological Science* 48 (Lithic Microwear Method: Standardisation, Calibration and Innovation): 60–72. https://doi.org/10.1016/j.jas.2013.10.028.

PAIXÃO, E., A. PEDERGNANA, J. MARREIROS, L. DUBREUIL, M. PRÉVOST, Y. ZAIDNER, G. CARVER & W. GNEISINGER. 2021. Using mechanical experiments to study ground stone tool use: Exploring the formation of percussive and grinding wear traces on limestone tools. *Journal of Archaeological Science: Reports* 37: 102971. https://doi.org/10.1016/j.jasrep.2021.102971.

PAL, N., M.R. ALVAREZ, I. BRIZ, A. DOMÍNGUEZ & E.A. FAVRET. 2020. Archaeology, Stone Tools and RIMAPS Technique: A Quantitive Characterization of Use-Wear Traces. *Microscopy and Microanalysis* 26: 21–22. https://doi.org/10.1017/S1431927620000343.

PEDERGNANA, A. & A. OLLÉ. 2017. Monitoring and interpreting the use-wear formation processes on quartzite flakes through sequential experiments. *Quaternary*

International 427 (New Contributions to the Functional Analysis of Prehistoric Tools): 35–65. https://doi.org/10.1016/j.quaint.2016.01.053.

PEDERGNANA, A. & A. OLLÉ. 2018. Building an Experimental Comparative Reference Collection for Lithic Micro-Residue Analysis Based on a Multi-Analytical Approach. *Journal of Archaeological Method and Theory* 25: 117–54. https://doi.org/10.1007/s10816-017-9337-z.

PEDERGNANA, A., I. CALANDRA, A.A. EVANS, K. BOB, A. HILDEBRANDT & A. OLLE. 2020a. Polish is quantitatively different on quartzite flakes used on different worked materials. *Plos one* 15. Public Library of Science San Francisco, CA USA: e0243295.

PEDERGNANA, A., A. OLLÉ & A.A. EVANS. 2020b. A new combined approach using confocal and scanning electron microscopy to image surface modifications on quartzite. *Journal of Archaeological Science: Reports* 30: 102237. https://doi.org/10.1016/j.jasrep.2020.102237.

RODRIGUEZ, A., K. YANAMANDRA, L. WITEK, Z. WANG, R.K. BEHERA & R. IOVITA. 2021. The effect of worked material hardness on stone tool wear. *OSF Preprints*. https://osf.io/uhkbr/. https://doi.org/10.31219/osf.io/uhkbr.

ROTS, V. & N. TAIPALE. 2023. Functional Perspectives on Lithic Standardization. *Lithic Technology*. https://www.academia.edu/99025364/Functional_Perspectives_on_Lithic_Standardization.

ROTS, V., L. PIRNAY, Ph. PIRSON & O. BAUDOUX. 2006. Blind tests shed light on possibilities and limitations for identifying stone tool prehension and hafting. *Journal of Archaeological Science* 33: 935–52. https://doi.org/10.1016/j.jas.2005.10.018.

SEMENOV, S.A. 1957. Prehistoric technology : an experimental study of the oldest tools and artefacts from traces of manufacture and wear. *(No Title)*. https://cir.nii.ac.jp/crid/1130000796237817728.

—. 1964. *Prehistoric Technology*.

SEMENOV, S.A. & V.E. SHCHELINSKY. 1971. Micrometric study of working traces on the Palaeolithic tools. *Sovetskaya arkheologiya* 1: 19–30.

STEMP, W.J. 2014. A review of quantification of lithic use-wear using laser profilometry: a method based on metrology and fractal analysis. *Journal of Archaeological Science* 48 (Lithic Microwear Method: Standardisation, Calibration and Innovation): 15–25. https://doi.org/10.1016/j.jas.2013.04.027.

—. 2023. Ghosts in the Room and Elephants in the Machine: Data Acquisition in Surface Texture Analysis of Stone Tools. *Lithic Technology* 48. Routledge: 291–306. Evaluating Surface Cleaning Techniques of Stone Tools Using Laser Scanning Confocal Microscopy. https://doi.org/10.1080/01977261.2022.2142391.

STEMP, W.J. & S. CHUNG. 2011. Discrimination of surface wear on obsidian tools using LSCM and RelA: pilot study results (area-scale analysis of obsidian tool surfaces). *Scanning* 33: 279–93. https://doi.org/10.1002/sca.20250.

STEMP, W.J. & M. STEMP. 2003. Documenting Stages of Polish Development on Experimental Stone Tools: Surface Characterization by Fractal Geometry Using UBM Laser Profilometry. *Journal of Archaeological Science* 30: 287–96. https://doi.org/10.1006/jasc.2002.0837.

STEMP, W.J., H.J. LERNER & E.H. KRISTANT. 2013. Quantifying Microwear on Experimental Mistassini Quartzite Scrapers: Preliminary Results of Exploratory Research Using LSCM and Scale-Sensitive Fractal Analysis. *Scanning* 35: 28–39. https://doi.org/10.1002/sca.21032.

STEMP, W.J., A.S. WATSON & A.A. EVANS. 2015. Surface analysis of stone and bone tools. *Surface Topography: Metrology and Properties* 4. IOP Publishing: 013001. https://doi.org/10.1088/2051-672X/4/1/013001.

STEVENS, N.E., D.R. HARRO & A. HICKLIN. 2010. Practical quantitative lithic use-wear analysis using multiple classifiers. *Journal of Archaeological Science* 37: 2671–78. https://doi.org/10.1016/j.jas.2010.06.004.

TAFELMAIER, Y., G. BATAILLE, V. SCHMID, A. TALLER & M. WILL. 2022. Microscopic Use-Wear Analysis, in Y. Tafelmaier, G. Bataille, V. Schmid, A. Taller & M. Will (ed.) *Methods for the Analysis of Stone Artefacts : An Overview*: 57–63 (Essentials). Wiesbaden: Springer Fachmedien. https://doi.org/10.1007/978-3-658-39091-4_7. https://doi.org/10.1007/978-3-658-39091-4_7.

TRINGHAM, R., G. COOPER, G. ODELL, B. VOYTEK & A. WHITMAN. 1974. Experimentation in the Formation of Edge Damage: A New Approach to Lithic Analysis. *Journal of Field Archaeology* 1. Routledge: 171–96. https://doi.org/10.1179/jfa.1974.1.1-2.171.

TUMUNG, L. 2019. Functional Analysis of the Lithic Assemblages from the Middle and Upper Paleolithic sites of Khorramabad Valley (Western Iran), with special reference to Kaldar Cave. *TDX (Tesis Doctorals en Xarxa)*. Ph.D. Thesis, Universitat Rovira i Virgili. https://www.tdx.cat/handle/10803/668723.

VERGÈS, J.M. & A. OLLÉ. 2011. Technical microwear and residues in identifying bipolar knapping on an anvil: experimental data. *Journal of Archaeological Science* 38. Elsevier: 1016–25.

WABER, N.H. 2020. Open lithics : applying open source technologies to problems in lithic use wear experimentation and analysis. University of British Columbia. https://open.library.ubc.ca/cIRcle/collections/ubctheses/24/items/1.0388821. https://doi.org/10.14288/1.0388821.

WADLEY, L., M. LOMBARD & B. WILLIAMSON. 2004. The first residue analysis blind tests: results and lessons learnt. *Journal of Archaeological Science* 31: 1491–1501. https://doi.org/10.1016/j.jas.2004.03.010.

WHITE, T.D. & P.A. FOLKENS. 2005. Chapter 19 - THE SKELETAL BIOLOGY OF INDIVIDUALS & POPULATIONS, in T.D. White & P.A. Folkens (ed.) *The Human Bone Manual*: 359–418. San Diego: Academic Press. https://www.sciencedirect.com/science/article/pii/B9780120884674500223. https://doi.org/10.1016/B978-0-12-088467-4.50022-3.

List of Figures

List of Tables

Annexes Figures

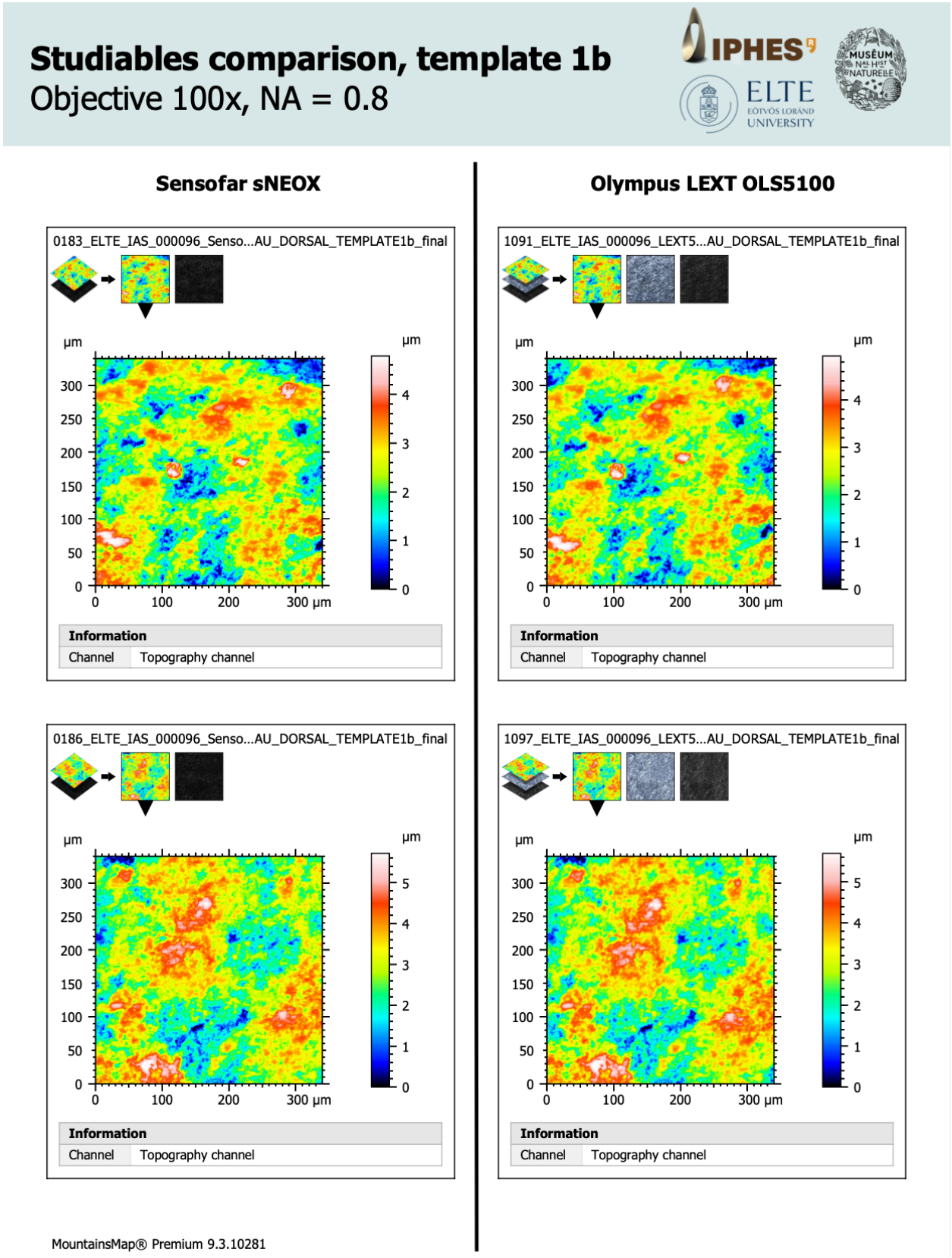

Annex figure 1: A.'96a'. - Figure 183 and Figure 1091; B. '96b.'- Figure 186 and Figure 1097

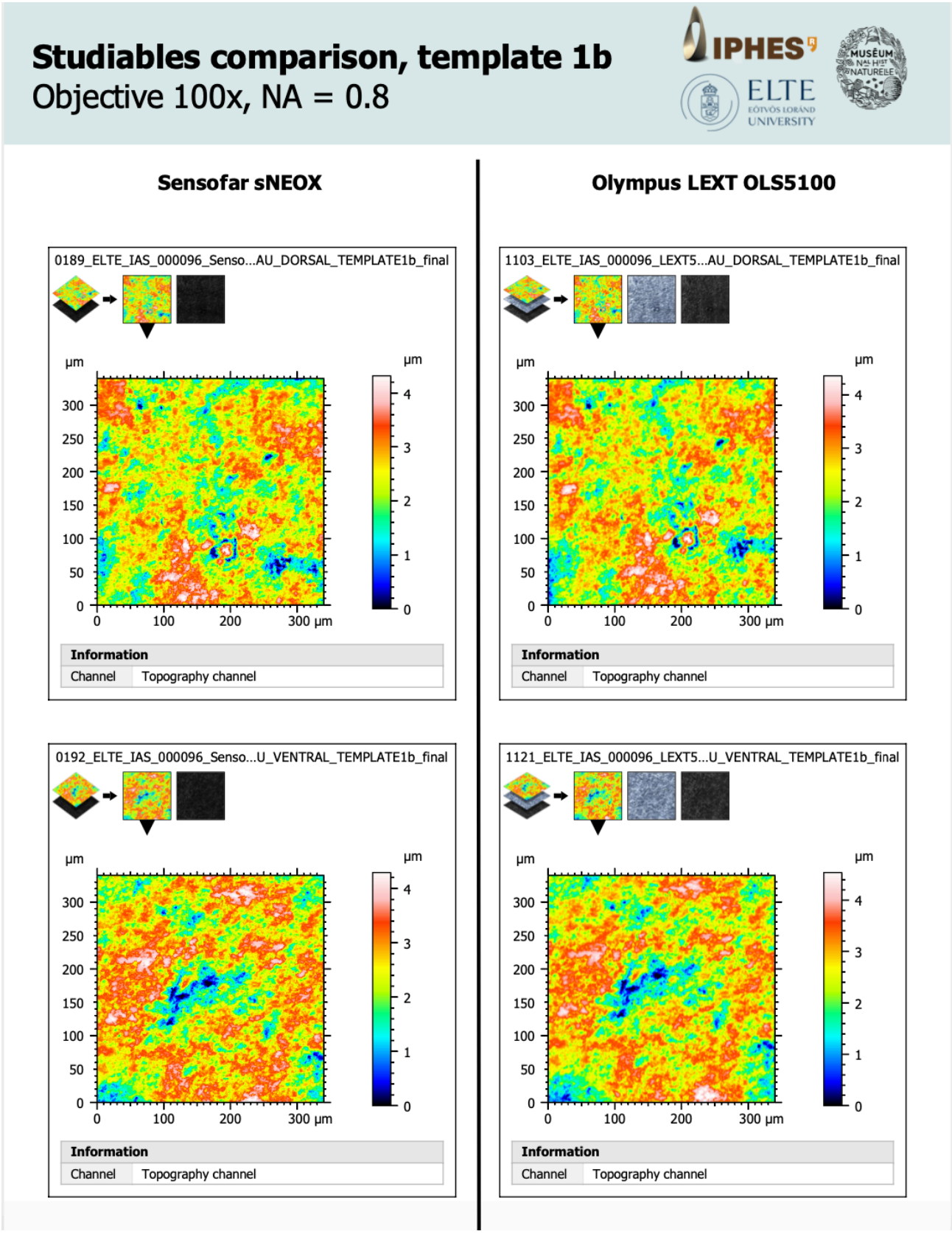

Annex figure 2: A.'96c'. - Figure 189 and Figure 1103; B. '96d.'- Figure 192 and Figure 1121

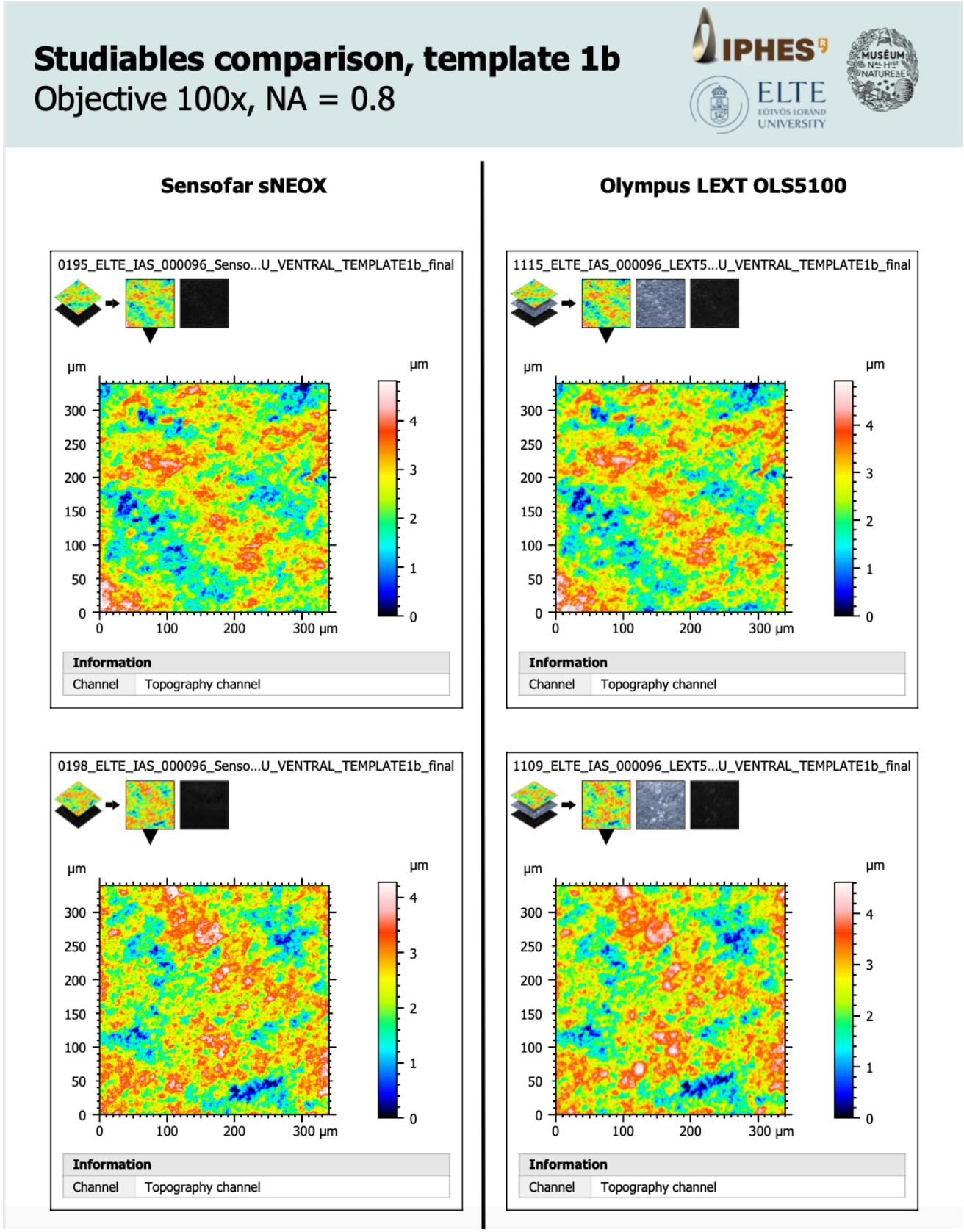

Annex figure 3: A.'96e'. - Figure 195 and Figure 1115; B. '96f.'- Figure 198 and Figure 1109

Studiables comparison, template 1b
Objective 100x, NA = 0.8

Sensofar sNEOX

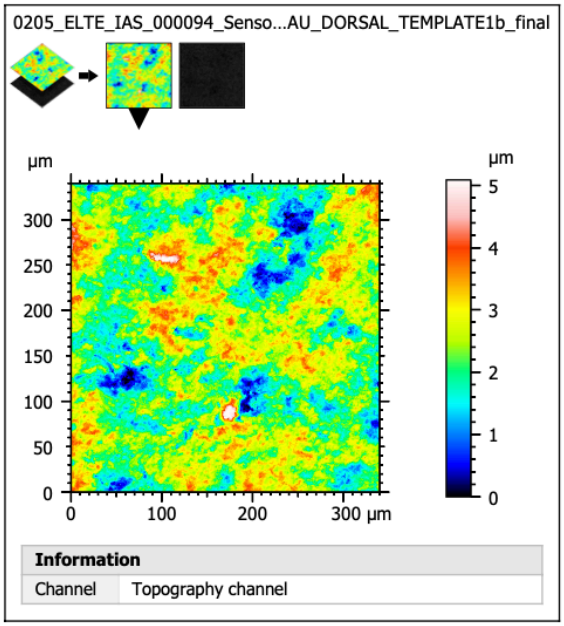

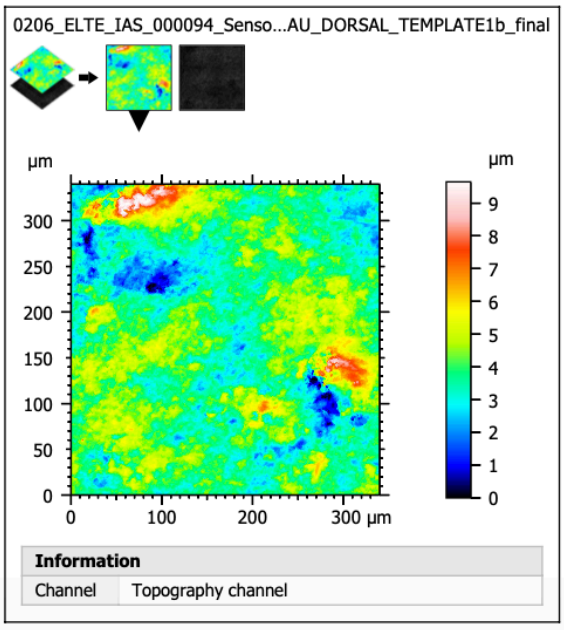

Olympus LEXT OLS5100

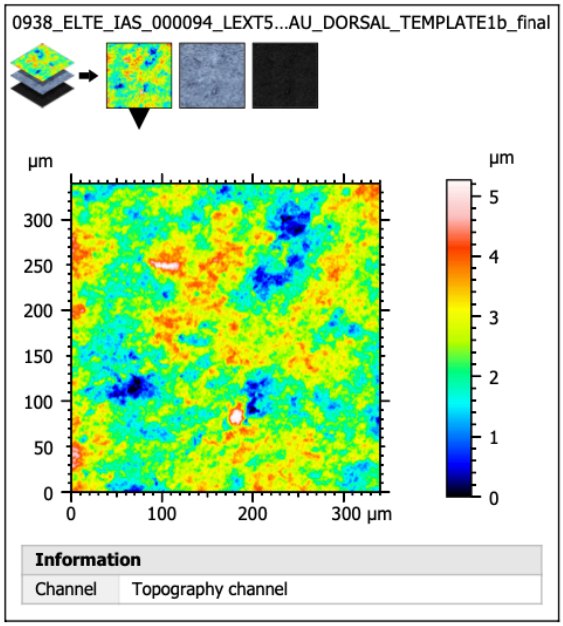

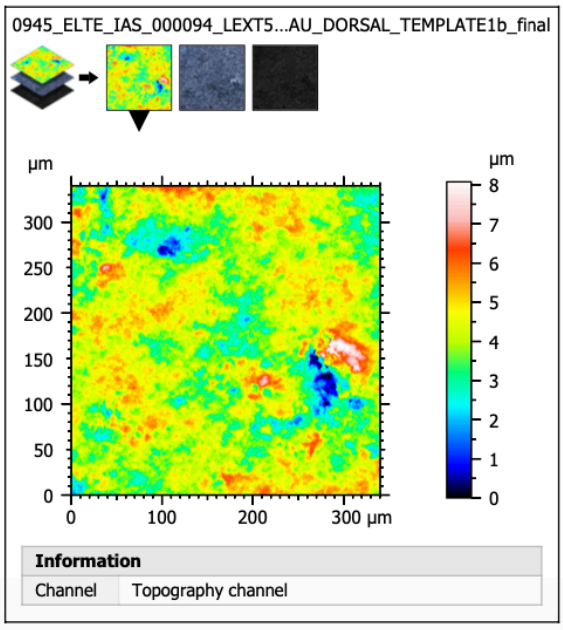

Annex figure 4: A.'94a'. - Figure 205 and Figure 938; B. '94b.'- Figure 206 and Figure 945

Studiables comparison, template 1b
Objective 100x, NA = 0.8

Sensofar sNEOX

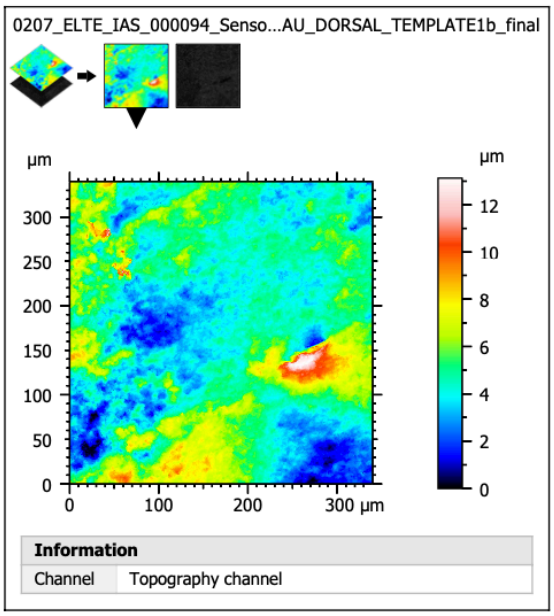

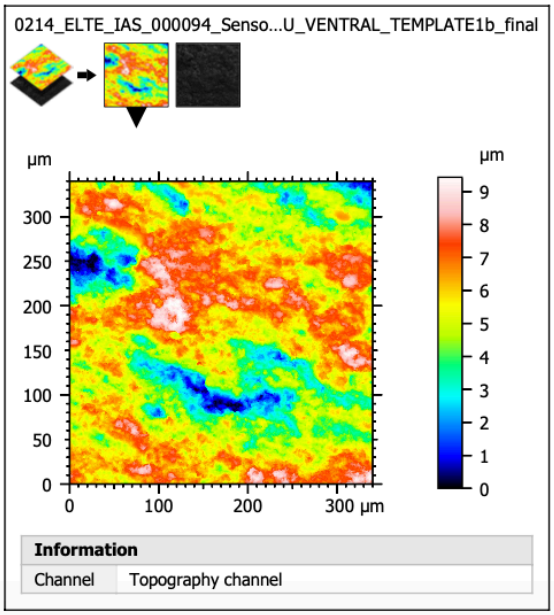

Olympus LEXT OLS5100

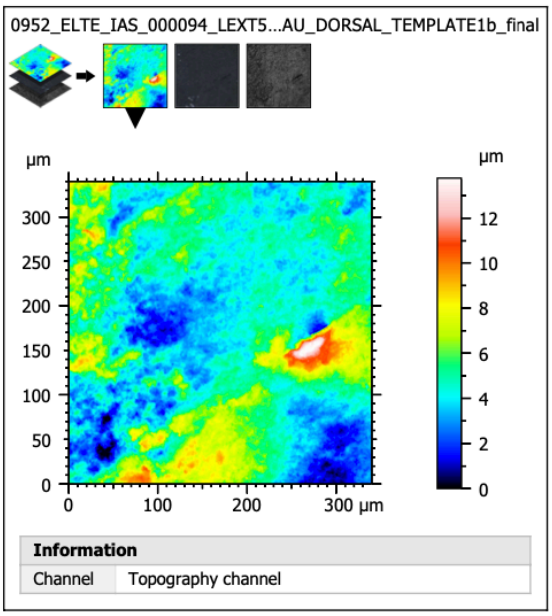

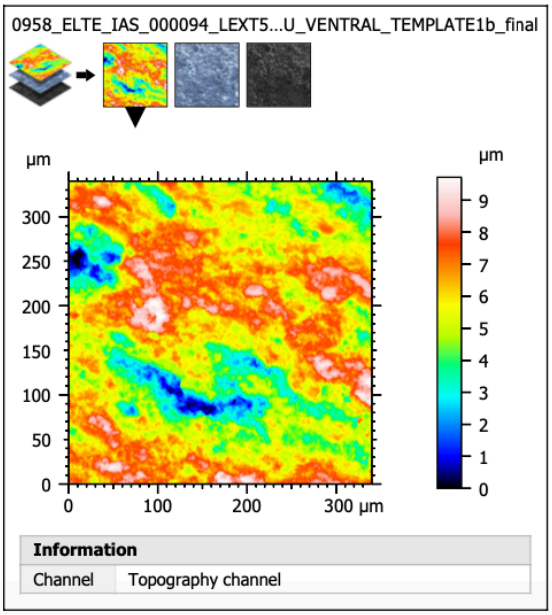

Annex figure 5: A.'94c'. - Figure 207 and Figure 952; B. '94d.'- Figure 214 and Figure 958

Studiables comparison, template 1b
Objective 100x, NA = 0.8

Sensofar sNEOX

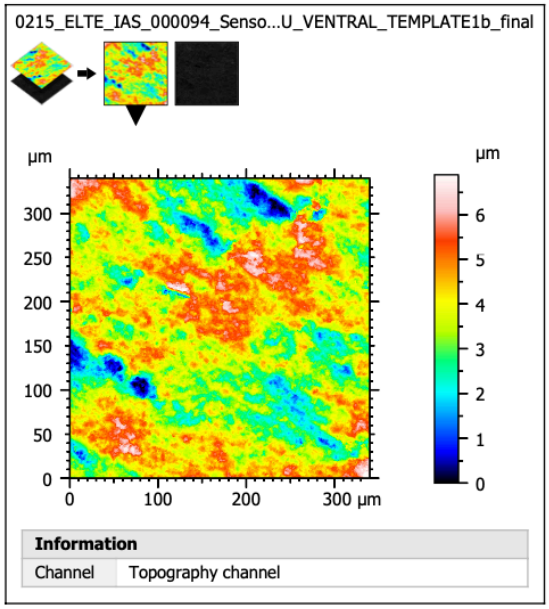

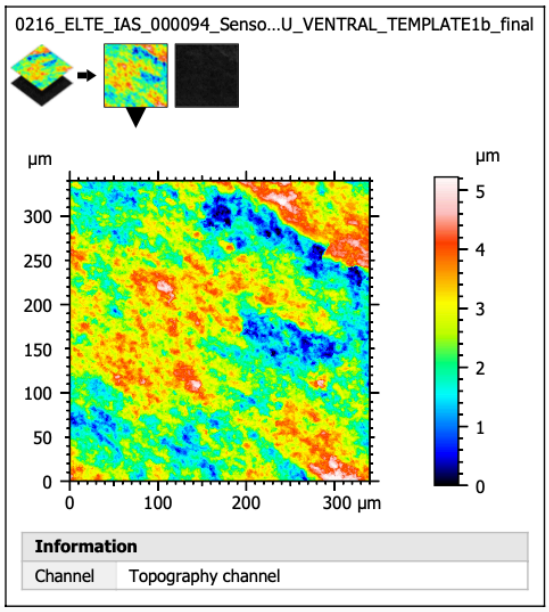

Olympus LEXT OLS5100

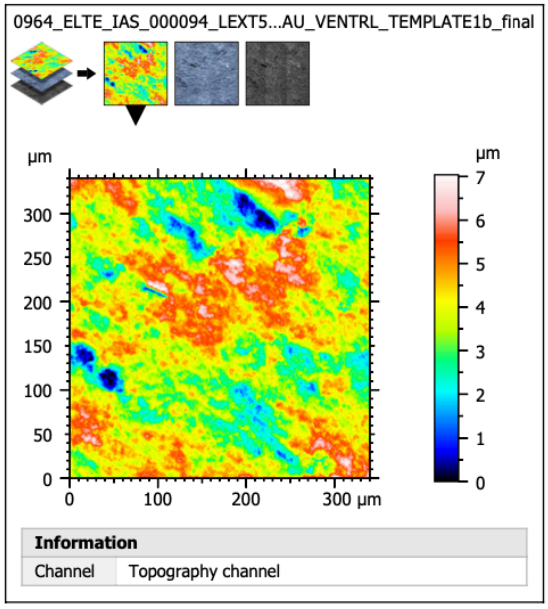

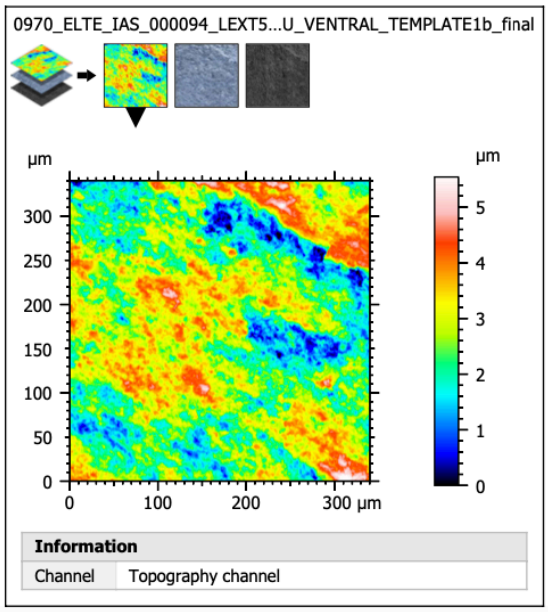

Annex figure 6: A.'94f'. - Figure 215 and Figure 964; B. '94f.'- Figure 216 and Figure 970

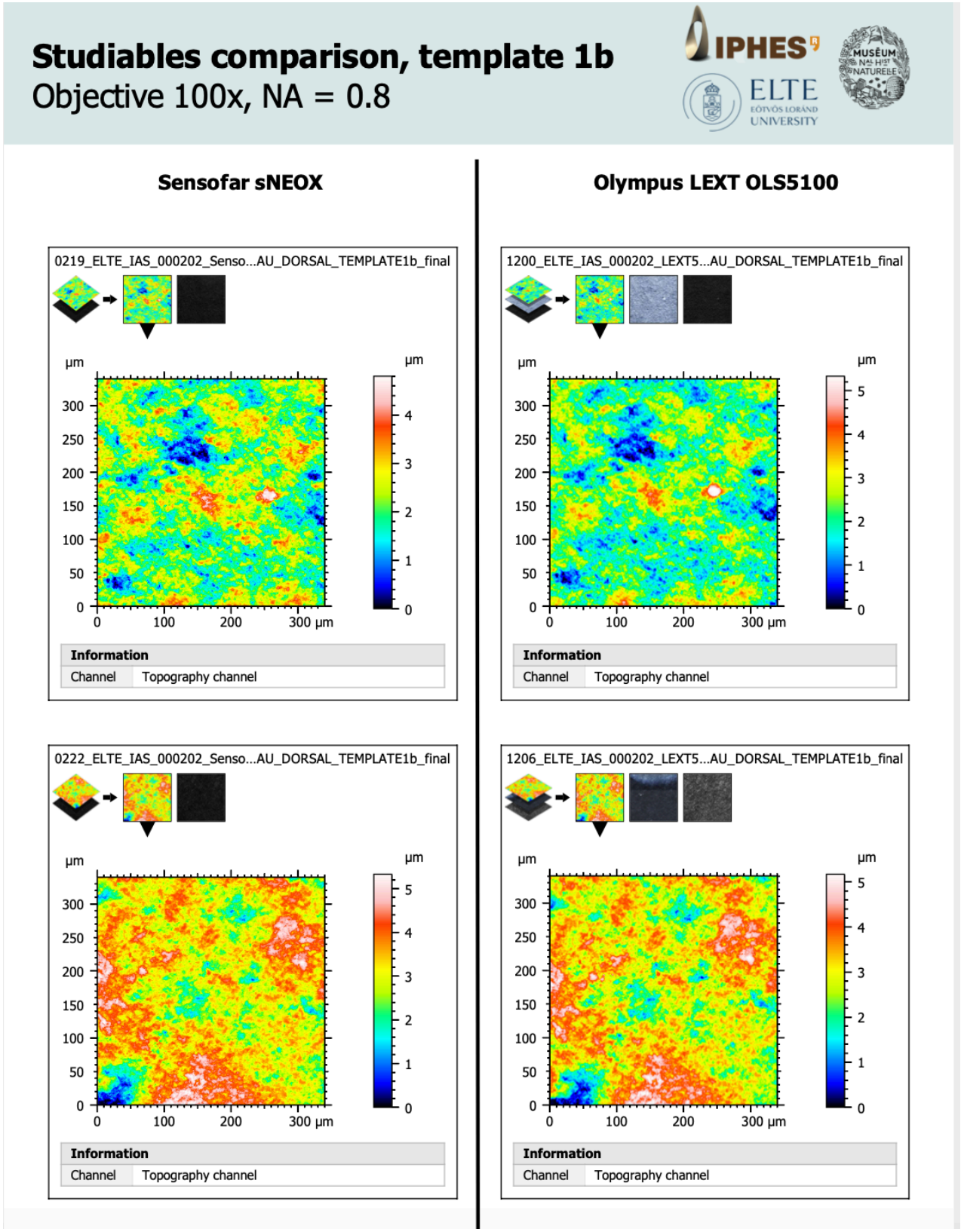

Annex figure 7: A.'202a'. - Figure 219 and Figure 1200; B. '202b.'- Figure 222 and Figure 1206

Studiables comparison, template 1b
Objective 100x, NA = 0.8

Sensofar sNEOX

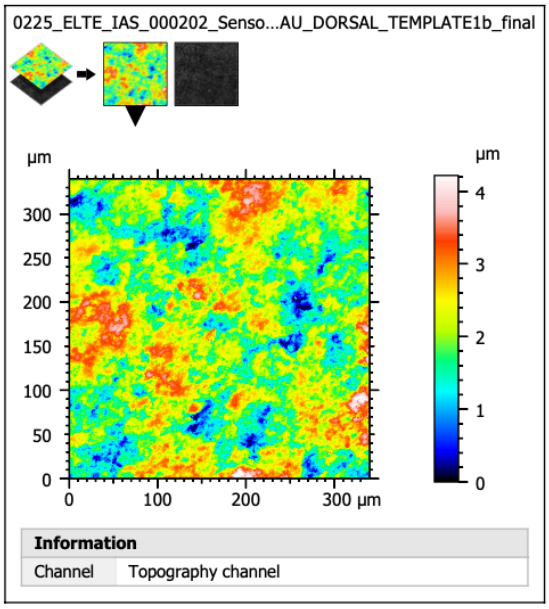

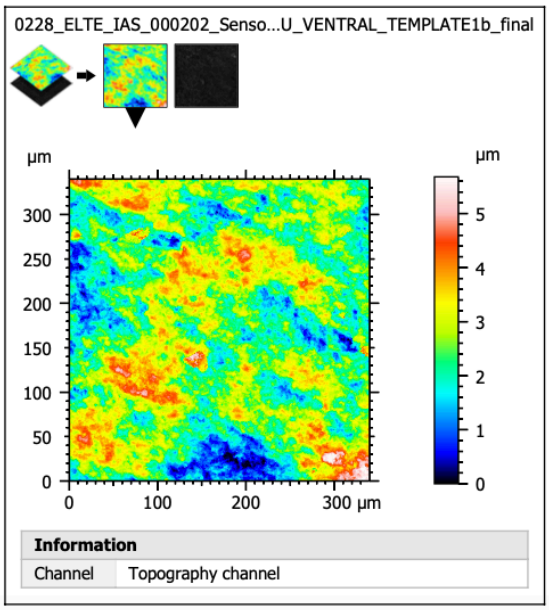

Olympus LEXT OLS5100

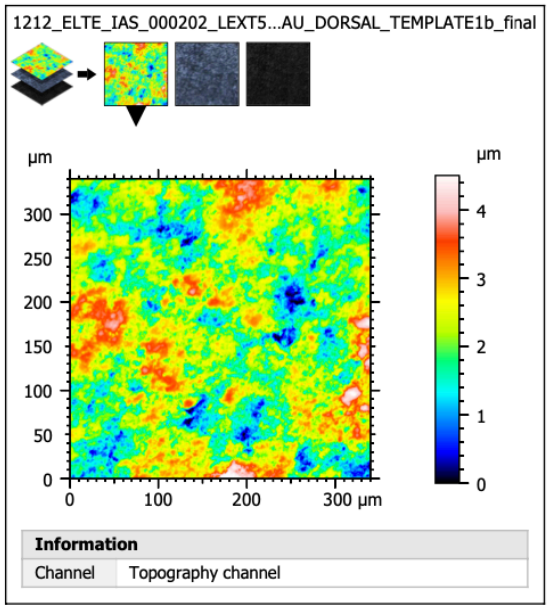

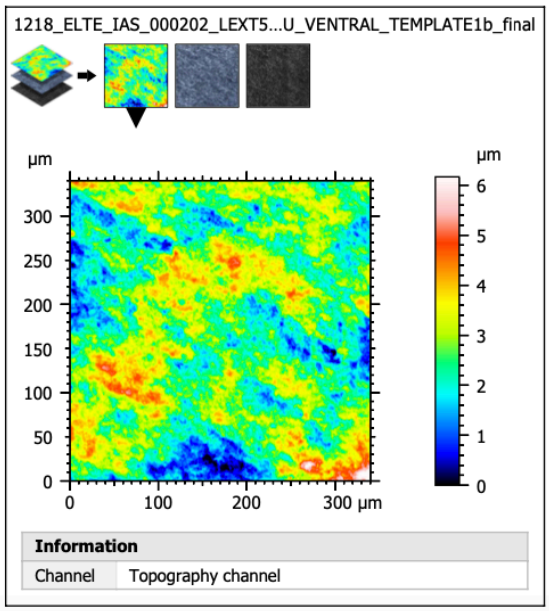

Annex figure 8: A.'202c'. - Figure 225 and Figure 1212; B. '202d.'- Figure 228 and Figure 1218

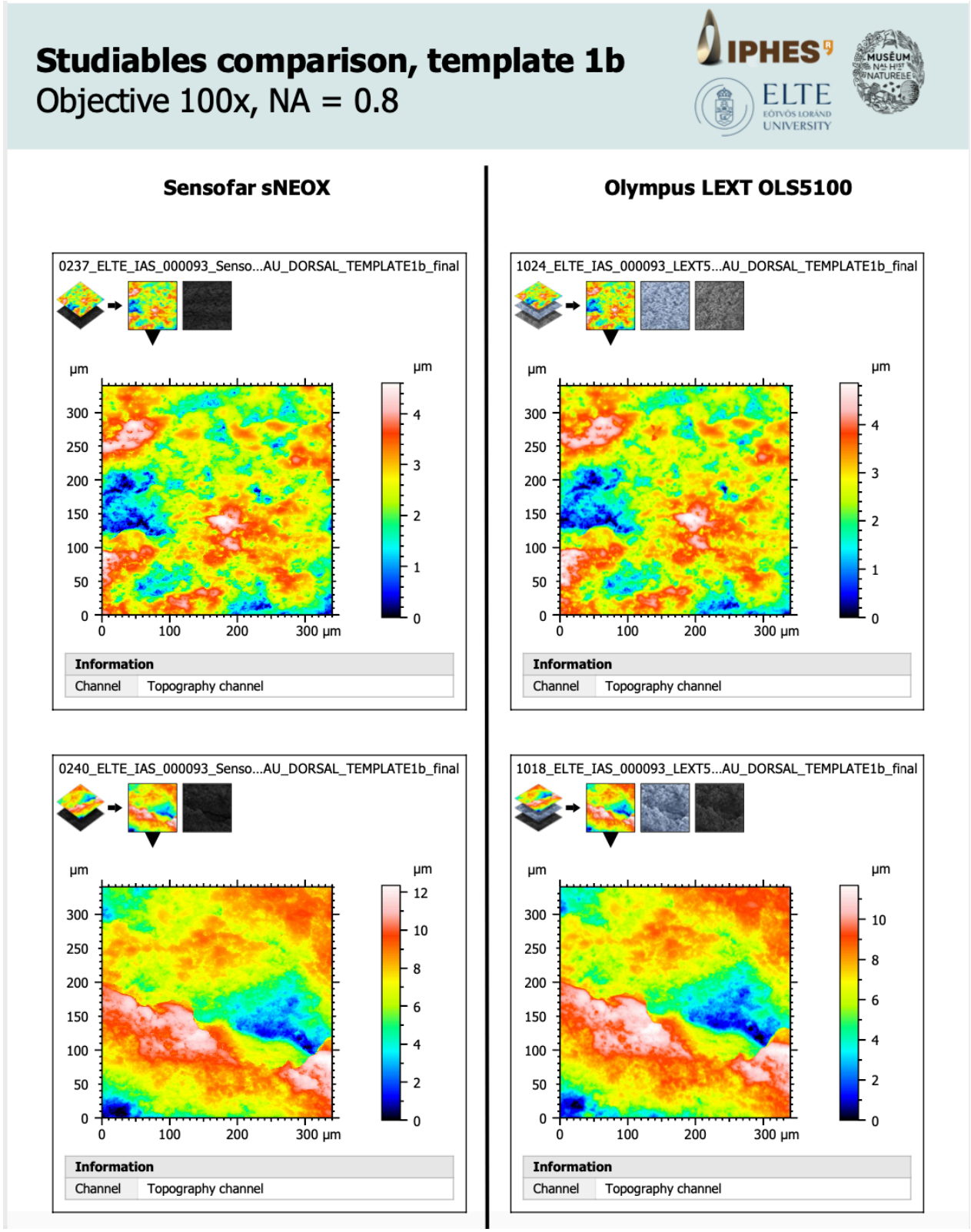

Annex figure 9: A.'93a'. - Figure 237 and Figure 1024; B. '93b.'- Figure 240 and Figure 1018

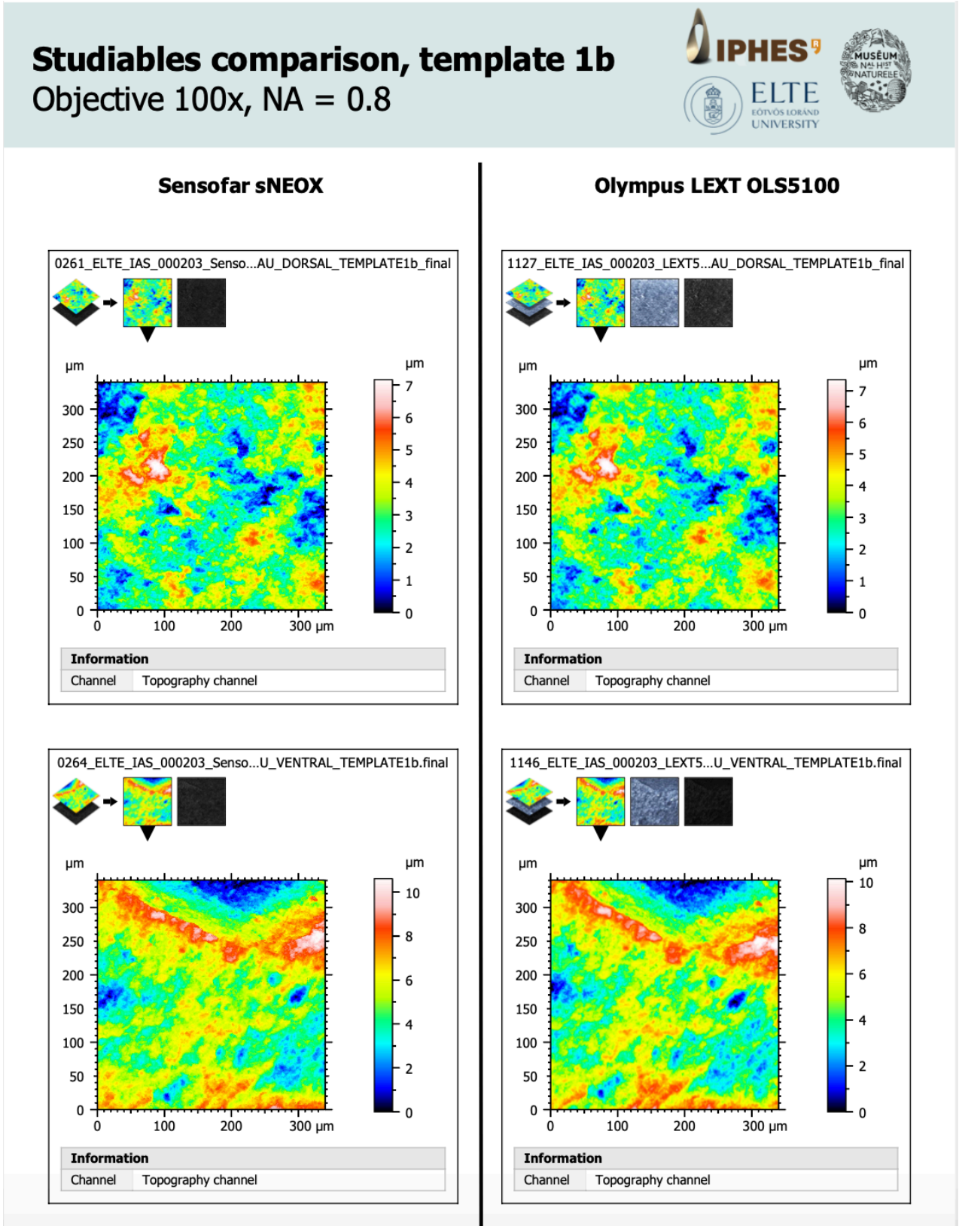

Annex figure 10: A. '203c' Figure 261 and Figure 1127; B. '203d.'- Figure 264 and Figure 1146

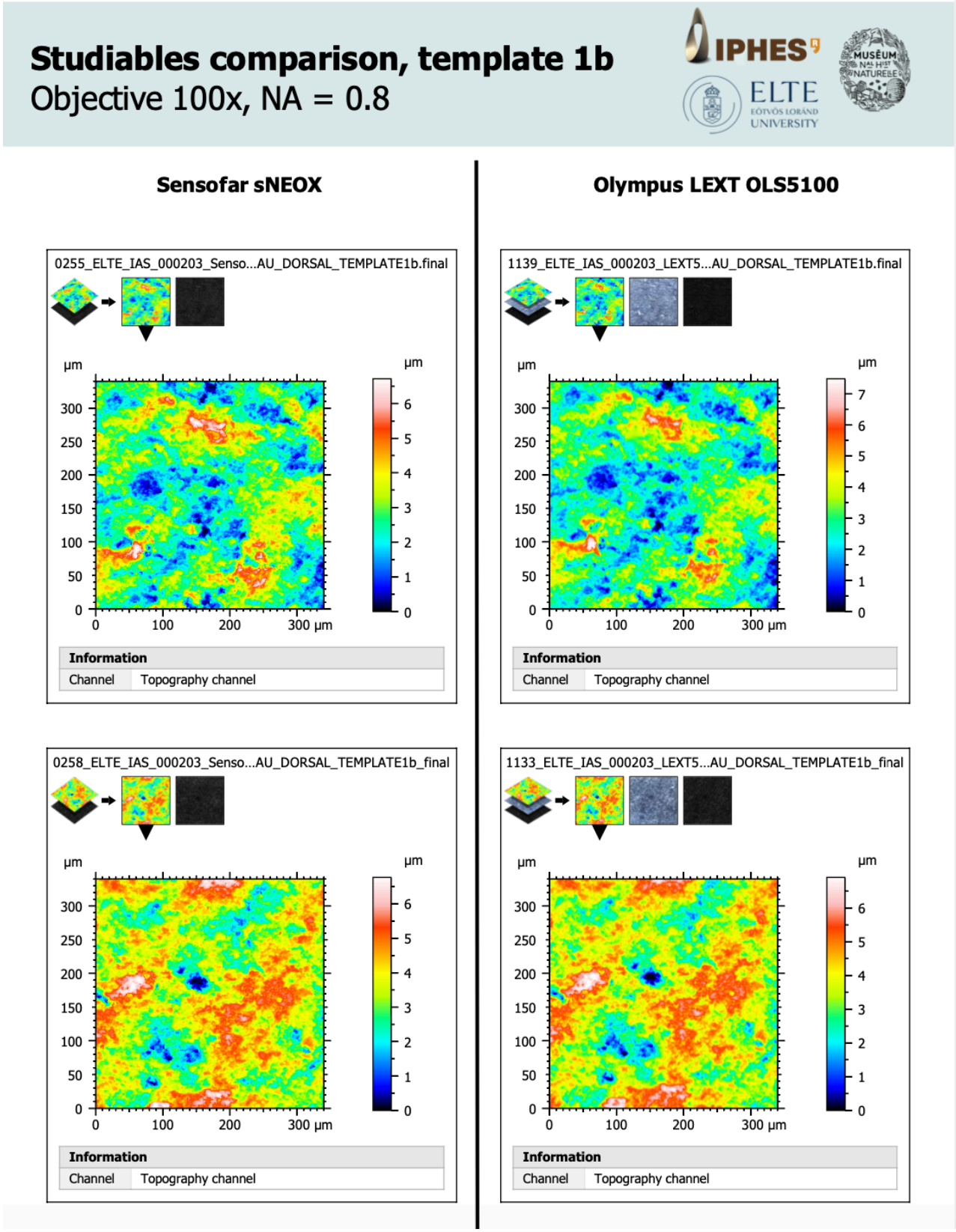

Annex figure 11: A. '93f' Figure 255 and Figure 1139; B. '203b.'- Figure 258 and Figure 1133

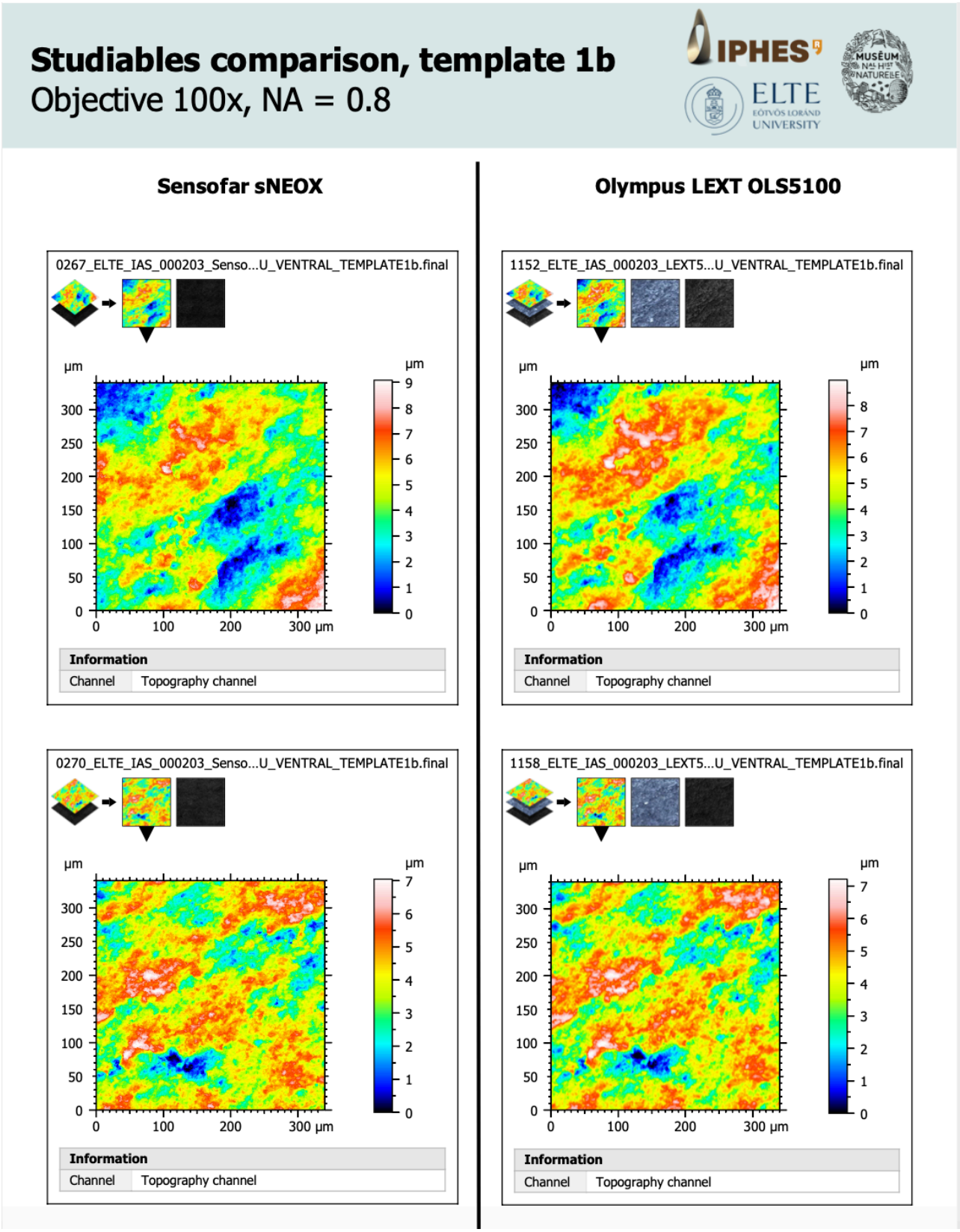

Annex figure 12: A.'203e'. - Figure 267 and Figure 1152; B. '203f.'- Figure 270 and Figure 1158

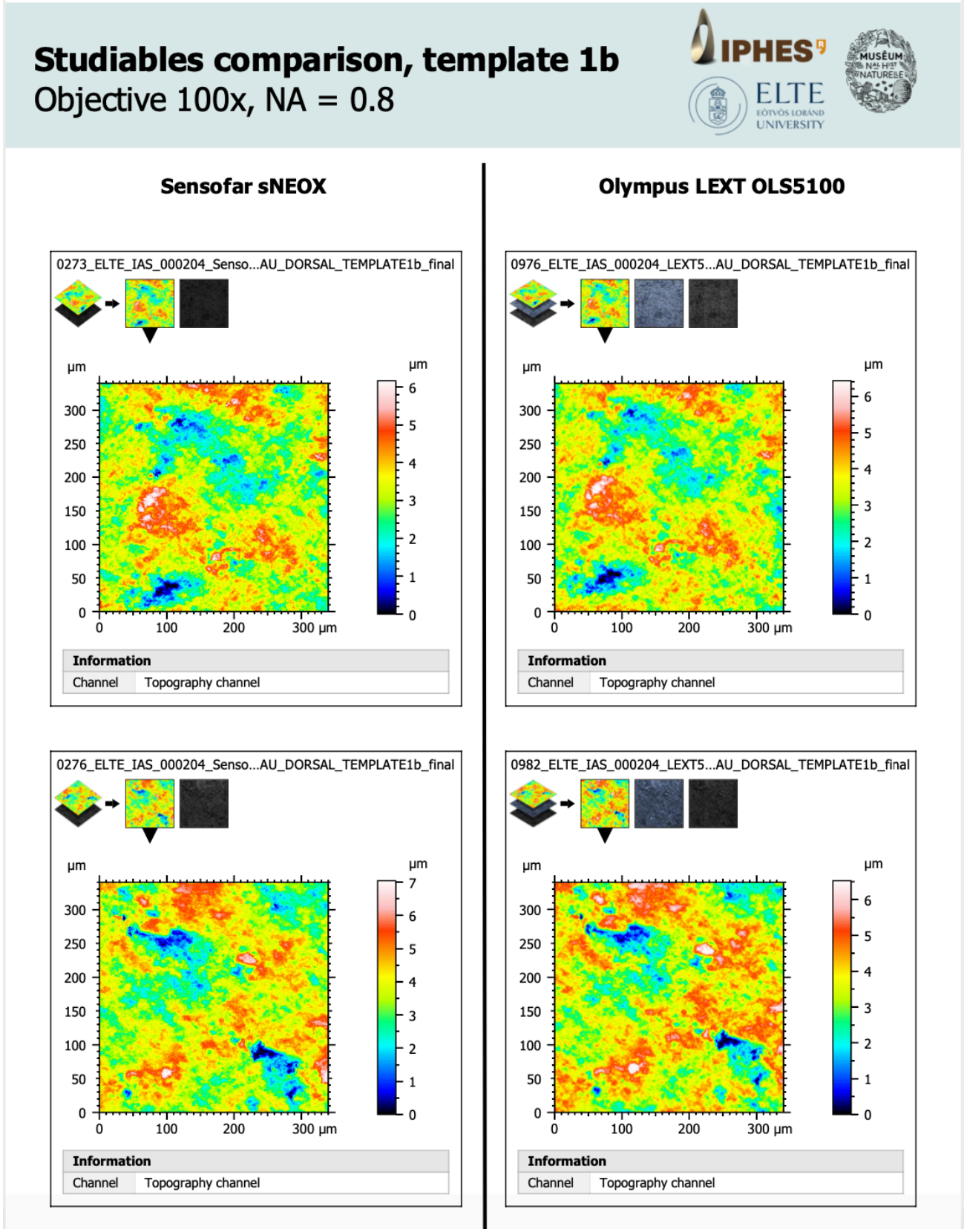

Annex figure 13: A.'204a'. - Figure 273 and Figure 976; B. '204b.'- Figure 276 and Figure 982

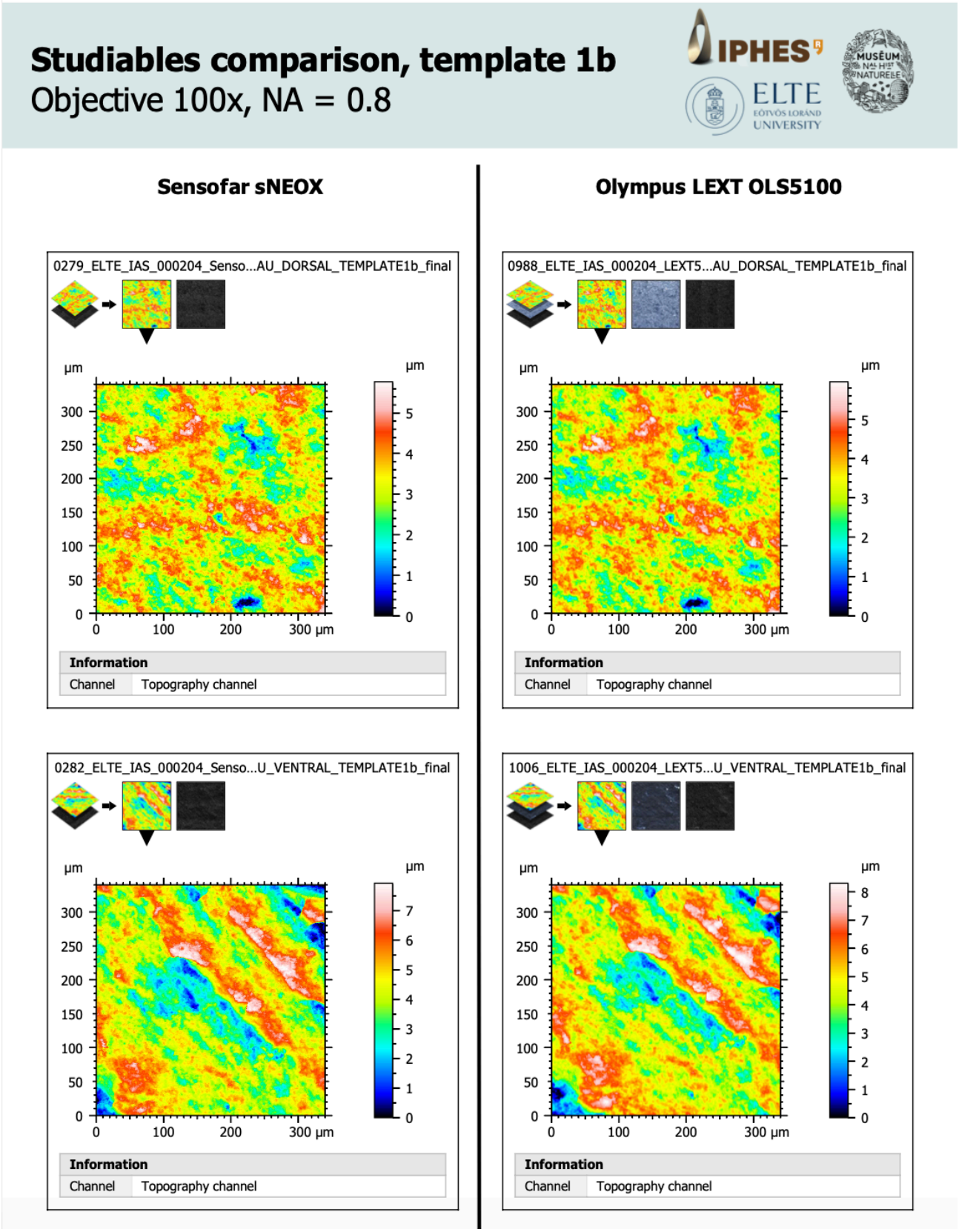

Annex figure 14: A.'96a'. - Figure 279 and Figure 988; B. '204d.'- Figure 282 and Figure 1006

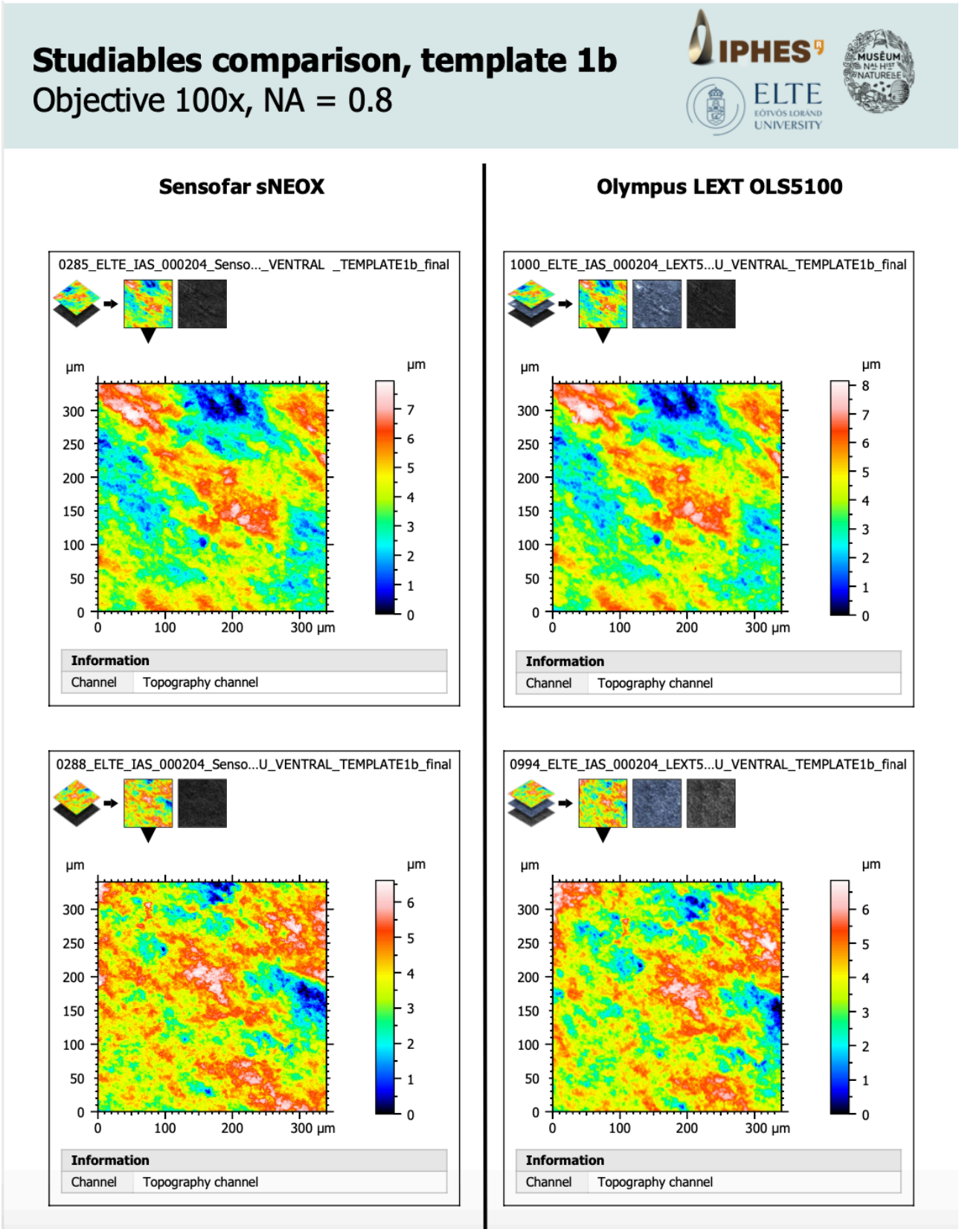

Annex figure 15: A.'204e'. - Figure 285 and Figure 1091; B. '204f.'- Figure 288 and Figure 994

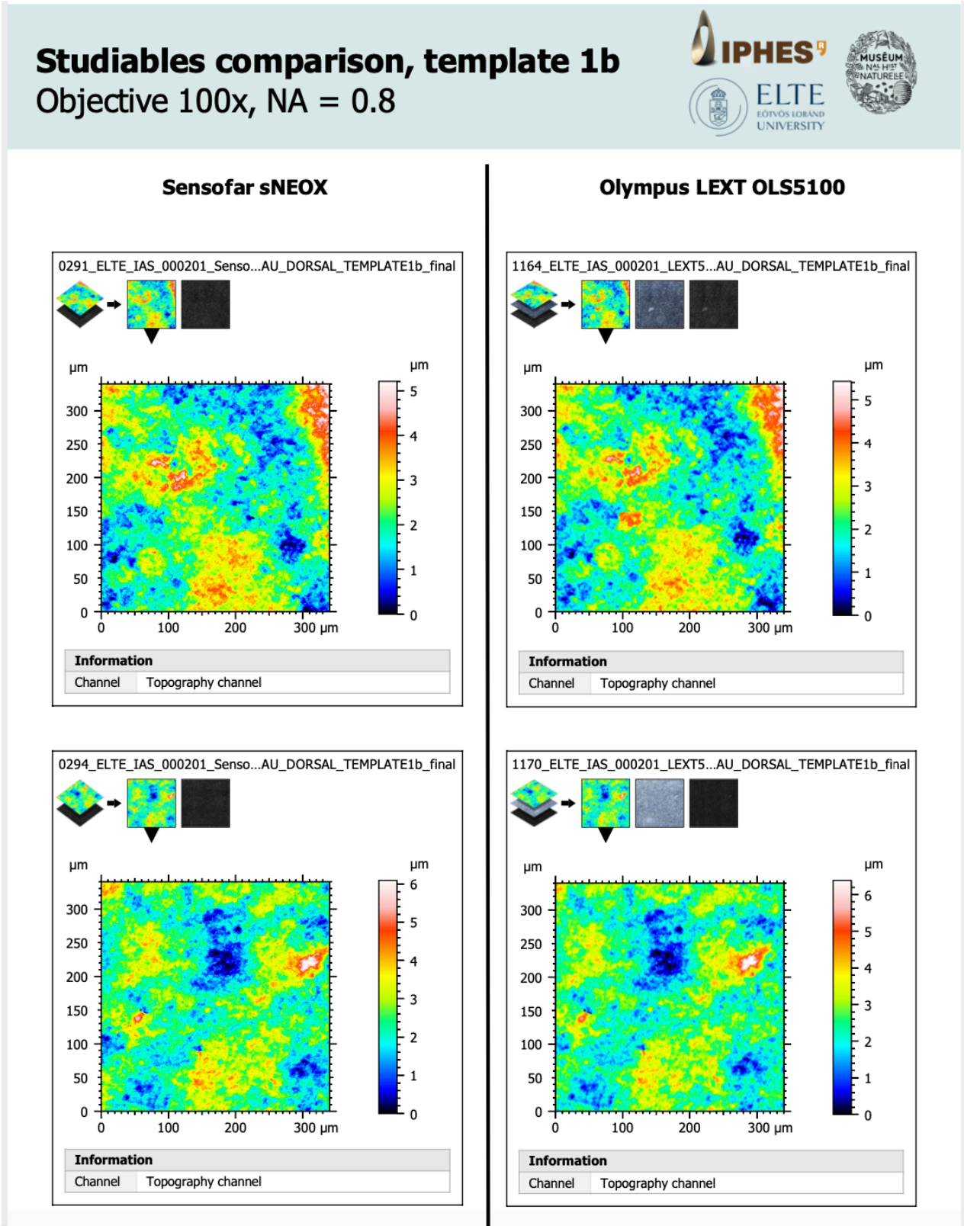

Annex figure 16: A.'201a'. - Figure 291 and Figure 1164; B. '201b.'- Figure 294 and Figure 1170

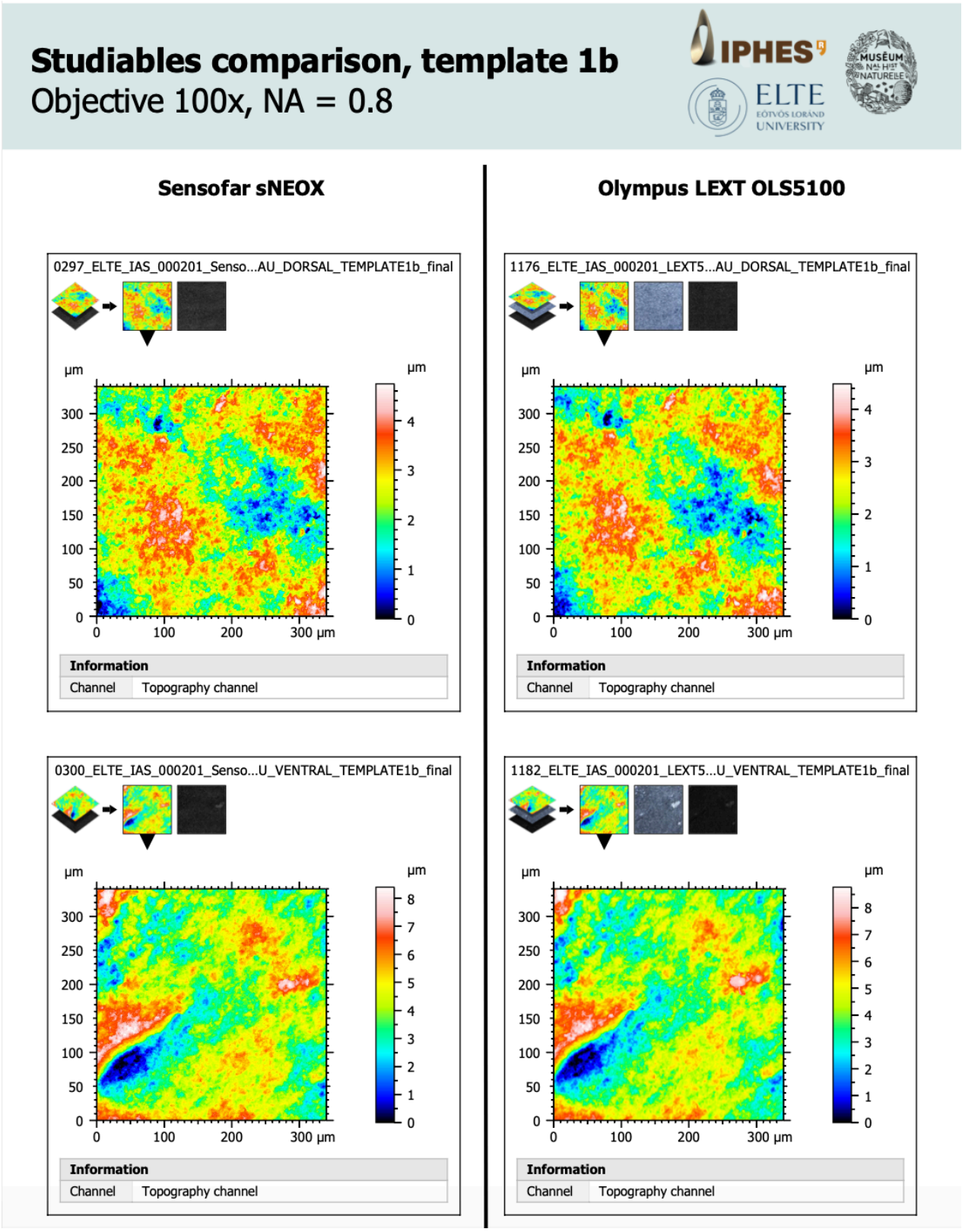

Annex figure 17: A.'201c'. - Figure 297 and Figure 1176; B. '201d.'- Figure 300 and Figure 1182

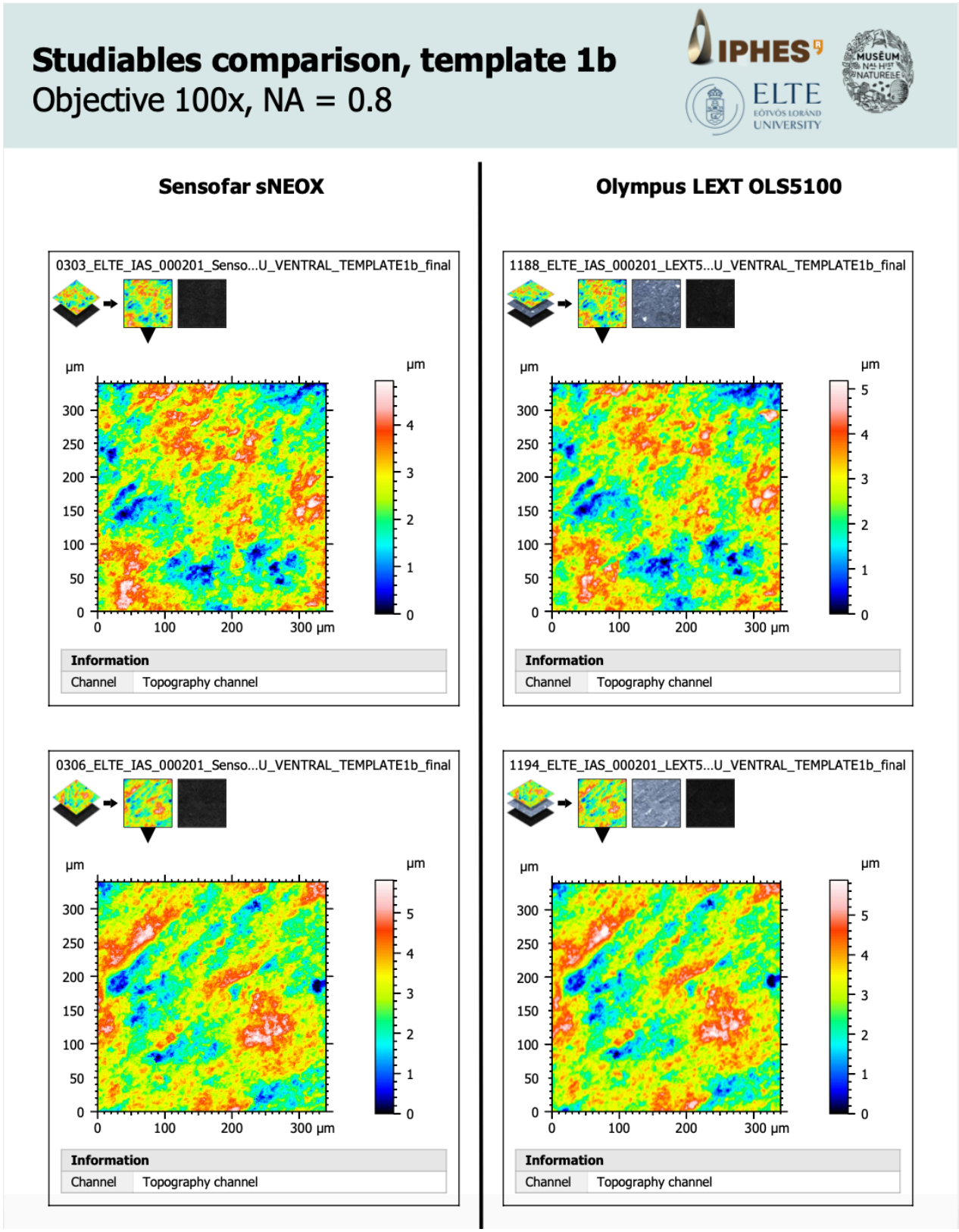

Annex figure 18: A.'201e'. - Figure 303 and Figure 1188; B. '201f.'- Figure 306 and Figure 1194

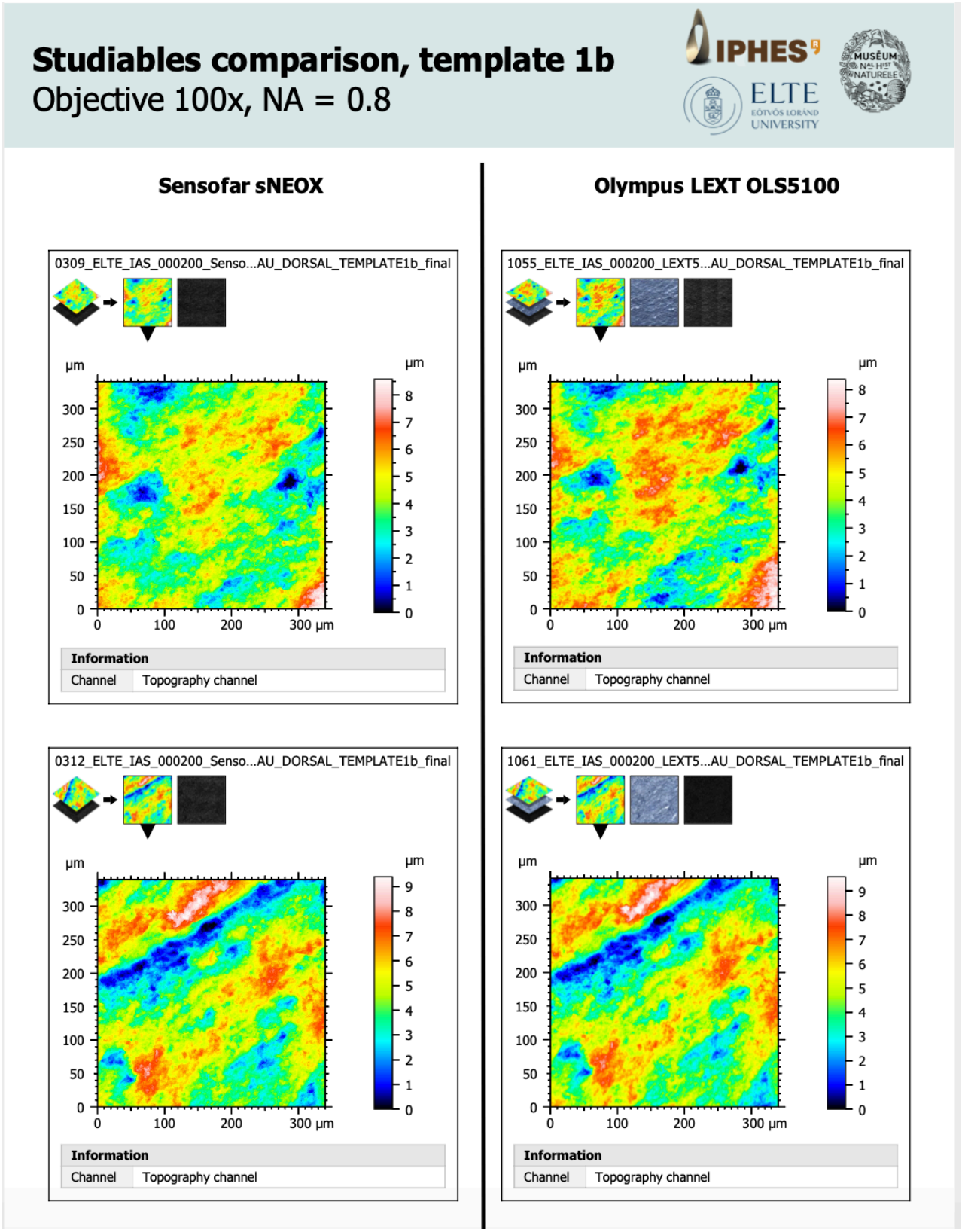

Annex figure 19: A.'200a'. - Figure 309 and Figure 1055; B. '200b.'- Figure 312 and Figure 1061

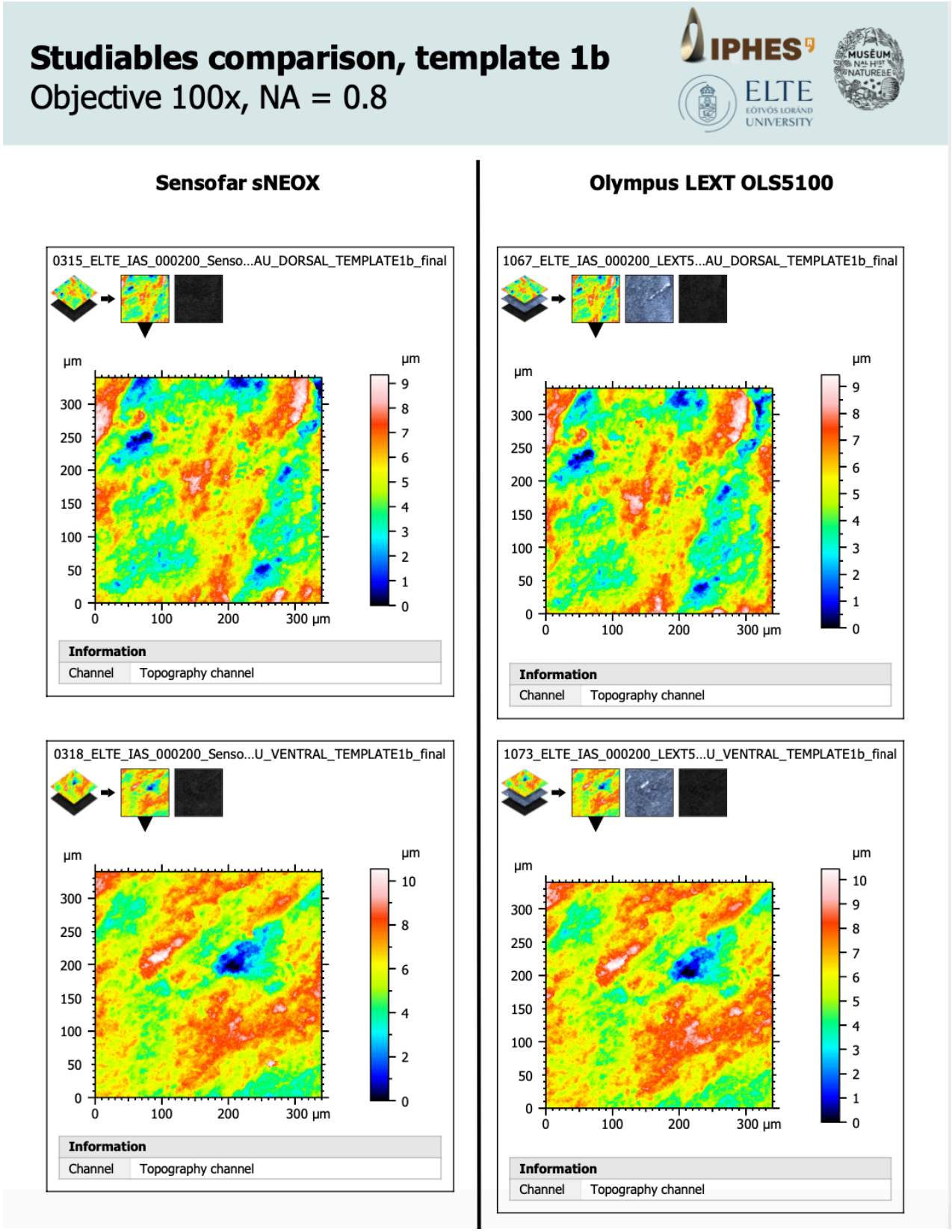

Annex figure 20: A.'200c'. - Figure 315 and Figure 318; B. '200d.'- Figure 318 and Figure 1073

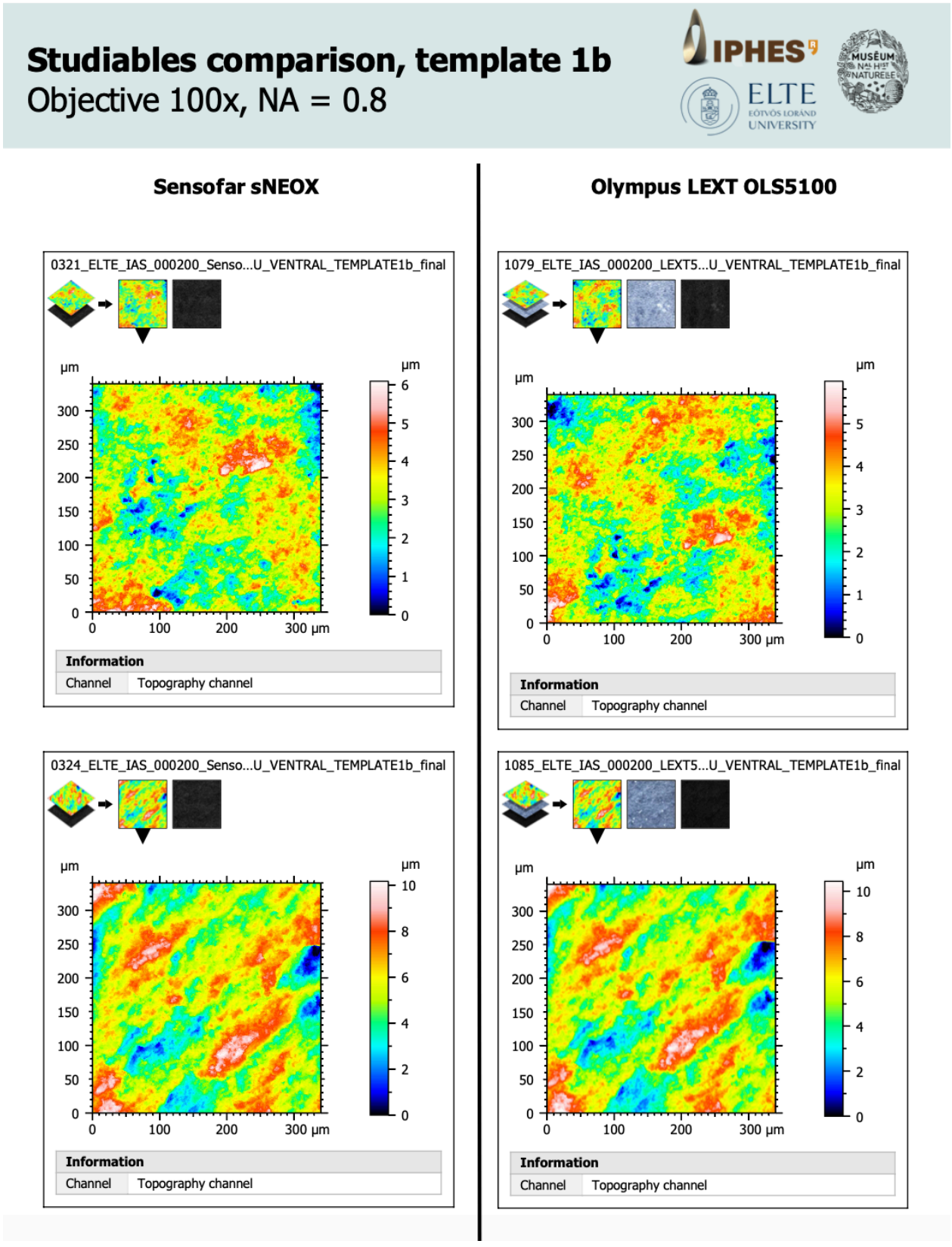

Annex figure 21: A.'200e'. - Figure 321 and Figure 1079; B. '200f.'- Figure 324 and Figure 1085

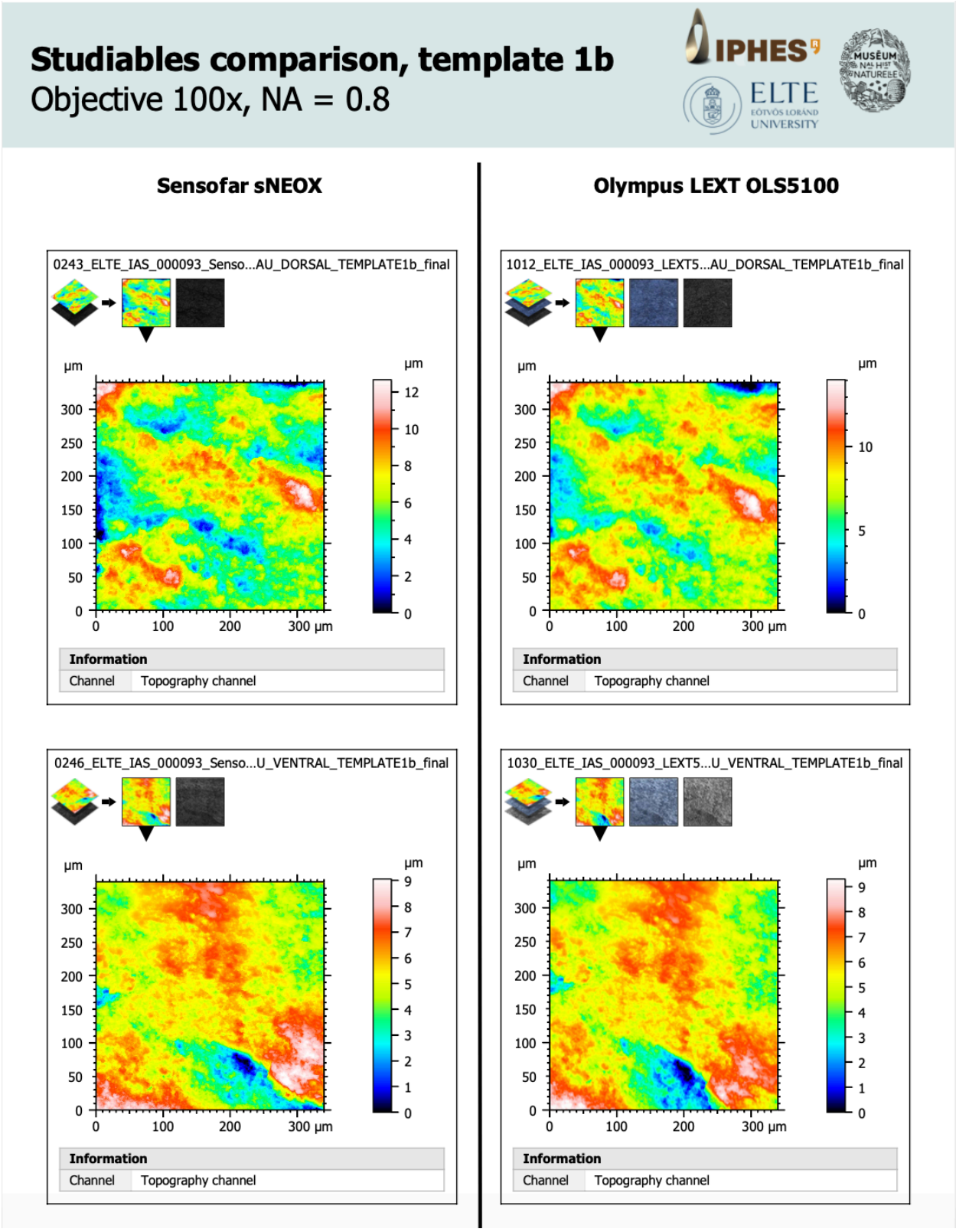

Annex figure 22: A.'93c'. - Figure 243 and Figure 1012; B. '93d.'- Figure 246 and Figure 1030

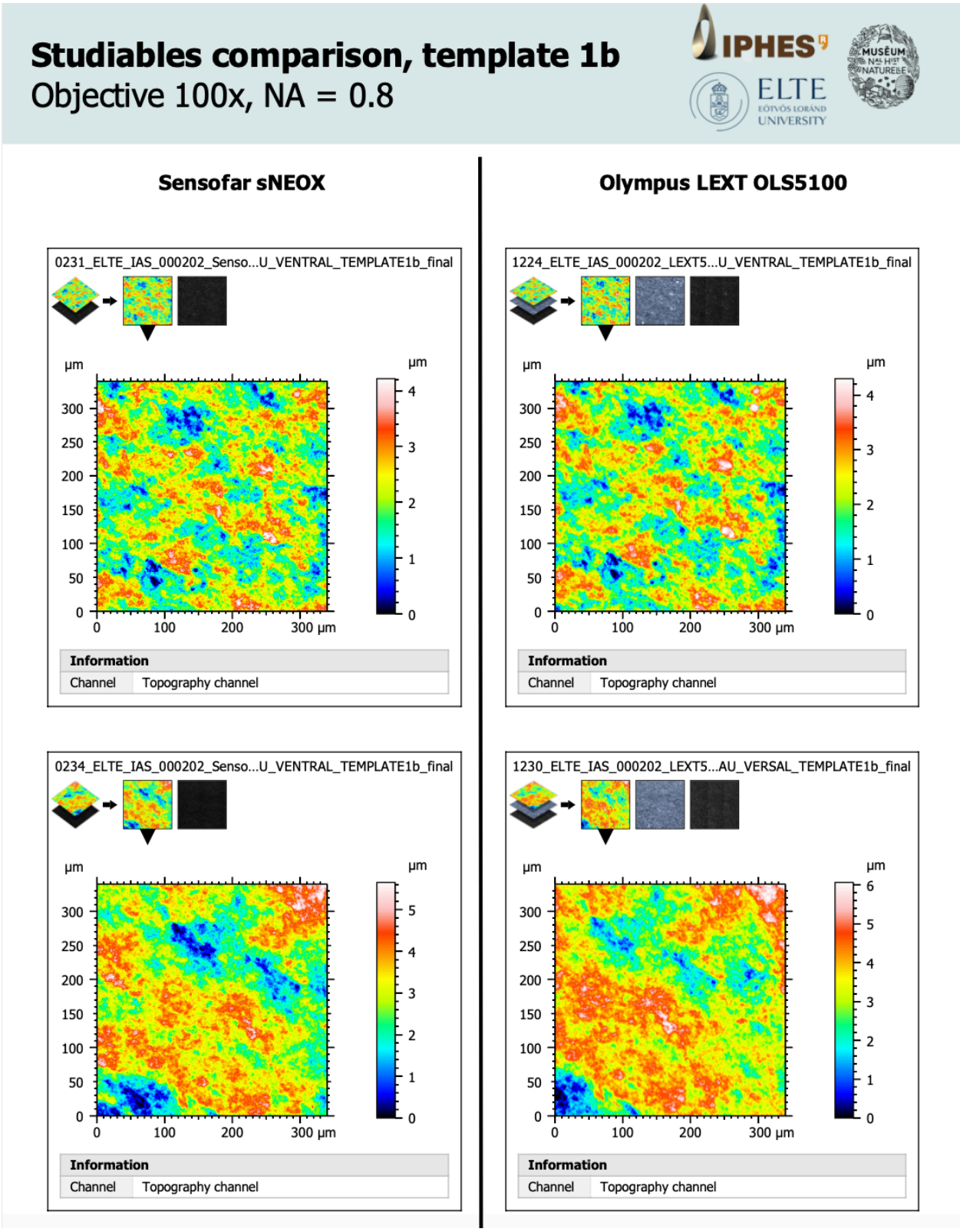

Annex figure 23: A.'202e'. - Figure 231 and Figure 1224; B. '202f.'- Figure 234 and Figure 1230

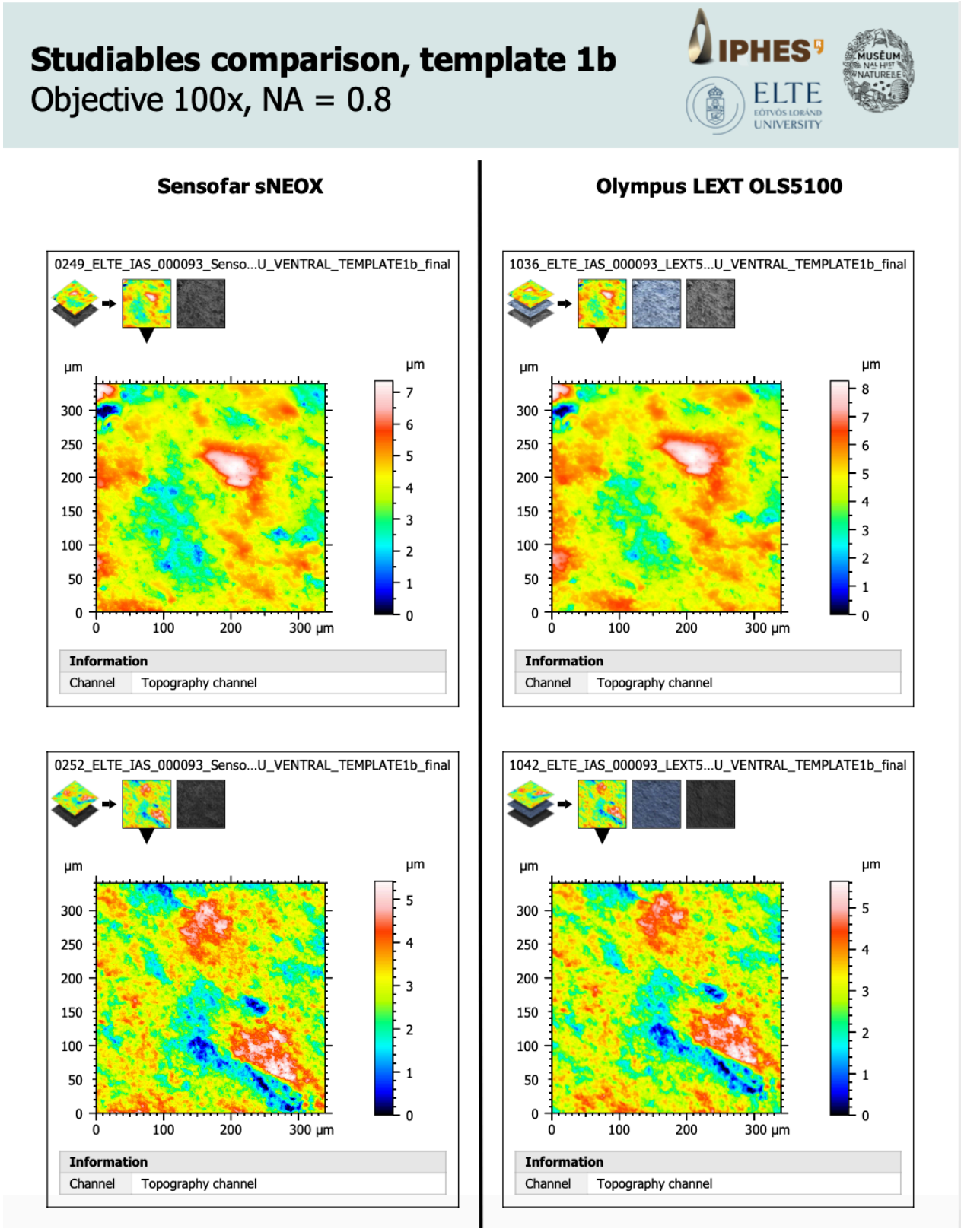

Annex figure 24: A.'93e'. - Figure 249 and Figure 1036; B. '93f.'- Figure 252 and Figure 1042